POLITECNICO DI TORINO

Corso di Laurea Magistrale

in Automotive Engineering

Tesi di Laurea Magistrale

Design, Manufacturing and Experimental Testing of a Composite Leaf-Spring Suspension Shackle using "Tailored Fiber Alignment (TFA)"

Relatore
prof. Giovanni Belingardi

Candidato
Martino Taffetani

Anno Accademico 2018/2019

Index of Contents

1. Introduction

1.1 General overview

Current global scenario features a day-by-day growing interest in the application of composite materials in the automotive field. From the aerospace industry, the concepts of lightweighting and smart usage of the material are now being ported to the automotive industry. This trend, in most cases, is not pushed by a whimsical research for exotic and expensive materials, but from the increasing importance that some concepts, like CO_2 emissions and waste of materials reduction, are gaining worldwide in general, and within the automotive sector in particular.

Lightweighting is a well-known multidisciplinary approach which, thanks to the continuous development of materials and technologies, can be adopted in more and more applications and designs. There are several drivers for lightweighting: performance enhancement by unconventional mass reduction systems, compliance to CO_2 emissions and fuel consumption regulations, reduction of Total Cost of Ownership, etc. Lightweighting does not simply consist in removing excess weight from a certain component or part, but it is a thorough approach which involves part and functional integration, choice of new materials and manufacturing processes and costs optimization. Lightweighting may also be considered as a virtuous circle which, through the reduction of Body In White mass, enables the reduction of chassis mass, which in turn allows a reduction of fuel tank capacity, keeping constant the mileage target of the vehicle, which presents, as a downstream effect, the possibility to reduce the performances of the powertrain, without affecting the overall performances of the entire vehicle. Chassis and body might represent up to two thirds of the total weight of a vehicle, this obviously implies that their optimization play a relevant role in the reduction of fuel consumption and CO_2 emissions and, even if regulations are not uniform across the world, the general trend aims to a CO_2 emission reduction. The average weight of cars has increased in years, mainly pushed by safety regulations, comfort equipment, driving dynamics improvement, etc. but in recent years, thanks to the development of new materials and technologies, lightweighting might be seen as the key to revert this weight increasing trend.

In this optic, the implementation of composite materials comes naturally. Carbon fiber can be considered a good alternative to traditional lightweight materials, e.g. high strength steel or aluminum, due to the its light weight, high strength and durability. The broad range of forms in which the fiber is used it is decisive in the choice of this material for several structural and non-structural components. Epoxy matrix resins systems are being developed whose cure time is getting closer and closer to being fully compatible with a mass production cycle-time. Thermoplastics are more and more considered for the advantage of easier manufacturing processes and, not less important, recyclability. Processes and tools are now available for high-speed, quality manufacturing, compliant with the standards required by the automotive industry. Nevertheless, even if this 'democratization' process of the composites is undergoing, one of its biggest obstacles is cost. Carbon fiber composites manufacturing costs around ten times more than aluminum and magnesium, and even more if compared to high strength steels. (Jaeger, 2014)[1] Other challenges to be faced are the recycling of carbon fibers, and the process/component integration in the multi-material manufacturing process of a vehicle.

As far as composite parts, the development is now focusing on improving the mechanical properties of the composite components, enhancement of structural integrity and, last but not least, optimization of load bearing capability of the material. Focusing on the latter, it is obvious that the performance of the material is fully exploited only when the internal forces are directed along the fibers' direction. However, this condition is neither easily nor often obtained, and this is because the manufacturing of fiber reinforced laminates typically consists in stacking layers of unidirectional tape or fabrics, each oriented in discrete directions (e.g. 0, ±45 and 90°) with reference to a defined structural axis, in order to obtain a multidirectional laminate. The direct consequence of this approach is that fiber alignment to load direction is always a trade-off, and the optimal alignment is seldom obtained. When this happens, load transfer is partially or completely discharged also on the matrix, which can be seen as the 'weak link' of the system, limiting the overall performance of the component or structure. (Tosh & Kelly, 2000)[2] Cracks and failures of the material are very frequently started exactly where applied loads are discharged on the matrix component of the composite, and several studies (Crothers & al., 1996) (Gliesche & al., 2002) (Koricho & al., 2014) (Zhu & al., 2018)[3] show that this phenomenon is even more accentuated in

[1] Hubert Jaeger, SGL, 2014 from https://www.reuters.com/article/sgl-fibres/cheaper-carbon-fibre-will-slash-auto-making-costs-manufacturer-idUSL5N0MP2RP20140328 consulted on 10/2018

[2] Tosh, Kelly, "*On the design, manufacture and testing of trajectorial fibre steering for carbon fibre composite laminates*", 2000

[3] Crothers et al., "*Tailored fibre placement to minimize stress concentrations*", 1996; Gliesche et al., "*Application of the tailored fibre placement (TFP) process for a local reinforcement of an "open-hole" tension plate from*

all the applications featuring notches and holes, them being necessary for functional integration, joining or even simple weight saving. The advantage of high strength and stiffness of carbon fibers is then lost and the traditional way to recover is to add more material increasing thickness and overall dimensions of the component or structure. This leads to negative effects on the load efficiency of the component and, by doing so, the choice of composites to replace standard metal parts is often hindered, also because of limited clearances and critical safety issues. Clearly, this opens a wide margin for improving the efficiency of the whole system: material could be used more efficiently allowing the reduction of surplus and the saving in material usage is anyway advantageous from both the economic point of view and the environmental one.

1.2 Tailored Fiber Alignment (TFA)

It is exactly with this aim in mind that TFA was studied at the beginning at the Institute of Polymer Research of Dresden. TFA technology aims to fully exploit the anisotropic properties of a continuous fiber reinforced compound. Since only along the fiber direction we have the optimal mechanical characteristics, and keeping in mind that even a small misalignment between fiber orientation and maximum stress angle can critically compromise the load bearing capacity, TFA technique is the way to locate the fibers so that they follow the stress field in the component under the considered load case. By using analytical and numerical tools the stresses in the components can be evaluated and the optimal fiber alignment can be defined.

carbon/epoxy laminates", 2002; Koricho et al., "*Innovative tailored fiber placement technique for enhanced damage resistance in notched composite laminate*", 2014; Zhu et al., "*Variable Angle Tow reinforcement design for locally reinforcing an openhole composite plate*", 2018

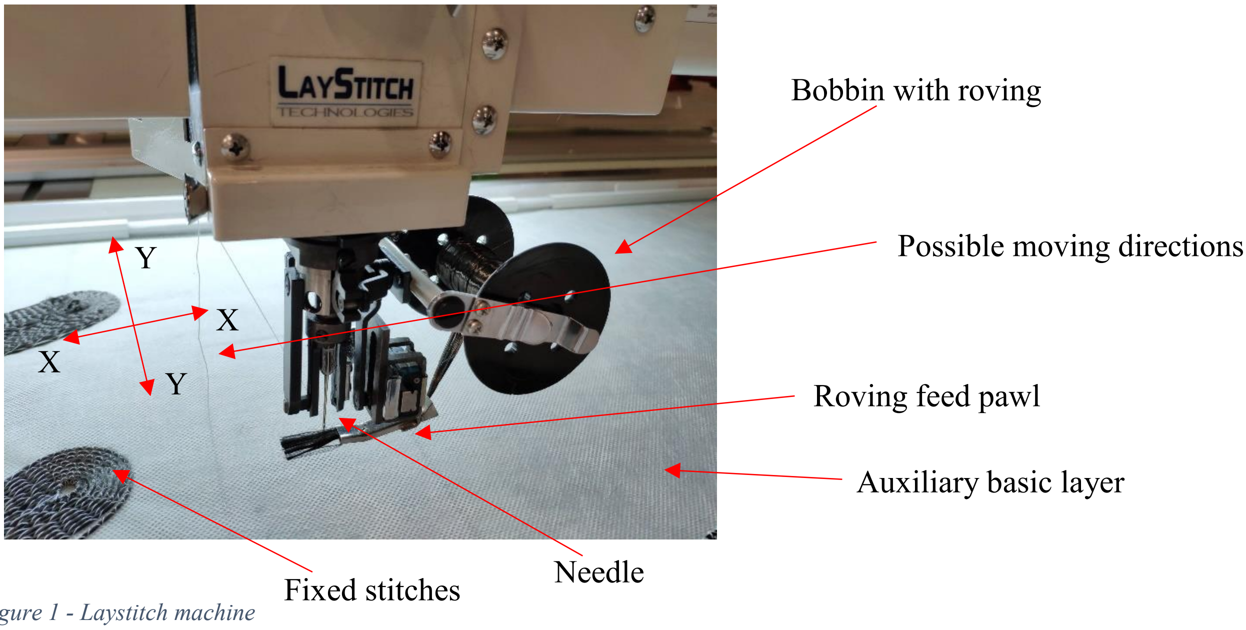

Figure 1 - Laystitch machine

The process can be summarized in this way: roving is positioned along a given path on a base layer of supporting material. The fibers are fixed in position by stitching them on the base material and usually the machine adopts a zig-zag stitching pattern. The advantage of this technique is that there is almost no constraint on the fiber orientation, so that the roving feed sleeve can follow any radius of curvature.

The manufacturing tools consist of the stitching head and a table with a moving frame so that it is possible to have relative movement in the two plane directions (X and Y) to follow the given pathway. It is also possible to manufacture preforms with more than one layer and of course this depends also on the specific machine used. The base material can be removed later or can be part of the final component, depending if the preform is going to be a single part/component or is a reinforcement which is going to be attached to another laminate. There is also the possibility to stitch directly the reinforcement on the laminate, but this may result in a loss of strength due to the damage to the laminate fibers caused by the stitching process itself. Some studies (Khaliulin & al., 2014)[4] suggest that the increase of strength coming from the optimal arrangement of the fibers may cover this loss, but every application should be evaluated in its particular conditions.

The advantages of the TFA consists, as already mentioned, in: the freedom to place the fiber in any angle ranging from 0° to 360°; stitching of multiple layers in the same area to achieve desired thickness distribution; reduced costs and time effort to convert the desired stitching pathway into a fiber placement pattern for the embroidery machine; production of near-net-shape preforms

[4] Khaliulin et al., "*Prospects of Applying the Tailored Fiber Placement (TFP) Technology for Manufacture of Composite Aircraft Parts*", 2014

which enhances the efficiency of the whole process by reducing material waste and maximizing the exploitation of the placed fibers; and the compatibility with a broad range of fibers from natural, glass, aramid up to carbon and ceramic ones.

Consolidation of TFA preforms to composites may be performed with regular techniques such as resin transfer molding (RTM), vacuum bag molding, pressing and autoclaving. For what concerns thermoplastic composites the matrix material can be placed together with the fibers, in this case the base material could be a thermoplastic ply which melts during the consolidation phase and becomes part of the matrix.

Another big advantage in the use of TFA can be seen whenever a notched component is considered. (Koricho & al., 2014)[5] In fact, very often laminate components integration (functional integration or joining) leads to the necessity of drilling holes through them. Conventional methods, however, bring a very limiting consequence: the fiber continuity in the hole is interrupted. Studies show that this can critically reduce the load bearing capacity of the component. Using TFA allows to steer the fibers around the hole/notch and to keep their continuity, and in this way the strength of the component is maintained almost similar to the unnotched one, while keeping unchanged the functional aspect.

1.3 Outline of the project

This project in particular focuses on the design, manufacturing and testing of an automotive leaf spring shackle. The role of this component in the leaf spring assembly is to allow the sliding motion of one of the leaf spring hinges, to obtain the expected behavior from the suspension.

[5] Koricho et al., "*Innovative tailored fiber placement technique for enhanced damage resistance in notched composite laminate*", 2014

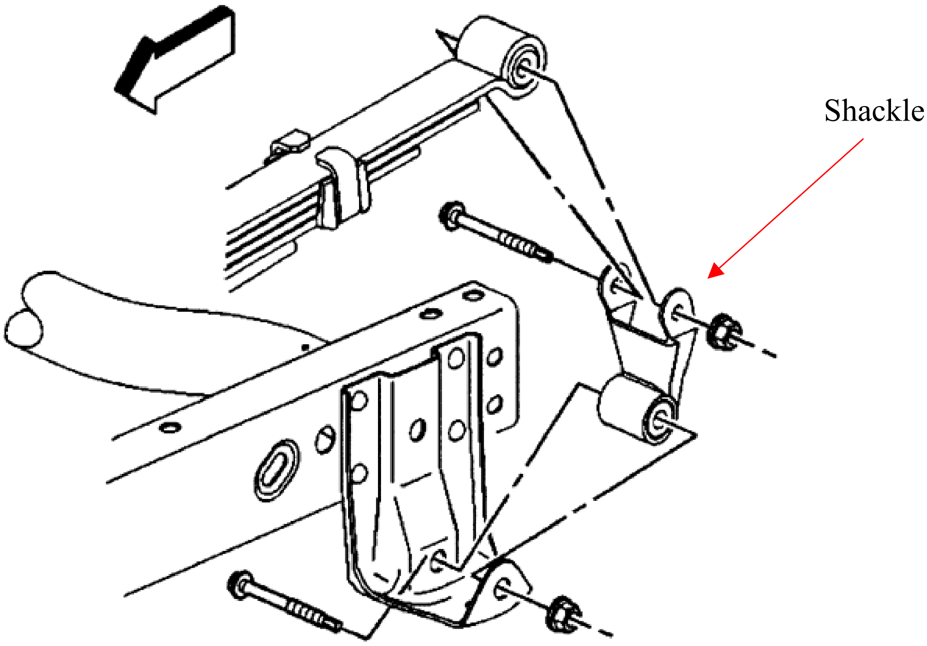

Figure 2 - Leaf spring assembly (from https://www.asvahosting.com)

Usually this component is realized in steel, the purpose of this thesis project was to exploit the TFA technique to realize a lightweight, optimized component, able to withstand the same rated load, but weighing less than the standard one. The innovation is not only in the use of a composite material, but also in the TFA technique, which allows to save material by optimizing fiber alignment and usage.

At first, an FE model of the shackle plate has been developed and tested in a FE analysis to evaluate the stress distribution and the load-paths. The fiber placement path has been defined by evaluating those results and the components have been stitched using the LayStitch machine in the Composite Vehicle Research Center of the Michigan State University. The material has been characterized by manufacturing and testing tensile coupons in order to validate the FE simulations. A mold has been designed and manufactured to obtain good quality components. Finally, the components have been tested to prove their mechanical qualities and a final analysis has been carried out on the results to understand the positive aspects and the drawbacks of this composite design compared to the traditional steel one.

1.4 Materials

In this paragraph, a brief presentation of the materials used in the composite manufacturing is given.

1.4.1 Fibers

Fibers are the elements which carry the load in the composite component. There are several types of fibers, each one characterized by its own mechanical properties and behavior. The characterization of the material is fundamental in any design, especially to validate the results of the simulations.

It is possible to distinguish four different types of fibers used as reinforcement material:

- Natural fibers (wool, etc.)
- Organic fibers (all plastic fibers)
- Inorganic fibers (glass, boron, etc.)
- Metal fibers (steel, aluminum, copper, etc.)

As Daniel Pichler, Managing Director at CarbConsult GmbH points out in an article entitled "*The Carbon Fiber Market*" (Pichler, 2019)[6], "in 2018, the global demand for carbon fiber was approximately 85,000 metric tons. […] In recent years, demand for carbon fiber has grown by 10 to 15 percent per year, and this same growth rate is expected to continue for the coming years".

As far as the production of glass fibers, "global […] capacity was 10.9 billion pounds in 2018 and is currently running at 91 percent utilization." (Mazumdar, 2019)[7]

[6] Pichler D., "The Carbon Fiber Market", 2019, on http://compositesmanufacturingmagazine.com consulted on 02/27/2019

[7] Dr. Mazumdar S., "The glass fiber market", 2019, on http://compositesmanufacturingmagazine.com consulted on 02/27/2019

Year 2018	Glass fibers	Carbon fibers
Production (metric tons)	4,950,000	85,000

Table 1 - 2018 annual production of carbon and glass fibers (metric tons)

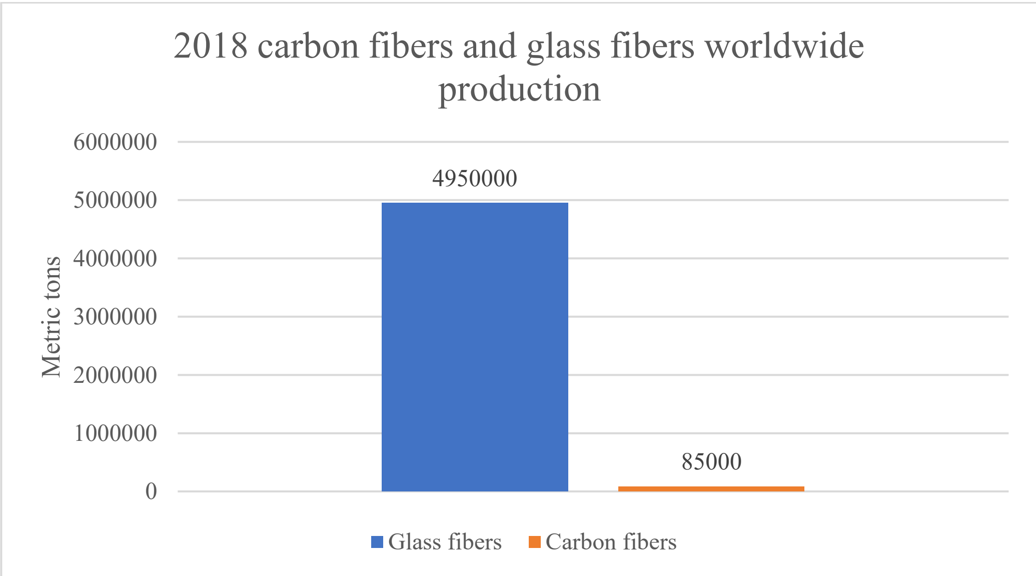

Figure 3 – 2018 worldwide carbon and glass fibers worldwide production bar chart

It is impossible not to notice that carbon fiber production is much smaller than glass fibers. Both, as reported in the previous cited articles about the worldwide composite industry, both types are facing a constant increasing trend year by year.

1.4.1.1 Glass Fibers

Glass fibers are the most common reinforcement adopted for plastics. Their main characteristics are low density associated to the high strength of the fibers. The cost is relatively low if compared to other fibers. The most adopted are the ring and the circular cross sections, even if elliptic shapes provide an improved bonding to the matrix. The design engineer can choose among 6 different kinds of glass fibers (E- low electrical conductivity, S- high strength, C- high chemical durability, M- high stiffness, A- high alkali or soda lime glass, D- low dielectric constant). The most frequently used is the low-cost general-purpose E-glass, whose basis is a calcium alumino-silicate. S-glass, D-glass, A-glass, ECR-glass (high corrosion resistance), ultrapure silica fibers, hollow fibers and trilobal fibers are special-purpose ones.

Positive aspects of use of glass can be summarized as:

- High tensile strength in relation to the specific mass
- Good draping properties
- Inflammable
- Low cost production

Negative aspects include: relatively low Young's modulus, no special material orientation and their tendency to brittle material failure. Their behavior is isotropic. The elastic range is quite large, this allows their use in cases where a high failure strain is requested. Glass fibers are subject to strength drops if exposed to high temperature over a long time (see Figure 2). (Salil & Manas, 2006) [8]

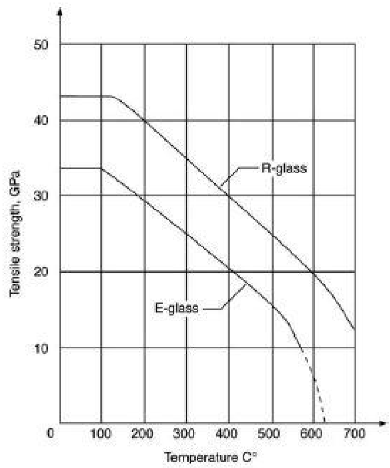

Figure 4 - Strength retention of R-glass and E-glass at elevated temperatures. Drawn from data contained in French patent 1,435,739, to Saint Gobain Company (Chambrey, France Patent No. 1435739, 1963)[9]

[8] Salil K. Roy Manas Chanda, "*Plastics Technology Handbook*", 2006

[9] French Patent no. 1435739 to St. Gobain Company, Chambrey, France, 1963

1.4.1.2 Carbon fibers

Carbon fibers are one of the top ten emerging high-tech materials for the future (Carbon composites one of top 10 emerging technologies, 2014)[10]. Their top-notch properties have been known since a long time, and research institutions worldwide are currently investing a lot of economical and time effort in studying and developing efficient and cost-effective methods to manufacture carbon components.

C-fibers are produced from PAN (Polyacrylnitril) fibers. The carbonization process of the PAN in a carbon atmosphere allows to achieve the high strength and Young's modulus which characterize C-fibers. Applying a different graphitization method together with an elongation of the fiber enables the possibility to obtain the desired Young's modulus. Then the surface is treated to increase the adhesion between the fibers and the matrix. During the production process, there is a build-up of stable oxides on the surface of the fibers, these protect the fibers from environmental agents.

The atomic structure of graphite is constituted by layers. This feature, in theory, allows to very high mechanical properties (E_l = 1000000 N/mm^2 and R_l=E_l/10=100000 N/mm^2) (Fitzer & Kunkele, 1990)[11]. In practice, defects lower these values. Several different types of carbon fibers have been developed featuring different strength and stiffness values.

[10] World Economic Forum, "*Carbon composites one of top 10 emerging technologies",* 2014
[11] Fitzer, Kunkele, High Temp. - High Pressures journal 22(3), pp.239-266, 1990

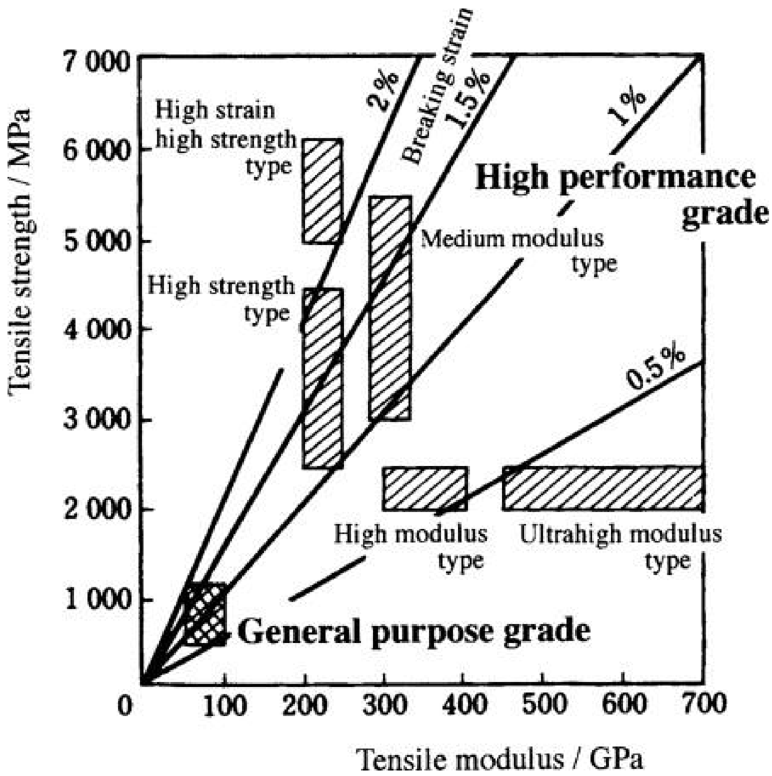

Figure 5 - Classification of carbon fibers on the basis of mechanical performance (Inagaki, 2000)[12]

It is possible to distinguish these categories:

- High-Tensile – HT
- Ultrahigh-Tensile – UT
- Intermediate Modulus/Strength – IMS
- High-Modulus – HM
- High-Modulus / Strength – HMS
- Ultrahigh-Modulus/Strength – UMS

Unlike glass fibers, carbon fibers exhibit anisotropic behavior. Tensile modulus in the material direction is about one order of magnitude higher than the one in the transverse direction. As far as the cracking behavior, it is brittle and the elongation at fracture is very low.

[12] Inagaki, in New Carbons - Control of Structure and Functions, 2000

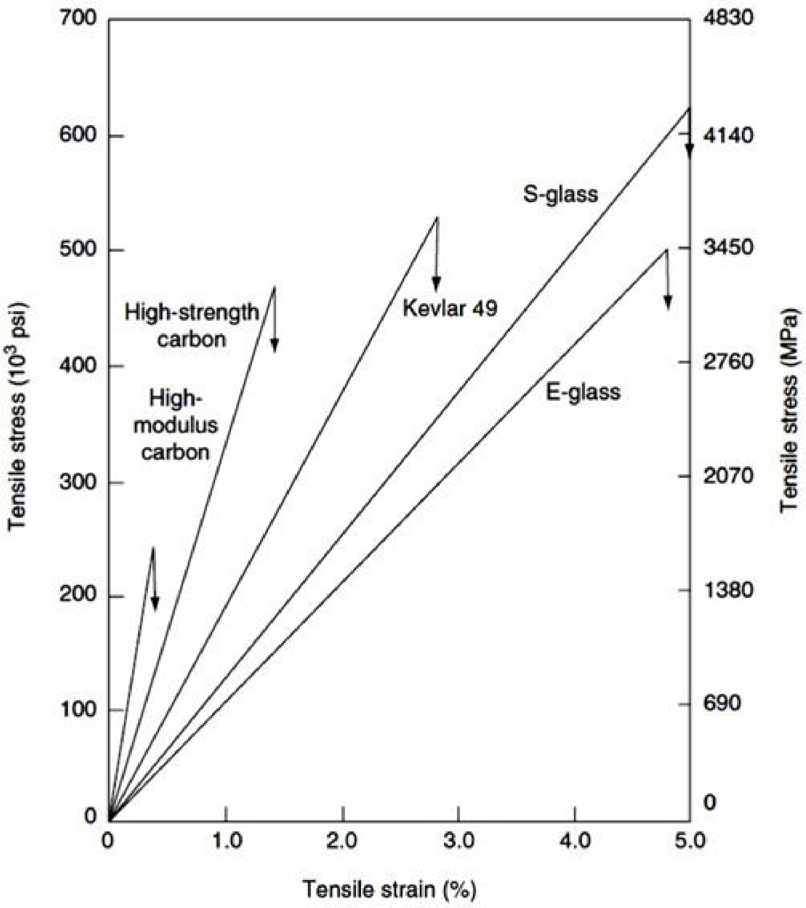

Figure 6 - Stress-strain curve for some typical fibers (Gotro, 2016)[13]

1.4.2 Semi-finished products

Common manufacturing techniques do not allow to arrange unprepared fibers according to the design schematic. That is why different semi-finished products are available. The product is chosen accordingly to the manufacturing method. Also, the finite element model is affected by the chosen manufacturing method. Neither the mechanical behavior is uninfluenced by the manufacturing process.

[13] Gotro, "*Polymer Composites Part 3: Common Reinforcements Used in Composites"* on https://polymerinnovationblog.com, 2016, consulted on 02/27/2019

The simplest semi-finished product is the roving. It is used to produce filament winded components but is also used as base material for other products. The most common ones are e.g. unidirectional (UD) tapes or woven fabrics. Their advantage is the ease of their assembly, in fact the weaving prevents the alteration of the fiber direction. The main downside of the woven fabrics is the loss of strength caused by the undulation of the fibers. There are three main categories of woven fabrics, each one characterized by specific properties: plain weave, twill weave and satin weave.

Due to the strength and stiffness loss of woven fabrics, multidirectional tapes consisting of non-crimp fabrics were developed. The individual yearns of these fabrics are stitched together using small threads, up to 8 layers with different orientations.

The above-mentioned products are considered as long-fiber reinforcements. The other group is the short-fiber reinforcement. Fibers with a length below 50 mm are considered short fibers.

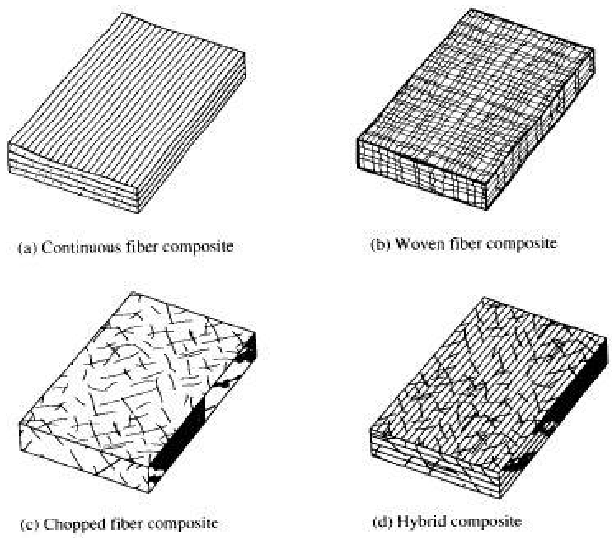

Figure 7 - Types of fiber-reinforced composites (Gibson, 2011)[14]

[14] Gibson, "*Principles of Composite Material Mechanics*", 2011

1.4.3 Matrix materials

In the context of a composite product, the matrix not only transfers the loads between the fibers, but also keeps the fibers in their position and supports them under a compressive load. It also joins the various layers and distribute the load between them. If a crack is started in a layer, the matrix can stop it from propagating to the other layers. The strength of the whole component under transverse or shear loading is basically defined by the matrix properties. Another important function of the matrix is to protect the fibers from the external environment. The plastic materials which satisfy these requirements are mainly thermosets and thermoplastics.

1.4.3.1 Thermosets

Thermosets solidify thanks to a chemical cross-linking process. After the curing process, all the cross-links are formed, and the thermoset polymers cannot be melted and reshaped. Therefore, welding of thermosets is impossible. The material features a low viscosity, ideal for the fiber wetting.

The major limit of thermosets is the long manufacturing time. As already mentioned, this is the main limiting factor which prevents industries such as the automotive one, to adopt them for manufacturing composite components for passenger vehicles. Other drawbacks are the low failure strain and impact strength.

One parameter which is of fundamental importance for thermosets plastic is the Glass Transition Temperature: it defines the dimensional stability under heat.

Most popular thermosets for fiber composites are epoxy and polyester resins.

1.4.3.2 Thermoplastics

Thermoplastics can offer some advantages over thermosets, mainly due to their ductility and larger failure strain. Their manufacturing time is low, which makes the production of the composite cheaper. In addition to that, the handling of thermoplastics is easier and a post thermoforming after initial manufacturing is allowed. They have a high melting temperature, though, which makes nearly impossible the pre-impregnation for the manufacturing of semi-finished products.

The most diffused thermoplastic materials for composite structures are polypropylene (PP), polyethylene tetraphtalate (PET) and polyamide (PA).

1.5 Mechanics of laminates

In this paragraph a small overview over the mechanics of a single lamina as well as of the whole laminate is presented. A lot of peculiar phenomena arise due to the special characteristics of the material, and the understanding of these phenomena is of crucial importance to understand the following work.

1.5.1 Notation and adopted conventions

A lamina (single ply or layer) consists of fibers within a matrix. The fiber direction (longitudinal) is defined as the local or material 1-direction of the lamina. Therefore the 2-direction will be the transverse direction of the ply and the 3-direction represents the normal out-of-plane direction. In general, a composite component is made up of more than one lamina (Fig. 6). Usually several layers are stacked up with different directions (layup). To refer to a position in the laminate, the global x-y-z coordinate system is used.

The convention used to show the stacking sequence prescribes to write the orientation of each ply within brackets. The written number corresponds to the angle between the 1-direction of that specific layer and the global x-direction. A positive angle is associated to a positive rotation and a negative angle to a negative one. If the subscript *S* is used at the end of a stacking sequence, that indicates that the laminate is symmetric about the x-y plane.

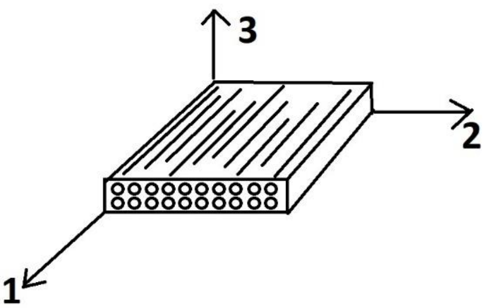

Figure 8 - Lamina with local coordinate system

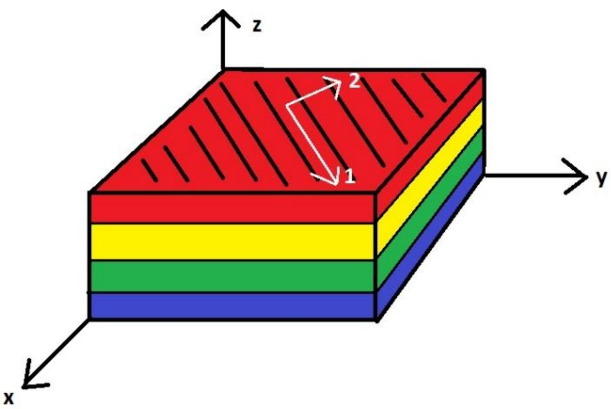

Figure 9 - Example of a 4 layers [A°,B°,C°,D°] stacking sequence of a laminate

1.5.2 Anisotropy of composites (Gibson, 2011)[15]

A lamina is considered as a homogeneous continuum with anisotropic material behavior. Considering a 3D-element, three normal stresses (σ_1, σ_2, σ_3) and six shear stresses (τ_{23}, τ_{32}, τ_{13}, τ_{31}, τ_{21}, τ_{12}) can be defined. Assuming a linear elastic behavior we can apply Hooke's Law which links the stresses and the strains through 81 coefficients. Applying the equilibrium equation, it is possible to demonstrate that $\tau_{23} = \tau_{32}$, $\tau_{13} = \tau_{31}$ and $\tau_{21} = \tau_{12}$ thus reducing the coefficients to 36.

[15] From Gibson, "*Principles of Composite Material Mechanics*", 2011

This configuration is defined as triclinic anisotropy. Through an energy-based approach, it is demonstrated that the stress and strain tensors are symmetric, which leads to a further reduction of the coefficients to 21.

$$\varepsilon_{ij} = C_{ijkl}\sigma_{kl}$$

Equation 1 - Hooke's Law

$$\begin{Bmatrix} \varepsilon_1 \\ \varepsilon_2 \\ \varepsilon_3 \\ \gamma_{23} \\ \gamma_{13} \\ \gamma_{12} \end{Bmatrix} = \begin{bmatrix} S_{11} & S_{12} & S_{13} & S_{14} & S_{15} & S_{16} \\ S_{21} & S_{22} & S_{23} & S_{24} & S_{25} & S_{26} \\ S_{31} & S_{32} & S_{33} & S_{34} & S_{35} & S_{36} \\ S_{41} & S_{42} & S_{43} & S_{44} & S_{45} & S_{46} \\ S_{51} & S_{52} & S_{53} & S_{54} & S_{55} & S_{56} \\ S_{61} & S_{62} & S_{63} & S_{64} & S_{56} & S_{66} \end{bmatrix} \begin{Bmatrix} \sigma_1 \\ \sigma_2 \\ \sigma_3 \\ \tau_{23} \\ \tau_{13} \\ \tau_{12} \end{Bmatrix}$$

Equation 2 – compliance matrix S in Voigt notation

If there is a symmetry plane in the element (monoclinic anisotropy), then the coefficients are further reduced to 9.

Whenever there are three perpendicular symmetry planes, the material behavior is defined as orthotropic. Only nine independent constants are present. In this case, the coupling between normal and shear strains vanishes. Only the coupling between longitudinal and transverse strain holds (see Equation 3).

$$\begin{Bmatrix} \varepsilon_1 \\ \varepsilon_2 \\ \varepsilon_3 \\ \gamma_{23} \\ \gamma_{13} \\ \gamma_{12} \end{Bmatrix} = \begin{bmatrix} S_{11} & S_{12} & S_{13} & 0 & 0 & 0 \\ S_{12} & S_{22} & S_{23} & 0 & 0 & 0 \\ S_{13} & S_{23} & S_{33} & 0 & 0 & 0 \\ 0 & 0 & 0 & S_{44} & 0 & 0 \\ 0 & 0 & 0 & 0 & S_{55} & 0 \\ 0 & 0 & 0 & 0 & 0 & S_{66} \end{bmatrix} \begin{Bmatrix} \sigma_1 \\ \sigma_2 \\ \sigma_3 \\ \tau_{23} \\ \tau_{13} \\ \tau_{12} \end{Bmatrix}$$

Equation 3

A UD lamina has the same transverse properties for every direction. It is possible, then, to draw an isotropic plane, which forms a specially orthotropic material behavior. Infinite perpendicular symmetry planes can be drawn. The isotropic plane is perpendicular to the fiber direction. This means that in every symmetry plane the material has the same properties. This assumption is correct until the fibers are homogeneously distributed in the matrix. The consequence is that some material coefficients become equal:

$$E_2 = E_3$$

$$G_{31} = G_{21}$$

$$\nu_{31} = \nu_{21}$$

Equation 4

According to the geometric relations for isotropic materials:

$$G_{23} = \frac{E_3}{2(1+\nu_{23})}$$

Equation 5

Due to the symmetry of the compliance matrix, this relationship is valid for the Poisson ratio:

$$\frac{E_1}{\nu_{21}} = \frac{E_2}{\nu_{12}}$$

Equation 6

This practically means that just one Poisson ratio has to be defined for a plane stress state. The resultant compliance matrix is:

$$\begin{Bmatrix} \varepsilon_1 \\ \varepsilon_2 \\ \varepsilon_3 \\ \gamma_{23} \\ \gamma_{13} \\ \gamma_{12} \end{Bmatrix} = \begin{bmatrix} S_{11} & S_{12} & S_{12} & 0 & 0 & 0 \\ S_{12} & S_{22} & S_{23} & 0 & 0 & 0 \\ S_{12} & S_{23} & S_{22} & 0 & 0 & 0 \\ 0 & 0 & 0 & S_{44} & 0 & 0 \\ 0 & 0 & 0 & 0 & S_{55} & 0 \\ 0 & 0 & 0 & 0 & 0 & S_{55} \end{bmatrix} \begin{Bmatrix} \sigma_1 \\ \sigma_2 \\ \sigma_3 \\ \tau_{23} \\ \tau_{13} \\ \tau_{12} \end{Bmatrix}$$

Equation 7

So, it is possible to calculate the stresses for a transversely isotropic material with equation 8:

$$\begin{Bmatrix} \sigma_1 \\ \sigma_2 \\ \sigma_3 \\ \tau_{23} \\ \tau_{13} \\ \tau_{12} \end{Bmatrix} = \begin{bmatrix} C_{11} & C_{12} & C_{12} & 0 & 0 & 0 \\ C_{12} & C_{22} & C_{23} & 0 & 0 & 0 \\ C_{12} & C_{23} & C_{22} & 0 & 0 & 0 \\ 0 & 0 & 0 & C_{44} & 0 & 0 \\ 0 & 0 & 0 & 0 & C_{55} & 0 \\ 0 & 0 & 0 & 0 & 0 & C_{55} \end{bmatrix} \begin{Bmatrix} \varepsilon_1 \\ \varepsilon_2 \\ \varepsilon_3 \\ \gamma_{23} \\ \gamma_{13} \\ \gamma_{12} \end{Bmatrix}$$

Equation 8

1.5.2.1 Plane stress state

In a plane stress state, the third, fourth and fifth row of the matrix equation 8 become trivial because $\sigma_3 = \tau_{13} = \tau_{23} = 0$. Row 1, 2 and 6 form the reduced compliance matrix of an orthotropic material under a plane stress state.

$$\begin{Bmatrix} \varepsilon_1 \\ \varepsilon_2 \\ \gamma_{12} \end{Bmatrix} = \begin{bmatrix} S_{11} & S_{12} & 0 \\ S_{21} & S_{22} & 0 \\ 0 & 0 & S_{66} \end{bmatrix} \begin{Bmatrix} \sigma_1 \\ \sigma_2 \\ \tau_{12} \end{Bmatrix}$$

Equation 9

It is possible to calculate the stress components from the in-plane strains from the following equation:

$$\begin{Bmatrix} \sigma_1 \\ \sigma_2 \\ \tau_{12} \end{Bmatrix} = \begin{bmatrix} Q_{11} & Q_{12} & 0 \\ Q_{21} & Q_{22} & 0 \\ 0 & 0 & Q_{66} \end{bmatrix} \begin{Bmatrix} \varepsilon_1 \\ \varepsilon_2 \\ \gamma_{12} \end{Bmatrix}$$

Equation 10 – Reduced stiffness matrix

Note that in general $\varepsilon_3 \neq 0$.

The above written equations for a plane stress state are the basis for the classical laminate theory.

1.5.3 Classical Lamination Theory (Gibson, 2011)[16]

Laminates are of a greater interest when considering the structural applications of composites. The Classical Lamination Theory allows to analyze nonsymmetric laminates with plies oriented in several directions, causing coupling effects, whose consequences may be complex combinations of extensional, flexural and torsional deformations. It also takes into account in-plane loading due to shear and axial forces and both bending and twisting moments. However, the biggest limitation of CLT is that for each ply is assumed a plane stress state and no interlaminar stress is considered.

Even if the laminate is made up of several laminae, it is assumed that each individual lamina is perfectly bonded to the others, having a behavior of a unitary, nonhomogeneous, anisotropic plate. Interfacial slip is not permitted, and the interfacial bonds are considered perfect and not deforming in shear. The consequence is that displacements across lamina interfaces are assumed to be continuous.

Defining the coordinate system as in the following figure:

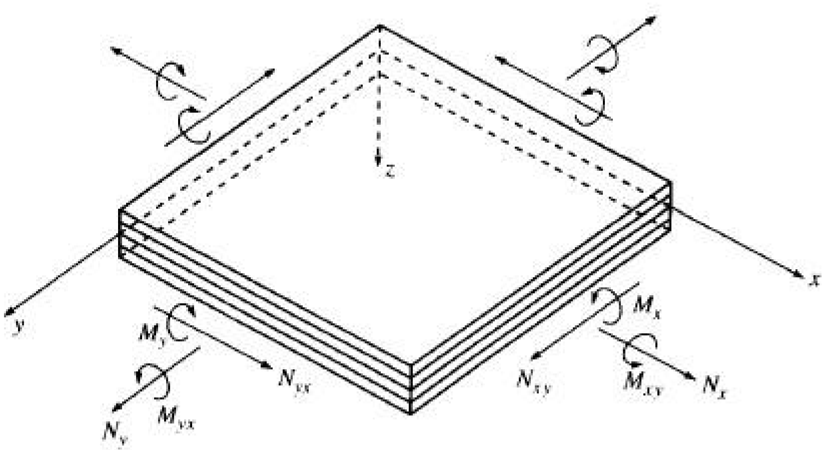

*Figure 10 - Coordinate system and stress resultants for laminated plate (from Gibson, "*Principles of Composite Material Mechanics*", 2011)*

[16] From Gibson, "*Principles of Composite Material Mechanics*", 2011

The *xyz* coordinate system has its origin on the middle surface of the plate, so that the middle surface lies in the *xy* plane. The displacements at one point (*x*,*y*,*z*) is (*u*,*v*,*w*). The basic assumptions of the Classical Lamination Theory are:

1. The plate consists of orthotropic laminae bonded together, with the principal material axes of the orthotropic laminae oriented along arbitrary directions with respect to the *xy* axes.
2. The thickness of the plate, *t*, is much smaller than the lengths along the plate edges, *a* and *b*.
3. The displacements *u*, *v*, *w* are small compared to the plate thickness.
4. The in-plane strains ϵ_x, ϵ_y and γ_{xy} are small compared with unity.
5. Transverse shear strains γ_{xz} and γ_{yz} are negligible.
6. Tangential displacements *u* and *v* are linear functions of the *z* coordinate.
7. The transverse normal strain ϵ_z is negligible.
8. Each play obeys Hooke's law.
9. The plate thickness *t* is constant.
10. Transverse shear stress τ_{xz} and τ_{yz} vanish on the plate surfaces defined by $z = \pm t/2$.

Assumption 5 is a consequence of assuming a plane stress in each ply, while assumptions 5 and 6 together define the Kirchoff deformation hypothesis for which normal to the middle surface remain straight and normal during the deformation. According to assumptions 6 and 7, the displacements can be written as:

$$
\begin{aligned}
u &= u^0(x,y) + zF_1(x,y) \\
v &= v^0(x,y) + zF_2(x,y) \\
w &= w^0(x,y) = w(x,y)
\end{aligned}
$$

Equations 11 - Displacements formulation

where u^0 and v^0 are the tangential displacements of the middle surface along the *x* and *y* directions. Due to the assumption 7, the transverse displacement at the middle surface, $w^0(x,y)$, is the same as the transverse displacement of any point having the same *x* and *y* coordinates.

Substituting the Equations 11 in the strain-displacement equations for the transverse shear strains and using assumption 5:

$$
\begin{aligned}
\gamma_{xz} &= \frac{\partial u}{\partial z} + \frac{\partial w}{\partial x} = F_1(x,y) + \frac{\partial w}{\partial x} = 0 \\
\gamma_{yz} &= \frac{\partial v}{\partial z} + \frac{\partial w}{\partial y} = F_2(x,y) + \frac{\partial w}{\partial y} = 0
\end{aligned}
$$

Equations 12

and:

$$F_1(x,y) = -\frac{\partial w}{\partial x} \quad F_2(x,y) = -\frac{\partial w}{\partial y}$$

Equation 13

Substituting the Equations 11 and 13 in the strain-displacement relations for the in-plane strains:

$$\epsilon_x = \frac{\partial u}{\partial x} = \epsilon_x^0 + z\kappa_x$$
$$\epsilon_y = \frac{\partial v}{\partial y} = \epsilon_y^0 + z\kappa_y$$
$$\gamma_{xy} = \frac{\partial u}{\partial y} + \frac{\partial v}{\partial x} = \gamma_{xy}^0 + z\kappa_{xy}$$

Equation 14

where the strains of the middle surface are:

$$\epsilon_x^0 = \frac{\partial u^0}{\partial x} \quad \epsilon_y^0 = \frac{\partial v^0}{\partial y} \quad \gamma_{xy}^0 = \frac{\partial u^0}{\partial y} + \frac{\partial v^0}{\partial x}$$

Equation 15

and the curvatures of the middle surface are:

$$\kappa_x = -\frac{\partial^2 w}{\partial x^2} \quad \kappa_y = -\frac{\partial^2 w}{\partial y^2} \quad \kappa_{xy} = -2\frac{\partial^2 w}{\partial x\,\partial y}$$

Equation 16

Therefore, it is possible to find the stresses along arbitrary *xy* axes in the *k*th lamina of a laminate by substituting equations 14 into the lamina stress-strain relationship:

$$\begin{Bmatrix} \sigma_x \\ \sigma_y \\ \tau_{xy} \end{Bmatrix}_k = \begin{bmatrix} \bar{Q}_{11} & \bar{Q}_{12} & \bar{Q}_{16} \\ \bar{Q}_{12} & \bar{Q}_{22} & \bar{Q}_{26} \\ \bar{Q}_{16} & \bar{Q}_{26} & \bar{Q}_{66} \end{bmatrix}_k = \begin{Bmatrix} \epsilon_x^0 + z\kappa_x \\ \epsilon_y^0 + z\kappa_y \\ \gamma_{xy}^0 + z\kappa_{xy} \end{Bmatrix}$$

Equation 17

where the subscript *k* refers to the *k*th lamina.

In the laminated plate analysis, it is convenient to use forces and moments per unit length rather than forces and moments. The forces and moments per unit length shown in Figure 10, are also referred to as stress resultants.

For example, the force per unit length, N_x, is:

$$N_x = \int_{-\frac{t}{2}}^{\frac{t}{2}} \sigma_x \, dz = \sum_{k=1}^{N} \left\{ \int_{z_{k-1}}^{z_k} (\sigma_x)_k \, dz \right\}$$

Equation 18

and the moment per unit length, M_x, is:

$$M_x = \int_{-\frac{t}{2}}^{\frac{t}{2}} \sigma_x z \, dz = \sum_{k=1}^{N} \left\{ \int_{z_{k-1}}^{z_k} (\sigma_x)_k \, z dz \right\}$$

Equation 19

where:

- t = laminate thickness
- $(\sigma_x)_k$ = stress in the *k*th lamina
- z_{k-1} = distance from middle surface to inner surface of the *k*th lamina
- z_k = corresponding distance from middle surface to outer surface of the *k*th lamina

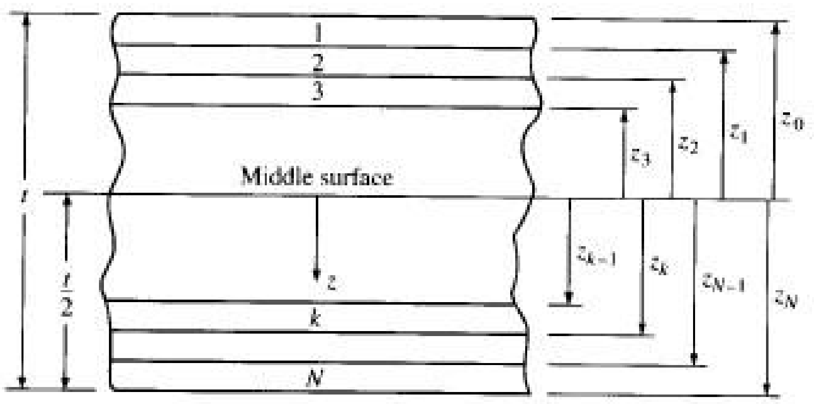

*Figure 11 – Laminated plate geometry and ply numbering system (from Gibson, "*Principles of Composite Material Mechanics*", 2011)*

Substituting the lamina stress-strain relationships from Equation 17 in Equations 18 and 19:

$$N_x = \sum_{k=1}^{N} \int_{z_{k-1}}^{z_k} \left\{ (\bar{Q}_{11})_k (\epsilon_x^0 + z\kappa_x) + (\bar{Q}_{12})_k \left(\epsilon_y^0 + z\kappa_y\right) + (\bar{Q}_{16})_k \left(\gamma_{xy}^0 + z\kappa_{xy}\right) \right\} dz$$

Equation 20

and:

$$M_x = \sum_{k=1}^{N} \int_{z_{k-1}}^{z_k} \left\{ (\bar{Q}_{11})_k (\epsilon_x^0 + z\kappa_x) + (\bar{Q}_{12})_k \left(\epsilon_y^0 + z\kappa_y\right) + (\bar{Q}_{16})_k \left(\gamma_{xy}^0 + z\kappa_{xy}\right) \right\} z\, dz$$

Equation 21

Combining terms and rearranging Equations 20 and 21:

$$N_x = A_{11}\epsilon_x^0 + A_{12}\epsilon_y^0 + A_{16}\gamma_{xy}^0 + B_{11}\kappa_x + B_{12}\kappa_y + B_{16}\kappa_{xy}$$

Equation 22

and

$$M_x = B_{11}\epsilon_x^0 + B_{12}\epsilon_y^0 + B_{16}\gamma_{xy}^0 + D_{11}\kappa_x + D_{12}\kappa_y + D_{16}\kappa_{xy}$$

Equation 23

where the laminate extensional stiffnesses are given by:

$$A_{ij} = \int_{-t/2}^{t/2} \left(\bar{Q}_{ij}\right)_k dz = \sum_{k=1}^{N} \left(\bar{Q}_{ij}\right)_k (z_k - z_{k-1})$$

Equation 24

the laminate coupling stiffnesses are given by:

$$B_{ij} = \int_{-t/2}^{t/2} (\bar{Q}_{ij})_k z \, dz = \frac{1}{2} \sum_{k=1}^{N} (\bar{Q}_{ij})_k (z_k^2 - z_{k-1}^2)$$

Equation 25

and the laminate bending stiffnesses are given by:

$$D_{ij} = \int_{-t/2}^{t/2} (\bar{Q}_{ij})_k z^2 \, dz = \frac{1}{3} \sum_{k=1}^{N} (\bar{Q}_{ij})_k (z_k^3 - z_{k-1}^3)$$

Equation 26

where the subscripts *i*, *j*= 1, 2 or 6. The other stress resultants can be written analogously, and the complete set of equations can be expressed in matrix form as:

$$\begin{Bmatrix} N_x \\ N_y \\ N_{xy} \\ M_x \\ M_y \\ M_{xy} \end{Bmatrix} = \begin{bmatrix} A_{11} & A_{12} & A_{16} & B_{11} & B_{12} & B_{16} \\ A_{12} & A_{22} & A_{26} & B_{12} & B_{22} & B_{26} \\ A_{16} & A_{26} & A_{66} & B_{16} & B_{26} & B_{66} \\ B_{11} & B_{12} & B_{16} & D_{11} & D_{12} & D_{16} \\ B_{12} & B_{22} & B_{26} & D_{12} & D_{22} & D_{26} \\ B_{16} & B_{26} & B_{66} & D_{16} & D_{26} & D_{66} \end{bmatrix} \begin{Bmatrix} \epsilon_x^0 \\ \epsilon_y^0 \\ \gamma_{xy}^0 \\ \kappa_x \\ \kappa_y \\ \kappa_{xy} \end{Bmatrix}$$

Equation 27

or in partitioned form as:

$$\begin{Bmatrix} N \\ M \end{Bmatrix} = \begin{bmatrix} A & B \\ B & D \end{bmatrix} \begin{Bmatrix} \epsilon^0 \\ \kappa \end{Bmatrix}$$

Equation 28

This clearly shows that there may be coupling effects at both lamina and laminate levels, but the two types are not necessarily related.

1.5.4 Interlaminar stresses

The key limitation of the CLT is the assumption of in-plane stress in the *xy* plane, and that interlaminar stresses associated with the *z* axis are neglected. These interlaminar stresses, however, can cause delamination.

A state of plane stress does exist in the laminae of a laminate in areas away from geometric discontinuities such as free edges. However, even in a laminate under simple uniaxial loading, there is a region along the free edges with a three-dimensional stress state.

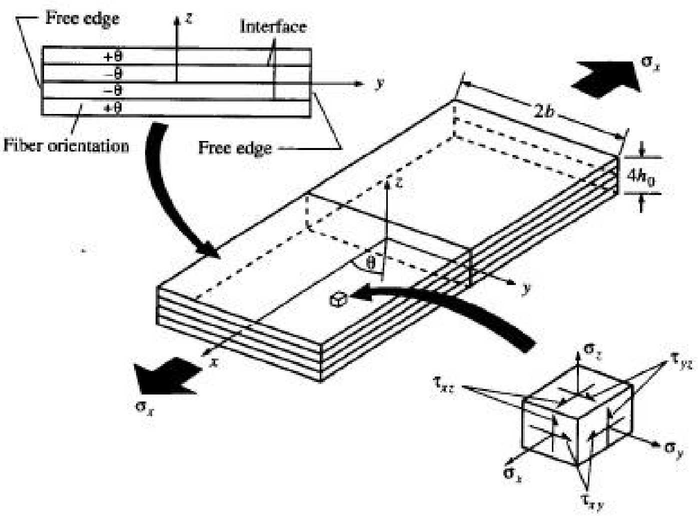

*Figure 12 - Pipes and Pagano model for analysis of interlaminar stresses in a laminate under uniaxial extension (from Gibson, "*Principles of Composite Material Mechanics*", 2011)*

Using the three stress equilibrium equations from the theory of elasticity:

$$\frac{\partial \sigma_x}{\partial x} + \frac{\partial \tau_{xy}}{\partial y} + \frac{\partial \tau_{xz}}{\partial z} = 0$$

Equation 29

$$\frac{\partial \tau_{yx}}{\partial x} + \frac{\partial \sigma_y}{\partial y} + \frac{\partial \tau_{yz}}{\partial z} = 0$$

Equation 30

$$\frac{\partial \tau_{zx}}{\partial x} + \frac{\partial \tau_{zy}}{\partial y} + \frac{\partial \sigma_z}{\partial z} = 0$$

Equation 31

For the uniaxially loaded laminate in Figure 12, considering a region near the free edges, where $y = \pm b$, and assuming that the stresses do not vary along the loading direction (x axis), then $\partial\sigma_x / \partial x = 0$ and from Equation 29, the interlaminar shear stress, $\tau_{xz}(z)$, is:

$$\tau_{xz}(z) = -\int_{-t/2}^{z} \frac{\partial \tau_{xy}}{\partial y}\, dz$$

Equation 32

Assuming that the in-plane stress, τ_{xy}, is constant in the interior region of the laminae, as we move along the y direction toward a free edge, τ_{xy} should decrease to zero at the stress-free surfaces where $y = \pm b$. It means that as $y \rightarrow \pm b$, $\partial\tau_{xy} / \partial y$ must increase. From Equation 32 it is clear that τ_{xz} must increase from zero in the interior region to a very large value as $y \rightarrow \pm b$.

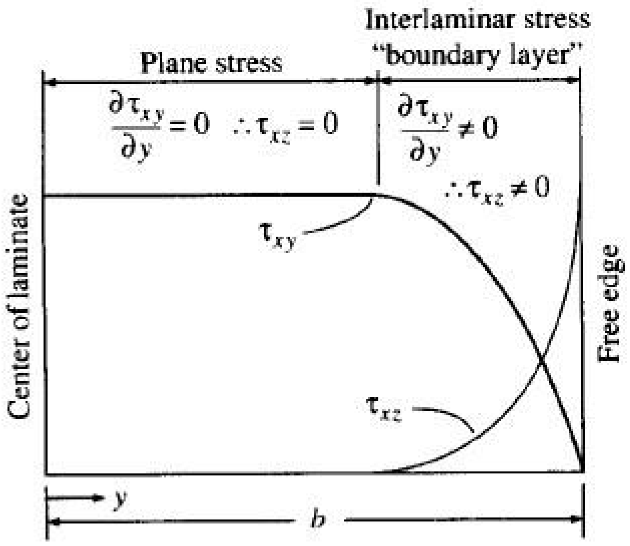

*Figure 13 - Schematic representation of in-plane shear stress and interlaminar shear stress distributions at ply interface (from Gibson, "*Principles of Composite Material Mechanics*", 2011)*

From Equations 30 and 31, the other interlaminar stresses are:

$$\tau_{yz}(z) = -\int_{-t/2}^{z} \frac{\partial \sigma_y}{\partial y}\, dz$$

Equation 33

$$\sigma_z(z) = -\int_{-t/2}^{z} \frac{\partial \tau_{yz}}{\partial y}\, dz$$

Equation 34

1.6 Failure of composites

In this paragraph the failure mechanisms and analysis approaches are analyzed. In order to understand the complex mechanisms of failure of laminates, the lamina fracture has to be clearly understood.

1.6.1 Lamina failure

FRP materials present many more failure modes than metals, and totally different ones. To be able to predict the failure of a composite component, it is mandatory to know which stress state causes which specific failure mode. Here a general overview of the failure mechanisms of fiber reinforced composites is given.

Crack initiation follows the same rules as in metals. The crack grows from material imperfections (e.g. broken fibers, debonding of matrix and fiber, micro-cracks, voids, inclusions and air bubbles). Other kinds of imperfections, especially for FRPs, can be the nonuniform distribution and the misalignment of fibers in the matrix (Ramesh & Singh, 2012)[17]. Because of the lower strength usually the cracks grow in the matrix material.

[17] Ramesh, Veer Singh, "*Damage and Failure of Composite Materials*", 2012

1.6.1.1 Fiber failure

The most catastrophic failure for FRPs is fiber failure. In fact, fibers are responsible for carrying the load in a laminate. Whenever a ply undergoes fiber failure, the whole component loses its load bearing capability. Every lamina has a certain amount of broken fibers, so the breakage of a single fiber is considered as an imperfection of the laminate. By fiber failure the breakage of many fibers is intended, thousands at the same time.

Three different fiber failure modes are listed:

- Fiber failure caused by longitudinal tension of the lamina
- Fiber micro buckling due to longitudinal compression
- Transverse fiber breakage (possible in theory, very unlikely in the reality)

1.6.1.2 Inter Fiber Failure

The strength of the matrix is much lower than the strength of the fibers. This means that cracks start to appear from the beginning of the load application to the laminate. Though, these cracks are not considered fatal, in fact the fibers in the load direction can still bear a high level of stress. These cracks in the matrix, anyway, lead to a continuous change of the laminate stiffness (i.e. it is subject to degradation).

1.6.1.3 Delamination

Unlike the previous failure modes, delamination occurs only in laminates. However, it has a very high affinity to the inter fiber failure.

The interface between the different laminas, constituted by the matrix, can be a weak link. Delamination is defined as the de-bonding of two or more laminas caused by a normal tension σ_3 or by an inter-laminar shear stress τ_{31} or τ_{32}. “Catastrophic failure of laminated structures is not the only undesirable result of delamination. The reduction in stiffness of a laminate during delamination growth may make the structure unsafe even if fracture does not occur". (Gibson, 2011)[18]

1.6.2 Failure criteria for a lamina

The design of a composite structure should prevent any irreversible damage under operational load. This is why the knowledge of the damage initiation mechanisms is fundamental. In the simple case of a single UD lamina under pure tension, the check of the maximum stress value of the component will provide enough information. The maximum stress criterion is enough to state whether or not the lamina will fail. Unfortunately, in real world components the stress state is much more complex: normal and shear stresses interact with each other and the maximum stress criterion is not anymore sufficient.

For metal materials this issue is addressed through the use of the Von Mises criterion, which allows to transform the 3D stress state in a single scalar, which is then compared to the tensile strength of the material.

However, this is not applicable to laminates. The anisotropic behavior makes impossible to define a single equivalent value. That is why in the past a lot of researchers have developed several failure criteria.

These are usually characterized by a certain ease of use. Most of them are second order elliptical equations using the strength values of the lamina to set the boundary conditions for the failure. A big drawback is the absence of the failure mode of the lamina, they just do not provide how the lamina will fail.

For a UD lamina, the five basic strengths parameters under in-plane loading are:

- $S_L^{(+)}$ = tensile strength in the fiber direction
- $S_L^{(-)}$ = compressive strength in the fiber direction

[18] From Gibson, "*Principles of Composite Material Mechanics*", 2011

- $S_T^{(+)}$ = tensile strength in the direction transverse to fibers
- $S_T^{(-)}$ = compressive strength in the direction transverse to fibers
- S_{LT} = shear strength

1.6.2.1 Maximum stress theory

According to this theory, a lamina fails if:

$$\sigma_1 = \begin{cases} S_L^{(+)} & \sigma_1 > 0, \\ S_L^{(-)} & \sigma_1 < 0, \end{cases}$$

$$\sigma_2 = \begin{cases} S_T^{(+)} & \sigma_2 > 0, \\ S_T^{(-)} & \sigma_2 < 0, \end{cases}$$

$$|\sigma_6| = S_{LT}.$$

Equation 35 - Maximum stress criterion

For combined loading, this criterion is not accurate because it does not consider stress interactions.

1.6.2.2 Maximum strain criterion

According to this criterion, failure occurs when:

$$\varepsilon_1 = \begin{cases} \epsilon_L^{(+)} & \varepsilon_1 > 0, \\ -\epsilon_L^{(-)} & \varepsilon_1 < 0, \end{cases}$$

$$\sigma_2 = \begin{cases} \epsilon_T^{(+)} & \varepsilon_2 > 0, \\ -\epsilon_T^{(-)} & \varepsilon_2 < 0, \end{cases}$$

$$|\varepsilon_6| = \epsilon_{LT}.$$

Where ε_i is the failure strain.

Equation 36 - Maximum strain criterion

1.6.2.3 Tsai-Hill criterion

This theory is based on the distortional failure theory of Von Mises. The stress is assumed to be plane in 1-2 plane, the material is assumed to be orthotropic and transversely isotropic.

$$\frac{\sigma_1^2}{S_L^2} - \frac{\sigma_1\sigma_2}{S_L^2} + \frac{\sigma_2^2}{S_T^2} + \frac{\tau_{12}^2}{S_{LT}^2} = 1$$

Where:

- S_L = longitudinal strength of the lamina
- S_T = transverse strength of the lamina
- S_{LT} = shear strength of the lamina

Equation 37 - Tsai-Hill criterion

1.6.2.4 Tsai-Wu criterion

This theory formulates a polynomial function of stress components. This is one of the most widely adopted criterion for laminae and it is based on the Hill theory.

$$F_i\sigma_i + F_{ij}\sigma_i\sigma_j = 1$$

Where:

- $i, j = 1, 2, \ldots, 6$
- F_i and F_{ij} are measured strengths

Equation 38 - Tsai-Wu criterion

1.6.2.5 Hashin criterion

The Hashin criterion takes into account both the matrix and the fiber failure. Compared to the previous criteria, this one, having four independent equations, is much more complex. Hashin formulated 3D failure criteria for UD composites in terms of quadratic stress polynomials. A UD composite is assumed to fail in one of four separate modes:

- Tensile fiber mode ($\sigma_1 > 0$)
- Compressive fiber mode ($\sigma_1 < 0$)
- Tensile matrix mode ($\sigma_2 + \sigma_3 > 0$)
- Compressive matrix mode ($\sigma_2 + \sigma_3 < 0$)

For a thin UD lamina, the equations are:

$$\left(\frac{\sigma_2}{S_L^{(+)}}\right)^2 + \left(\frac{\sigma_6}{S_{LT}}\right)^2 = 1, \qquad \sigma_1 > 0,$$

$$\sigma_1 = -S_L^{(-)}, \qquad \sigma_1 < 0,$$

$$\left(\frac{\sigma_2}{S_T^{(+)}}\right)^2 + \left(\frac{\sigma_6}{S_{LT}}\right)^2 = 1, \qquad \sigma_2 > 0,$$

$$\left(\frac{\sigma_2}{2S'_{LT}}\right)^2 + \left[\left(\frac{S_T^{(-)}}{2S'_{LT}}\right)^2 - 1\right]\frac{\sigma_2}{S_T^{(-)}} + \left(\frac{\sigma_6}{S_{LT}}\right)^2 = 1, \quad \sigma_2 < 0,$$

Where:

- S_{LT}' is the transverse shear strength

- S_{LT} is the axial shear strength

1.6.3 Laminate strength analysis

The described strength criteria can also be used on a ply-by-ply basis for a laminate for estimating which ply fails first under in-plane loads. However, it has been shown that interlaminar stresses in laminates must be taken into account because they may lead to a different failure mode: delamination.

1.6.3.1 First Ply Failure Due to In-Plane Stresses

This is a straightforward application of the appropriate multiaxial lamina strength criterion in combination with the lamina stress analysis from the CLT. The loads causing the first ply failure may anyway not be the laminate failure loads, since a laminate has, in general, plies in several orientations. This means that a sequence of ply failures will take place culminating eventually in the laminate failure when all plies have failed. Therefore, the ultimate load capacity of the laminate might be considerably larger than the first ply failure load.

Every time a ply fails, the stiffness matrix of the laminate must be modified.

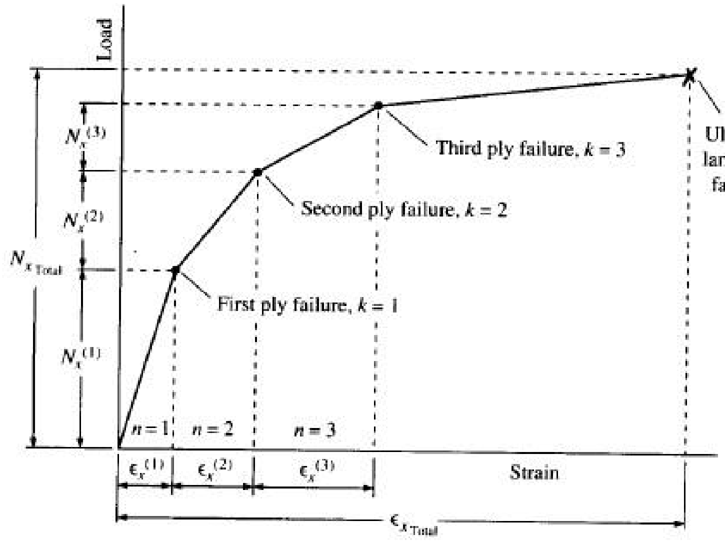

*Figure 14 – Load-strain curve for uniaxially loaded laminate showing multiple ply failures leading up to ultimate laminate failure (from Gibson, "*Principles of Composite Material Mechanics*", 2011)*

In Figure 14 is presented a load-deformation curve with several "knees" due to ply failures. The total forces and moments at the *k*th knee in the curve are related to the corresponding forces and moments for the *n*th section of such a curve (where $n \leq k$) by the summation:

$$\begin{Bmatrix} N \\ M \end{Bmatrix}_{Total} = \sum_{n-1}^{k} \begin{Bmatrix} N^{(n)} \\ M^{(n)} \end{Bmatrix}$$

Equation 39

where the superscript (*n*) on a parameter denotes the particular value of that parameter associated with the *n*th section. The corresponding midplane strains and curvatures are given by:

$$\begin{Bmatrix} \epsilon^{0} \\ \kappa \end{Bmatrix}_{Total} = \sum_{n=1}^{k} \begin{Bmatrix} \epsilon^{0(n)} \\ \kappa^{(n)} \end{Bmatrix}$$

Equation 40

It is possible to approximate the load-deformation relationship for the *n*th section:

$$\begin{Bmatrix} N^{(n)} \\ M^{(n)} \end{Bmatrix} = \begin{bmatrix} A^{(n)} & B^{(n)} \\ B^{(n)} & D^{(n)} \end{bmatrix} \begin{Bmatrix} \epsilon^{0(n)} \\ \kappa^{(n)} \end{Bmatrix}$$

Equation 41

where the $[A^{(n)}]$, $[B^{(n)}]$ and $[D^{(n)}]$ are the modified stiffness matrices after the (n - 1)th ply failure. To calculate these modified laminate stiffnesses it is required to know the modified ply stiffnesses, $[Q^{(n)}]$, and before to be able to modify the ply stiffness matrices, it is required to know the type of failure. This means that if the ply failure is caused by the in-plane shear stress exceeding the shear strength, the shear modulus and transverse modulus of that ply may be severely degraded by longitudinal cracks; but the longitudinal modulus may not be affected significantly by these cracks. To stay on the safe side, it is possible to equate to zero all the ply stiffnesses for the failed ply, during the calculation of the degraded laminate stiffnesses.

1.6.3.2 Delamination Due to Interlaminar Stresses

This kind of failure could reduce the failure stress of the laminate below the one predicted by the in-plane failure criteria. Failure by delamination is not always the same as the initiation of delamination, though. The initiation of delamination is generally followed by stable delamination growth, and eventually can result in an unstable growth and ultimate failure.

Catastrophic failure of laminated structures is not the only undesirable effect of delamination. The reduction in stiffness of a laminate during delamination growth can make the structure unsafe even if no crack is created. It is also true that stiffness loss can be used to evaluate the growth of delamination.

2. Literature review

This chapter is a small recap of the papers that have been collected before and during the thesis work to gather ideas and hints on how to proceed and which elements and parameters to keep in mind while developing the project.

Of course, the first considered paper has been the one published by the advisor itself: Koricho, Khomenko, Fristedt, Haq, "*Innovative tailored fiber placement technique for enhanced damage resistance in notched composite laminate*", 2014. This paper underlined the benefits of the use of TFA especially for notched composite laminates and it has been the basement from which the project has been further developed. The main and most important result was that a notched composite plate with TFA was performing in the range of 80-90% of the unnotched plate, while a drilled notched plate showed a significant reduction in the strength performance. From this evidence, the idea of the new project has been to implement this advantage into a "finished" product.

Another paper which gave a good hint for the success of the process has been Gliesche, Hubner, Orawetz, "*Application of the tailored fibre placement (TFP) process for a local reinforcement on an 'open-hole' tension plate from carbon/epoxy laminates*", 2002. This paper gives indication on how TFA stitched reinforcements can improve the resistance of a plate with drilled holes, and different configurations and shape of reinforcements are tested, showing advantages and disadvantages of each one.

The paper from Tosh, Kelly, "*On the design, manufacture and testing of trajectorial fibre steering for carbon fibre composite laminates*", 2000 has proved itself very interesting, especially because they have considered the stress trajectories and load-paths not only of a plate with a hole under tension, but also of pin-loaded plates, which is the load case that has been developed in the shackle project.

A similarly interesting paper is from Crothers, Drechsler, Feltin, Herszberg, Kruckenberg, "*Tailored fibre placement to minimise stress concentrations*", 1996, in which the authors have studied the different cases of open-hole plate under tension with and without reinforcement, the pin-loaded plate and the 2-bolts loaded strut. Though the content has been useful to understand the importance of the fiber orientation, it has not been straight-forward applicable to the project because at that time the authors did not have the zig-zag stitching technology.

For what concerns the reinforcements, another paper that has been consulted is Zhu, Qin, Qi, Xu, Liu, Yan, "*Variable Angle Tow reinforcement design for locally reinforcing an openhole composite plate*", 2018 in which the different stitched reinforcements have been evaluated in the application to a base layup.

Finally, a paper from Khaliulin, Khilov, Toroptsova, "*Prospects of Applying the Tailored Fiber Placement (TFP) Technology for Manufacture of Composite Aircraft Parts*", 2014 has been used for its interesting content in terms of manufacturing and market applicability of the TFA technique.

Some other papers have been consulted and their content, even if maybe not directly applicable, has given a good point of view on topics which are anyway close to the one developed in this thesis. Here is a list of all the papers collected in the literature gathering step at the beginning of the project:

- Kiyono, Silva, Reddy, "*A novel fiber optimization method based on normal distribution function with continuously varying fiber path*", 2016;
- Gliesche, Hubner, Orawetz, "*Application of the tailored fibre placement (TFP) process for a local reinforcement on an 'open-hole' tension plate from carbon/epoxy laminates"*, 2002;
- Rettenwander, Fischlschweiger, Steinbichler, "*Computational structural tailoring of continuous fibre reinforced polymer matrix composites by hybridisation of principal stress and thickness optimization"*, 2013;
- Botzkowski, Galkin, Wagner, Sikora, Karger, "*Experimental and numerical analysis of bolt-loaded open-hole laminates reinforced by winded carbon rovings*", 2016;
- Leipprand, Bittrich, Spickenheuer, Heinrich, *"Experimental and Numerical Analysis of Material Properties of Unidirectional Composites Manufactured by Tailored Fiber Placement*", 2014;
- Uhlig, Tosch, Bittrich, Leipprand, Dey, Spickenheuer, Heinrich, "*Meso-scaled finite element analysis of fiber reinforced plastics made by Tailored Fiber Placement*", 2016;
- Tosh, Kelly, "*On the design, manufacture and testing of trajectorial fibre steering for carbon fibre composite laminates*", 2000;
- Wallin, Saarela, Law, Liehu, "*RTM Composite Lugs for High Load Transfer Applications*", 2006;
- Crothers, Drechsler, Feltin, Herszberg, Kruckenberg, "*Tailored fibre placement to minimise stress concentrations*", 1996;

- Rettenwander, Fischlschweiger, Machado, Steinbichler, "*Major Tailored patch placement on a base load carrying laminate: A computational structural optimisation with experimental validation*", 2014;
- Lopes, Gurdhal, Camanho, "*Tailoring for strength of composite steered-fibre panels with cutouts*", 2010;
- Spickenheuer, Schulz, Gliesche, Heinrich, "*Using tailored fibre placement technology for stress adapted design of composite structures*", 2008;
- Zhu, Qin, Qi, Xu, Liu, Yan, "*Variable Angle Tow reinforcement design for locally reinforcing an openhole composite plate*", 2018;
- Richther, Uhlig, Spickenheuer, Bittrich, Mader, Heinrich, "*Thermoplastic composite parts based on online spun commingled hybrid yarns with continuous curvilinear fibre patterns*", 2014;
- Wallin, Saarela, Pento, "Load Response and Failure of Thick RTM Composite Lugs", 2002;
- Khaliulin, Khilov, Toroptsova, "*Prospects of Applying the Tailored Fiber Placement (TFP) Technology for Manufacture of Composite Aircraft Parts*", 2014;
- Tatting, Gürdal, "*Automated Finite Element Analysis of Elastically-Tailored Plates*", 2003;
- Pejhan, Kuznetcov, Wang, Wu, Telichev, "*Design assessment of a multiple passenger vehicle component using load transfer index (U*) method*", 2017.

3. Product specifications and target values

The initial idea was to develop a real component, from a real vehicle, to have a direct comparison between a standard steel shackle and the newly designed composite one. Unfortunately, for Export Control reasons, which forbid non-US citizens to design finished products as an outcome of their research work, it was decided to design a pseudo-finished shackle. This means that the composite shackle coming out of this process is a plausible component, with realistic dimensions and load ratings, but it is not an actual or potential substitute for a steel shackle fitted in any current production vehicle.

In fact, the 2018 Toyota Tundra steel shackle was taken as a geometrical reference. This means that the steel thickness of .25” and the distance between the centers of the holes of 6” are coming from that particular model. As far as the load rating, the rear axle capacity of 4800 lbs. of the 2019 Ford F-150 has been considered. There has been no particular criterion in choosing which models to take as a reference, besides popularity and availability of technical data.

Since there are two leaf springs in the rear axle, and each one of them has a shackle assembly, which is made of two shackle plates working together, each shackle should bear a static load of:

$$\frac{4800\ lbs.}{6} = 600\ lbs. = 272.16\ kg \rightarrow 2669.84\ N$$

To summarize, the given data and constraints for the design were:

- center-to-center distance between the holes: 6”;
- static load rating of a single shackle plate: ~2.7 kN.

A so-called “boomerang” shape was chosen for the shackle plate to simulate the need of avoiding other imaginary suspension and chassis components. Though it is true that for the applied load to the component, a rectangular shape is the most obvious and recommended, this shape allows to demonstrate the capabilities of the TFA technique to lay and stitch the fibers following the exact desired orientation given as an input from the designer. It is also true that as it will be demonstrated in the next chapters, this shape has undermined the strength performance of the component in a critical way.

4. CAD model design

Once the geometric constraints were decided, the CAD model has been created using the commercially available software SolidWorks 2018. The model was created with a thickness of .25”, following the thickness of the reference steel one.

The radius around the holes has been set at 1”, and therefore the inner and outer radii of the “boomerang” shape were defined.

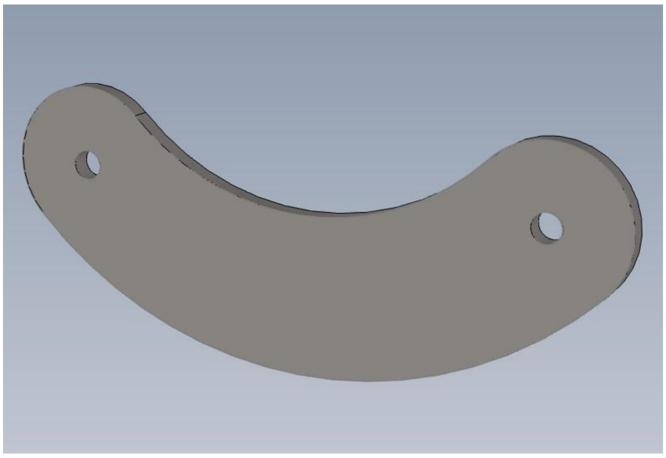

Figure 15 - Shackle CAD model

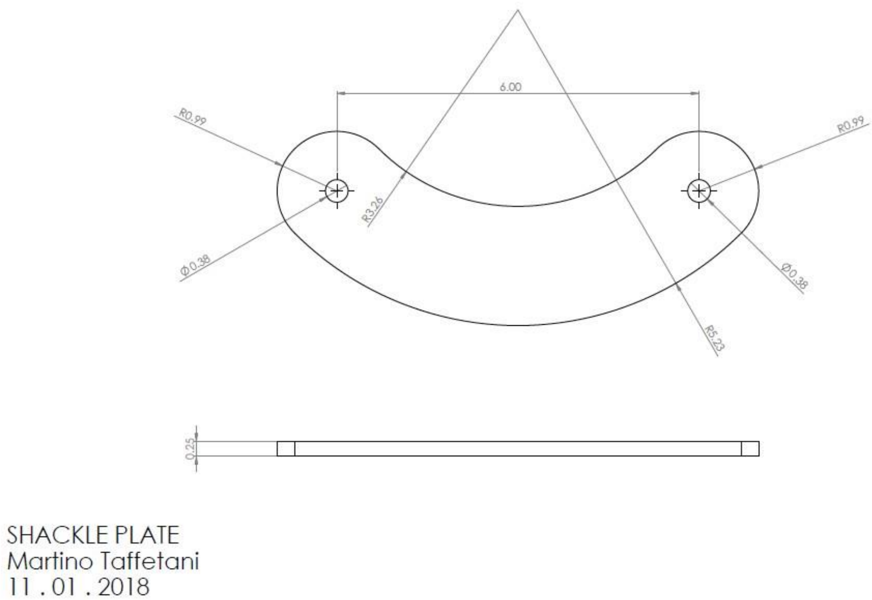

Figure 16 - Shackle CAD drawing

5. Preliminary Finite Element Analysis

At the beginning, a Finite Element Analysis has been set up to understand how the loads were transferred within the component. In this chapter a brief overview of the analysis is presented.

5.1 Input data

The CAD model of the shackle has been imported in the Abaqus CAE environment. It has been defined as a 3D, deformable shell part. The set material was steel, so to have an isotropic behavior and to understand the load-paths distribution without any "filter" from the use of a non-homogeneous material.

Material	Steel
Young's Modulus, E	210 GPa
Poisson's ratio, ν	0.3

Table 2 - Material data

A section property with the desired thickness of .25" was generated and linked to a section, which has been applied to the whole part geometry.

5.2 Mesh

The mesh of the component was created paying attention to have finer elements in the region alongside the holes, where the loads and constraints were going to be applied. S4R elements are 4-node general-purpose shell elements, reduced integration with hourglass control, designed for finite membrane strains.

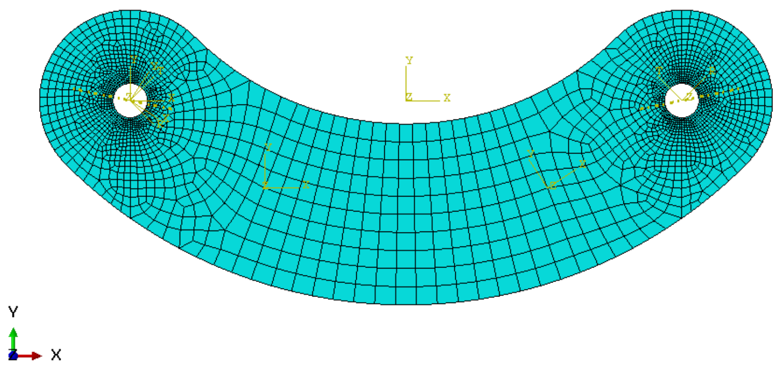

Figure 17 - Part mesh

5.3 Loads and constraints

The model has been setup to work under a tension load. The load is applied through a bolt in one hole, while the other hole is constrained by a fixed bolt. To simulate this condition the conditions have been applied to the external semi-circumferences of the two holes.

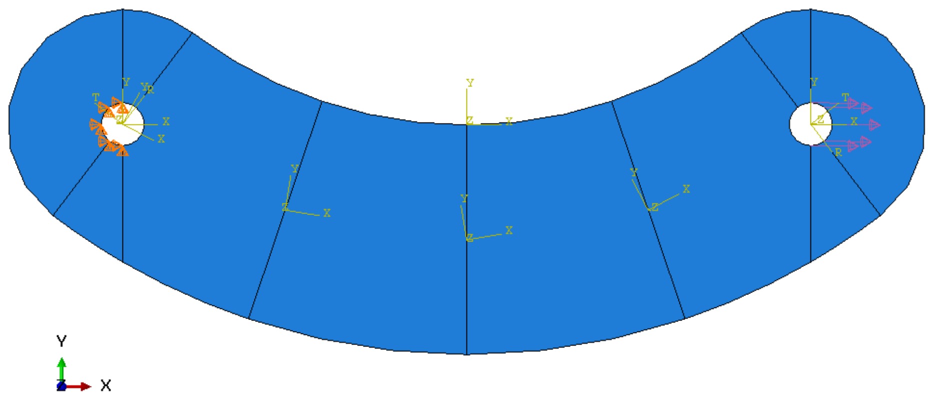

Figure 18 - Constraints and loads on the part

5.4 Results of the analysis

The analysis output has allowed to evaluate how the stresses are distributed along the component. The load-paths have been identified through the detailed analysis of the maximum principal stress tensor.

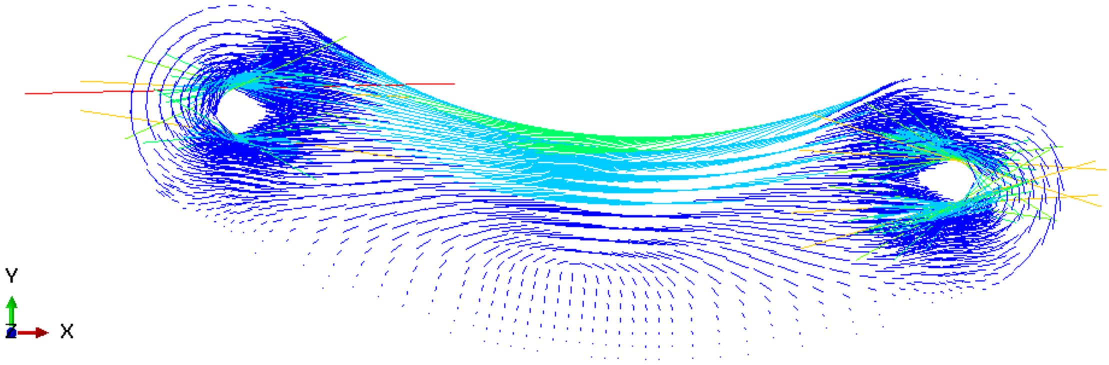

Figure 19 - Maximum principal stress tensor of deformed shape

The direction and magnitude of the vectors have been used as an indication of how to place the fiber rovings.

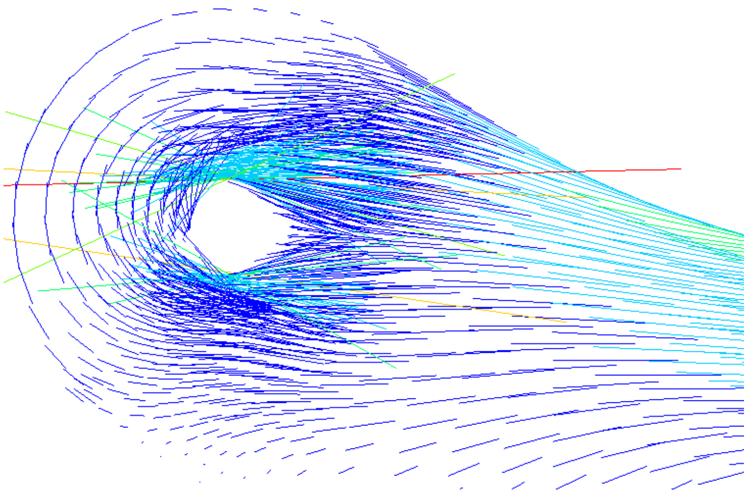

Figure 20 - Detail of maximum principal stress tensor around fixed hole

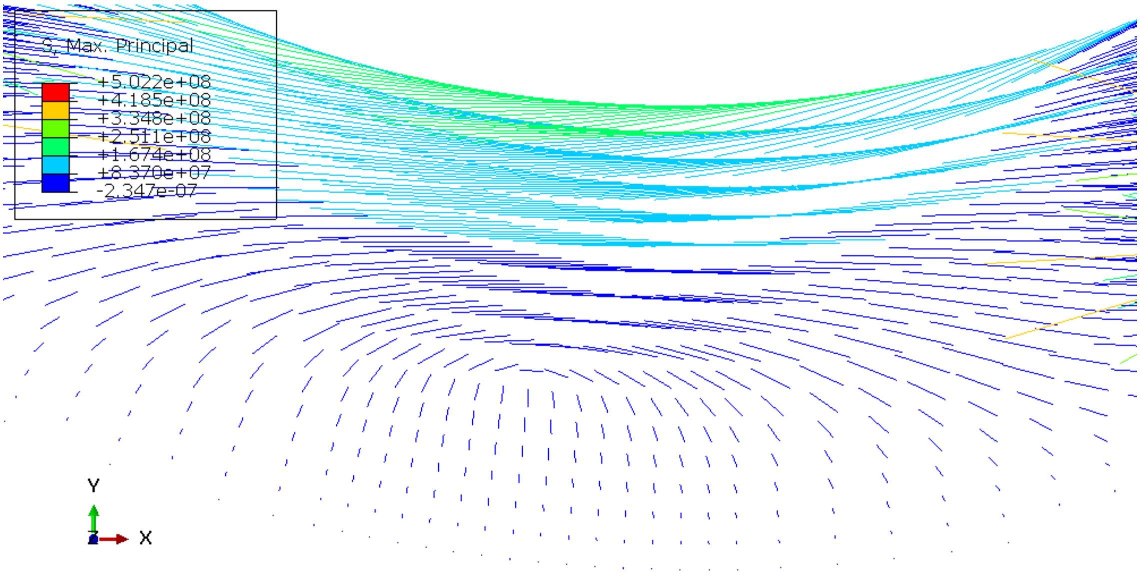

Figure 21 - Detail of maximum principal stress tensor in the middle section of the shackle

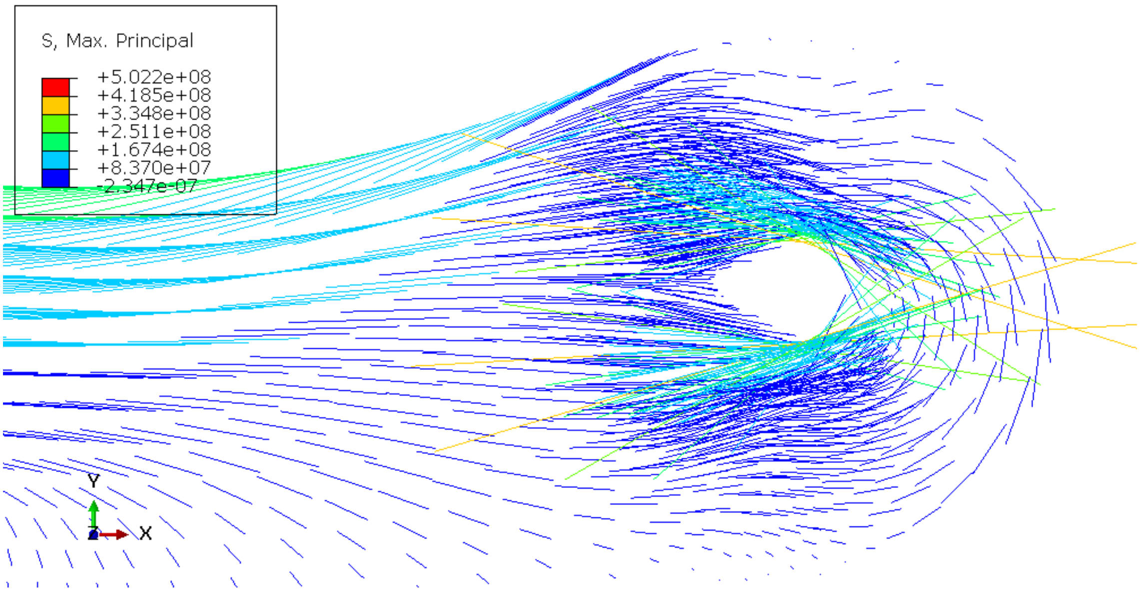

Figure 22 - Detail of maximum principal stress tensor around the loaded hole

In figures 20, 21 and 22, it is interesting to see how the loads are concentrated on the inner side of the curved middle section of the component, going in a direction as straight as possible from one hole to the other (the areas of application of external loads and constraints).

5.5 Net-shape definition

From the tensor plot analysis, it is also evident how some areas, in particular those in the lower, external curved side, are less loaded. This fact has suggested to further increase the possibility of material and weight saving in the component, by defining a 'net-shape' part. With this term, it is intended a part whose shape is designed upon considerations based on the material efficiency criterion and the directions of the load-paths across the component.

To realize this concept, the contour plot of the maximum principal stress tensor has been gradually filtered-out, by eliminating the parts whose stress was less than a threshold value.

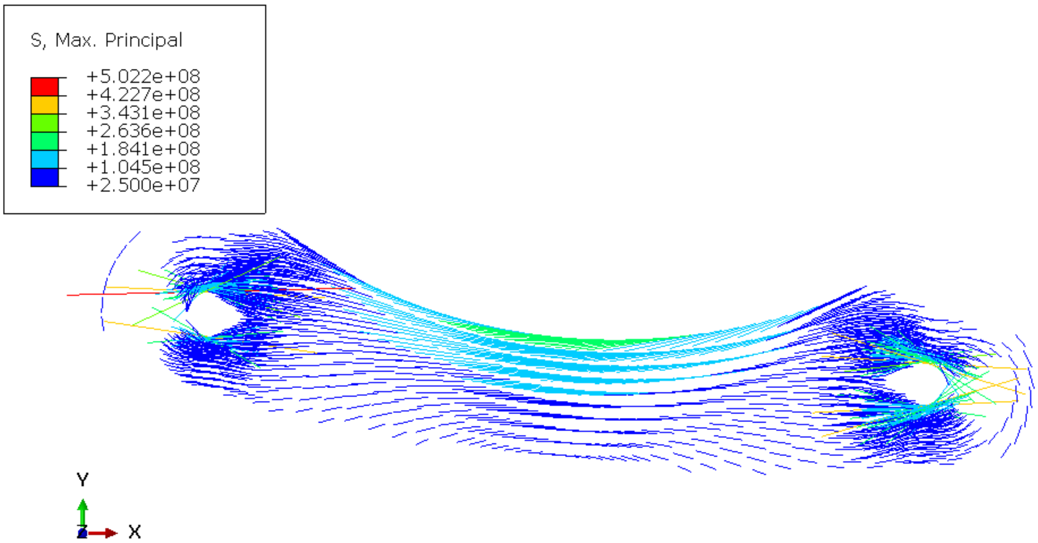

Figure 23 - Maximum principal stress tensor plot of elements above 25 MPa

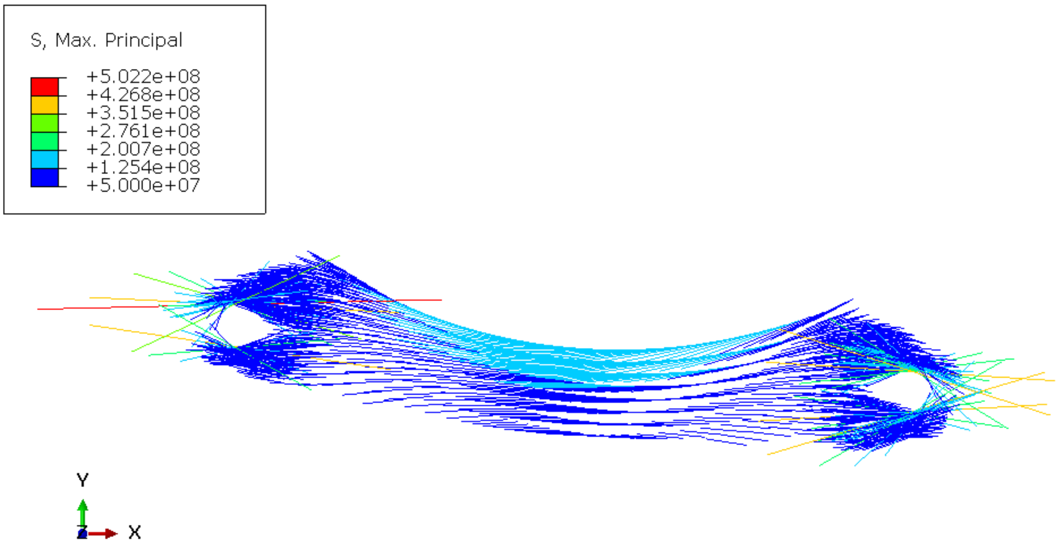

Figure 24 - Maximum principal stress tensor plot of elements above 50 MPa

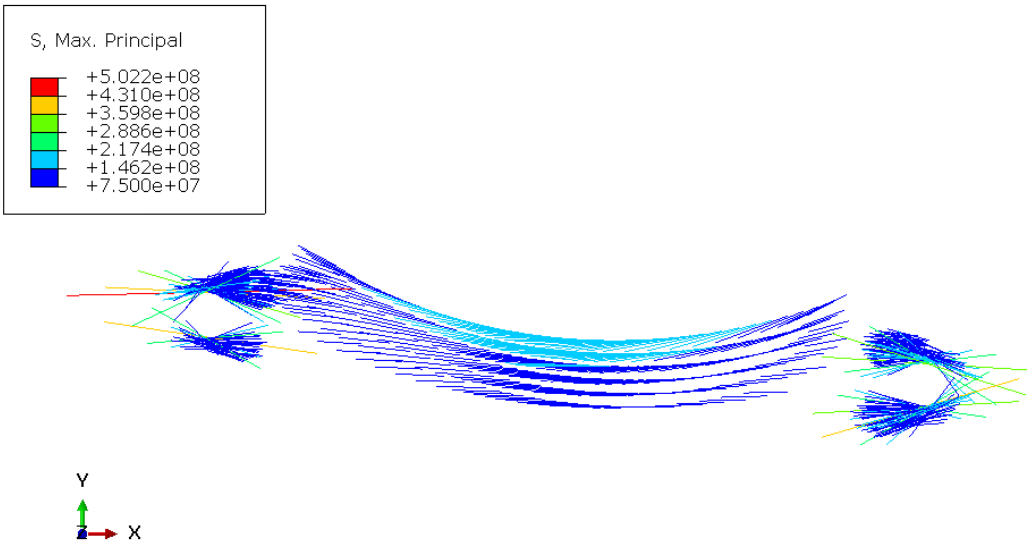

Figure 25 - Maximum principal stress tensor plot of elements above 75 MPa

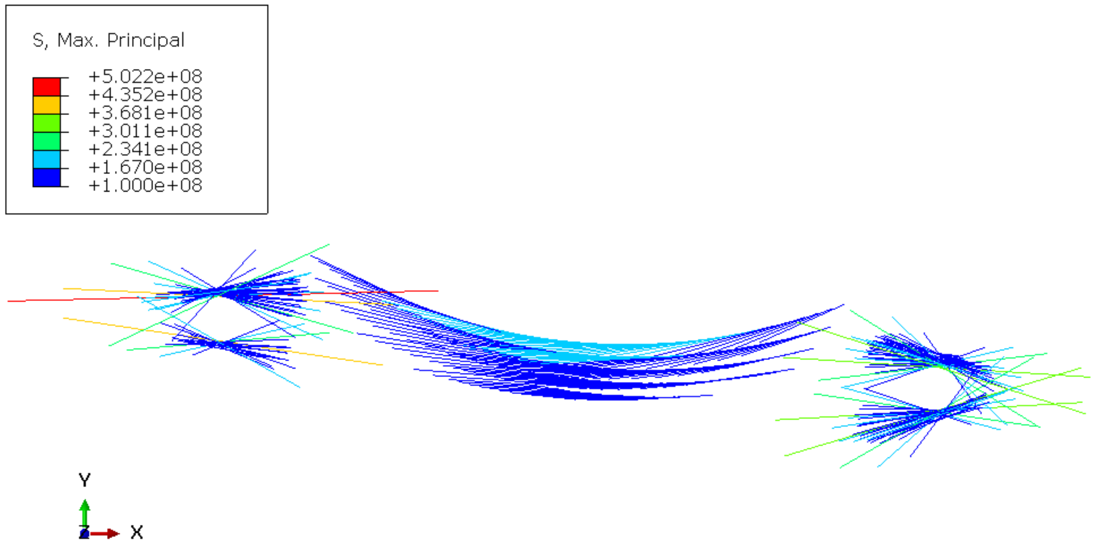

Figure 26 - Maximum principal stress tensor plot of elements above 100 MPa

This evaluation has given proof of the effectiveness of this criterion to select only significative elements. However, it could only be considered in a qualitative way, in fact the FE model was based on a steel component.

To have a closer representation of the actual composite model, with fibers laid down using the TFA method, another FE model has been developed in Abaqus. This model had the same geometry as the previous one and was using the same S4R elements for the mesh.

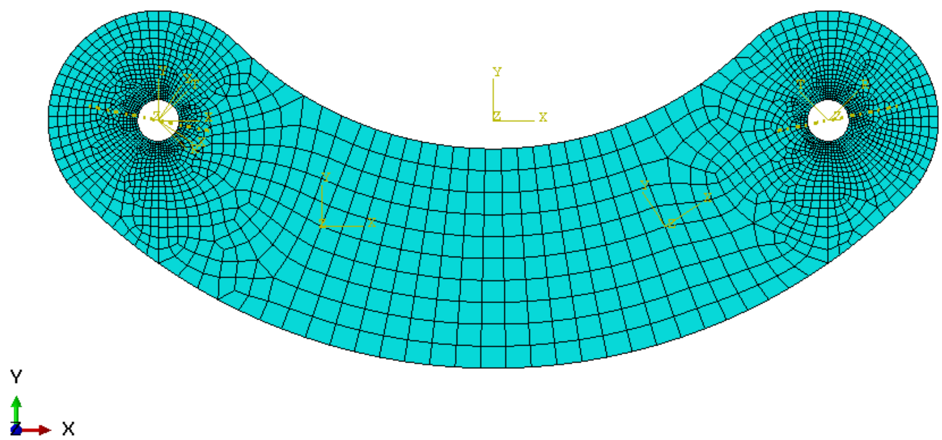

Figure 27 - Mesh of the FE model

The difference was in the specified material, in this case carbon fibers within an epoxy matrix. The material data have been set from previous experimental data and recommended values. The material has been defined through the engineering constants:

Engineering constant	Value
E_1	287 GPa
E_2	7.75 GPa
E_3	7.75 GPa
ν_{12}	0.3
ν_{13}	0.01
ν_{23}	0.55
G_{12}	5 GPa
G_{23}	3 GPa
G_{13}	5 GPa

Table 3 - Stitched fibers preliminary material data

Moreover, to be consistent with the Tailored Fiber orientation, the shell surface has been partitioned in 5 different sections, each one with its particular material orientation. In the areas around the holes, a circular reference system has been created so that the fibers follow the stitching pattern. In the areas of the main middle section of the shackle 3 different sections have been defined to discretize the continuous fiber stitching pattern, but to obtain a similar material orientation overall.

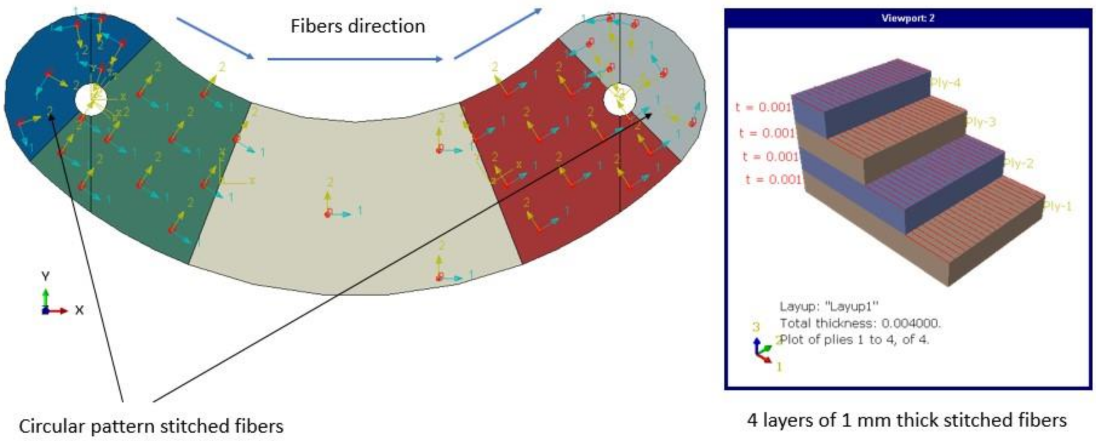

Figure 28 - Material orientations in the new FE model (left) and layup schematic (right)

In the left box of Figure 28 it is possible to see how the layup have been defined: 4 layers of fibers, each one having a thickness of 1 mm. This choice has been made considering the experimental results obtained during the first tests with the stitching machine. In fact, the available fiber tow had a 1 mm thickness and not more than 2 layers could be stitched one on top of the others. Considering the possibility of curing together 2 double-layer layers, one on top of the other, a maximum of 4 layers have been considered the best option to evaluate.

The results of this analysis showed a similar output as the previous one:

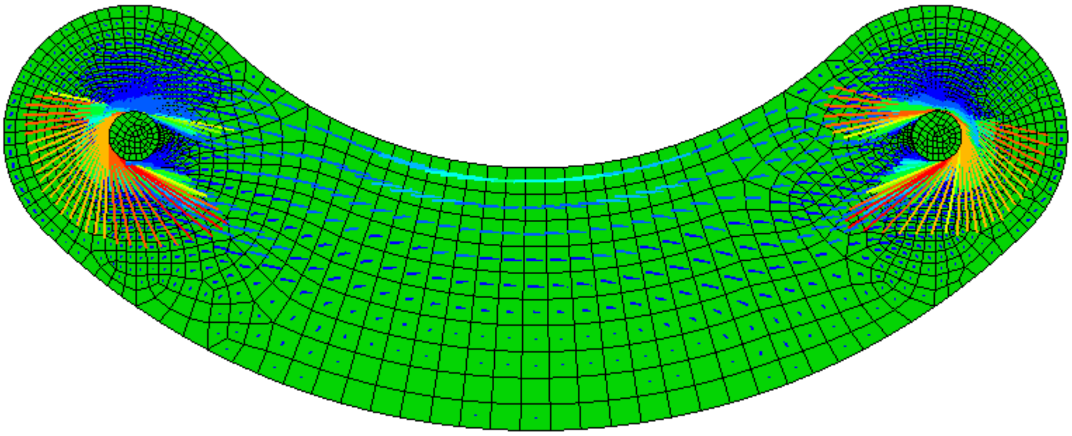

Figure 29 – Maximum principal stress tensor contour plot on the undeformed shackle

Plotting the elements has allowed to individuate and eliminate all the ones whose stress value was below 10 MPa:

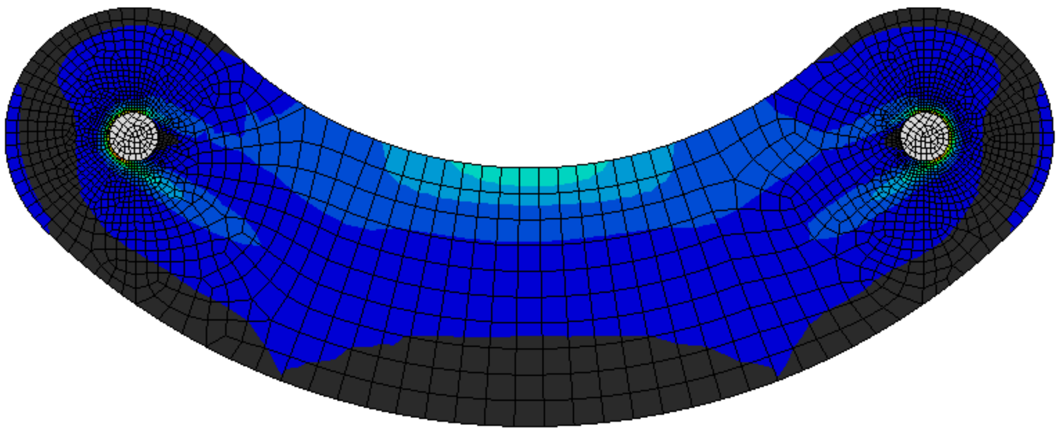

Figure 30 - Maximum principal stress plot with blackened areas below 10 MPa

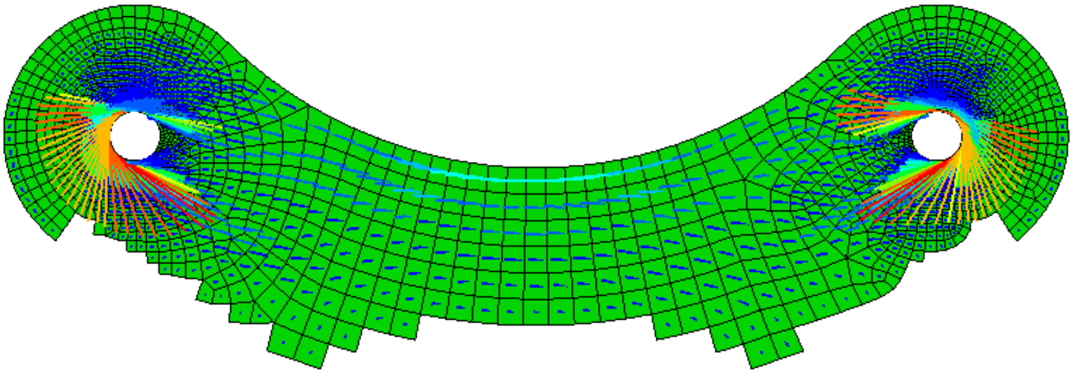

Figure 31 - Shackle model with no elements below 10 MPa

In this way, a net-shape was identified and defined applying not only plausible material properties, but also implementing the material orientation parameter, which was not considered in the very first model with the steel shackle.

6. Stitching process

After having defined both the 'reference' shape and the net-shape of the shackle, the next step has been the stitching of the fibers using the stitching machine available in the Composite Vehicle Research Center at the Michigan State University.

The process consists in:

1. Drawing the stitching pattern in AutoCAD;
2. Transferring the AutoCAD file to the laboratory laptop where the EDO Path software is installed;
3. Converting the AutoCAD .dxf drawing into a .edop file which can be read from the LayStitch machine;
4. Transferring the file from the laboratory laptop to the machine memory;
5. Setup of machine parameters;
6. Stitching.

6.1 Stitching pattern definition

The stitching pattern has been defined in a qualitative way. Even if the Polymerforschung Dresden has developed innovative advanced software (SpinCOM and AOPS, Advanced Optimization of Primary Stress) (Richter, et al., 2014)[19] which should automatically define the optimal stitching pattern based on the stresses' analysis, their cost has prevented their usage in this process. This led to the qualitative method of converting the results and considerations from the FEA to a stitching pattern. The adopted method consisted in the progressive off-set of the shape of the reference shape:

[19] Richter, Uhlig, Spickenheuer, Bittrich, Mäder, Heinrich, "THERMOPLASTIC COMPOSITE PARTS BASED ON ONLINE SPUN COMMINGLED HYBRID YARNS WITH CONTINUOUS CURVILINEAR FIBRE PATTERNS", 2014

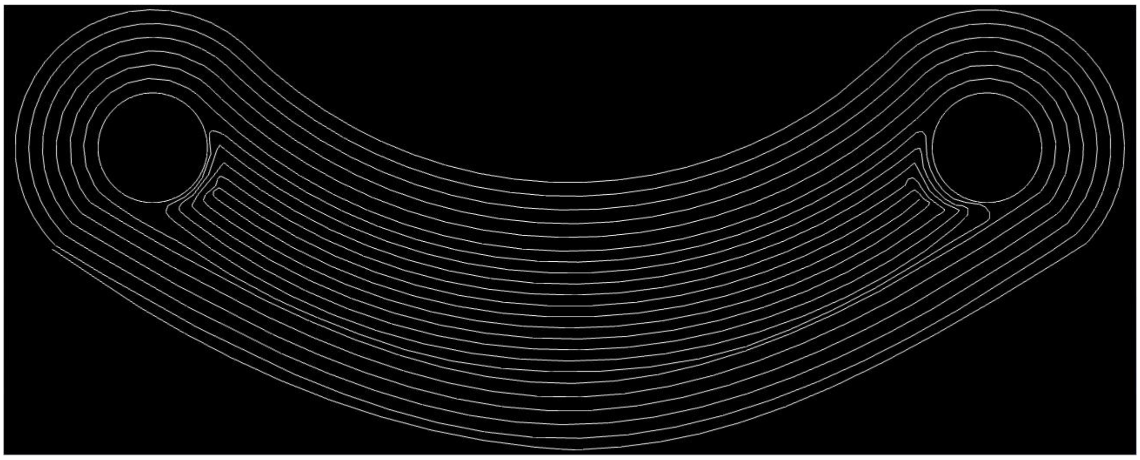

Figure 32 - Stitching pattern of the reference shape shackle

In Figure 32 it is possible to see the AutoCAD .dxf drawing. The white line represents the path that will be followed by the stitching head. The path is requested to be a single continuous line, though there are two additional independent lines, which are the two circles around the holes; those have been added to create a reinforcement around the holes and to help redistribute the stresses. Spacing between one row and the other has been a critical parameter; in fact, considering a 1 mm width of the fiber tow, the minimum spacing has to be 1 mm, but experimental testing with the stitching machine has shown that a slightly larger spacing allows a better allocation of the fibers. It is evident from Figure 32 that the central area stitching, where the line is not passing anymore around the holes, it is going to be a weak spot in the structural strength of the component, in fact the tension load is going to be locally converted in a transversal load in the area right between the hole and the middle section. The consequence is that the E_2 stiffness module will be the important one, due to the fact that the fibers are aligned exactly in the perpendicular direction of the load-paths. This is totally in contrast with the purpose of the project, however in the short time of the project it has been impossible to find a better alternative for this shape. One of the crucial issues to be solved in the future will be the positioning of the fibers.

The net-shape shackle had to be stitched, so an AutoCAD drawing has been designed also for it, too.

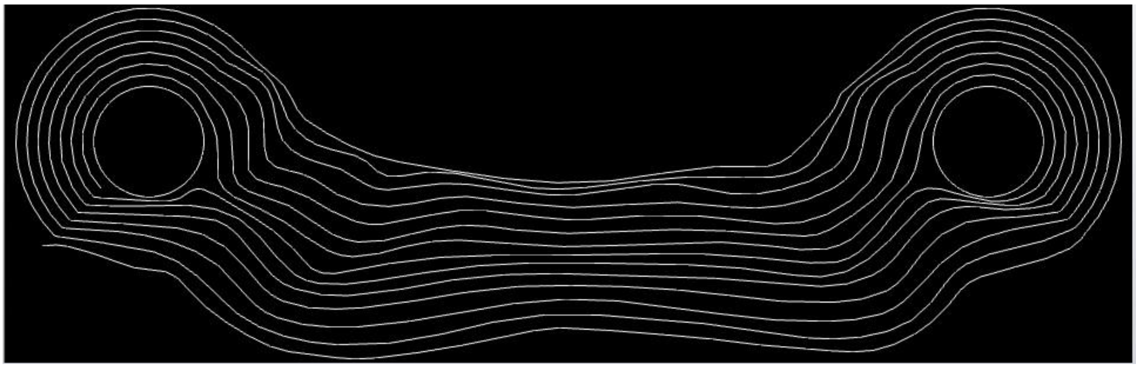

Figure 33 – Stitching pattern of the net-shape shackle

In Figure 33 it is possible to see the pattern of the net-shape shackle. Due to the smaller width of the component, it was possible to design a pattern in such a way so that all the fiber rows circled around the holes. The critical point here was the fiber distribution, that left a resin-rich area right next to the edges where the loads are applied. This is going to be very favorable for the initiation of a crack that may lead to a severe strength reduction of the component.

6.2 Stitching material and process parameters

The adopted stitching material was a carbon fiber tow designed as "Mitsubishi Chemical Carbon Fiber & Composites Grafil^{tm}" type: 34-24K WD. From the Grafil Inc. datasheet of the GRAFIL 34-700: "It is a continuous, high strength, PAN based fiber. It is available in 12K and 24K filament count tows. They can be supplied in either round or flat tow formats. The flat tow (designated by 'WD') is the ideal fiber to use in applications where spreading is required, e.g., tape production. The round tow is used in applications where spreading is not necessarily required, e.g., braiding and weaving."

Typical Fiber Properties			
Tow Tensile	Strength	4830 MPa	SRM 16
	Modulus	234 GPa	
Typical Density		1.80 g/cm^3	SRM 15
Typical Yield	12K	800 mg/m	SRM 13
	24K	1600 mg/m	SRM 13

Table 4 - Typical fiber properties of GRAFIL 34-700 (from www.grafil.com)

Typical Mechanical Properties				
Tensile Properties	0°	Strength	2572 MPa	ASTM D3039 / 0° 8 ply
		Modulus	137 GPa	ASTM D3039 / 0° 8 ply
	90°	Strength	81 MPa	ASTM D3039 / 0° 16 ply
		Modulus	9.2 GPa	ASTM D3039 / 0° 16 ply
Compressive Properties	0°	Strength	1365 MPa	ASTM D3410 / 0° 16 ply
		Modulus	127 GPa	ASTM D3410 / 0° 16 ply
	90°	Strength	210 MPa	ASTM D3410 / 0° 20 ply
		Modulus	10.2 GPa	ASTM D3410 / 0° 20 ply
Flexural Properties	0°	Strength	210 MPa	ASTM D790 / 0° 16 ply, L/D=32, Vf=61%
		Modulus	10.2 GPa	ASTM D790 / 0° 16 ply, L/D=32, Vf=61%
	90°	Strength	102 MPa	ASTM D790 / 0° 16 ply, L/D=16, Vf=61%
		Modulus	8.8 GPa	ASTM D790 / 0° 16 ply, L/D=16, Vf=61%
ILSS	Strength		97 GPa	ASTM D2344 / 0° 16 ply, L/D=4, Vf=59%

- 250F Epoxy Prepregs
- Resin: Mitsubishi Rayon #340 resin system
- Tensile and compressive properties are normalized to 60% fiber volume

Table 5 - Typical mechanical properties of GRAFIL 34-700 (from www.grafil.com)

The LayStitch machine has several parameters which can be set by the user using the control console:

- Zigzag Swing Stroke: controls the movement/distance the fiber guide is allowed to move during stitching;

Figure 34

- Swing Assist: Controls the movement/rotation of the bobbin during stitching;

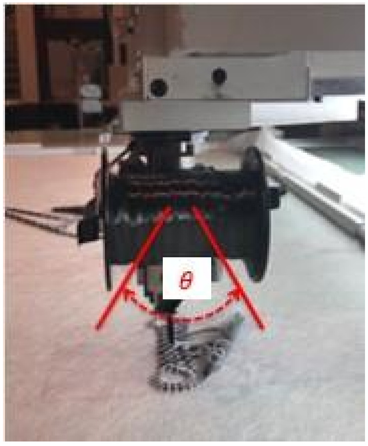

Figure 35

- Width: Changes the width of the stitch pattern in order to stitch across the entire fiber tow;
- Several more parameters about the stitching can be set in the EDOPath software during the conversion of the AutoCAD file into the .dst file that can be read by the machine system (e.g. the distance between one punch and the next one, the length of a straight stitching line along which to decrease the number of punches, the number of closer punches before and after a strong change in curvature or an edge, etc.) but all of them where left at the default configuration.

7. Manufacturing

The manufacturing process has been developed in two different stages. At the beginning a Vacuum Assisted Resin Transfer Molding (VARTM) process has been used, followed by a room temperature curing under vacuum. Then, due to some requirements on the quality of the parts, the process has been switched to a hand-layup in a one-sided mold, and then curing under vacuum in the oven.

7.1 VARTM

Vacuum Assisted Transfer Molding is a closed mold, out-of-autoclave composite manufacturing process. It is a variation of the classic Resin Transfer Molding (RTM) with the only difference being the replacement of the top portion of a mold tool with a vacuum bag and the use of the vacuum to help the flow of the resin. The use of the vacuum pump assists the resin flow into the fiber layup contained within a mold tool covered by a vacuum bag. After the impregnation, the composite part is allowed to cure at room temperature with an optional post cure sometimes carried out.

In general, this process uses a low viscosity resin along with glass or carbon fibers, to create a composite. Normally the produced composites have a fiber volume fraction of around 40-50%. Resins used in this process should have a low viscosity due to the limited pressure differential provided by the vacuum pump.

The most critical issue that can be present during VARTM, is air leakages. They can cause resin to flow in a not correct way through the mold and can lead to the formation of air bubbles. The air bubbles will then be present as air voids in the finite composites. Air leakage can be caused by a defect in the vacuum bag, an improper application of the sealant tape, or an improper seal at the points where the hose meets the vacuum bag.

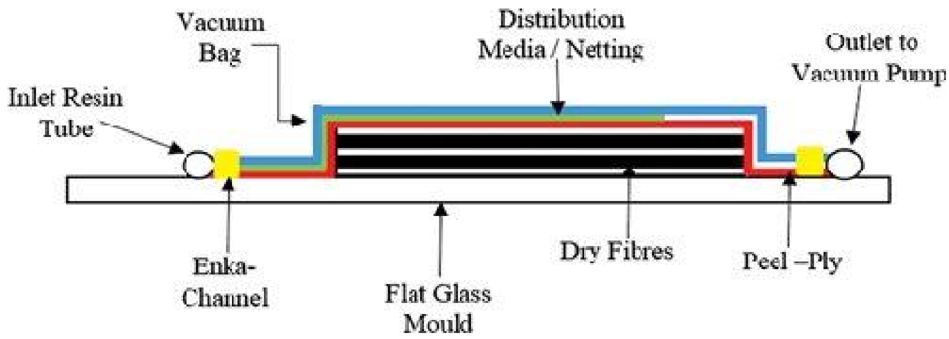

Figure 36 - Schematic of VARTM (from Tan, Azwan, Noorhafiza, "Delamination and Surface Roughness Analyses in Drilling Hybrid Carbon/Glass Composite", 2015)

7.1.1 Process

The first batch of stitched shackles was made of 2 reference shape shackles and 2 net-shape ones.

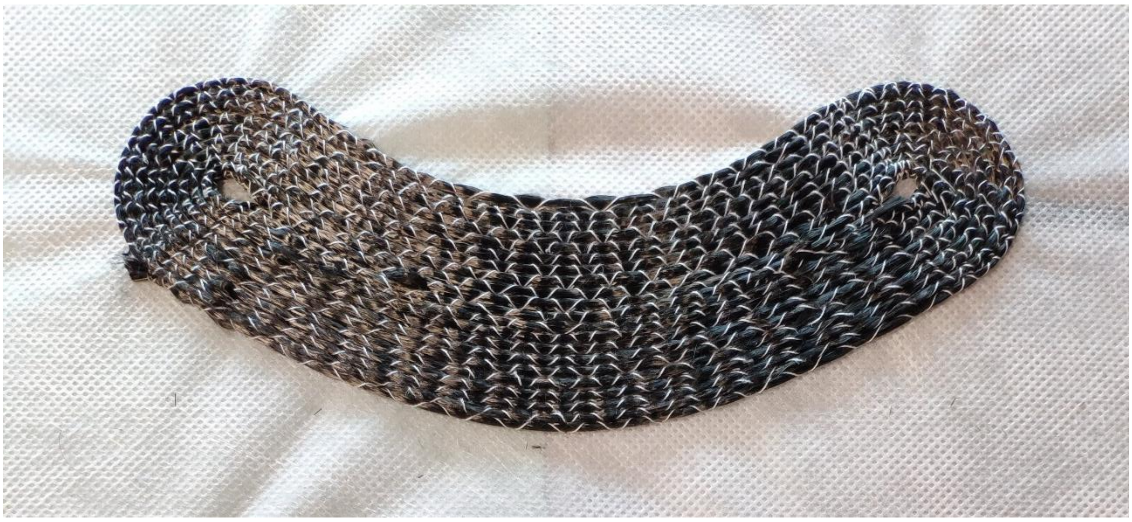

Figure 37 - Stitched reference shape shackle

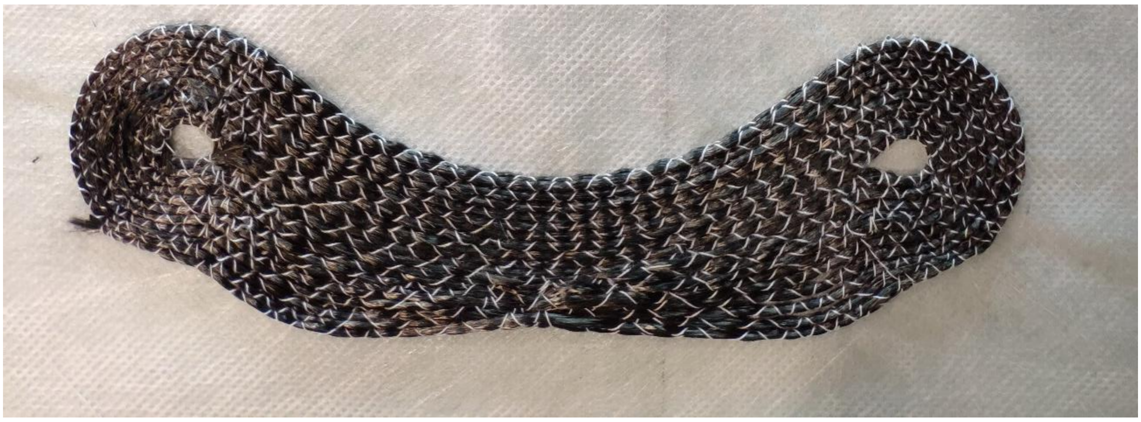

Figure 38 - Stitched net-shape shackle

The preforms were positioned on a flat aluminum plate (mold), the sealant tape was attached on a rectangle shape all around, then they were covered by the transfer media, the peel ply and the vacuum bag. Two hoses were connected to two holes in the opposite sides of the mold plate, the one to the inlet was sucking the resin from a can, while the other one, from the outlet, was connected to the vacuum pump to pull the vacuum. A breather cloth was put close to the outlet hole, to slow down the resin, in order to give it time to reach and impregnate the lower layers of the parts, closer to the mold surface.

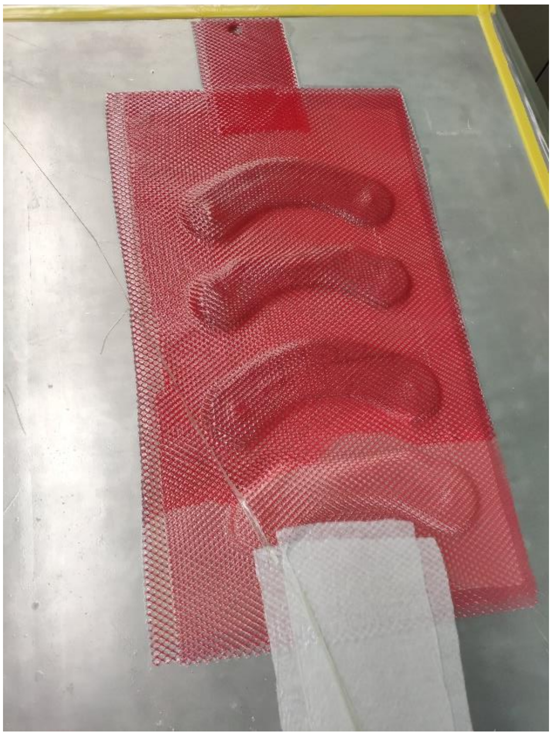

Figure 39 - VARTM setup during infusion

The adopted resin was the SC-15 resin. It is adopted in many industrial applications. It is developed by Applied Policeramic Inc. (Benicia, CA). This low-viscosity, epoxy-based resin is rubber toughened. It is a two-parts resin, and it has to be mixed at a 30:100 ratio hardener:resin. Immediately after mixing the two parts, it was degassed in a vacuum for 10 minutes to remove air bubbles. After that the VARTM process was started and the curing process lasted 24 hours at room temperature, with the vacuum pump kept active for 6 hours.

7.1.2 Results

Figure 40 - Cured parts after VARTM

The lack of a pin inserted in the holes during the curing process, has led to the closure of the holes, filled with hardened resin, and to possible misalignments of the two superimposed layers. As clearly visible from Figure 40, the parts also needed a finishing to remove the excess resin from the external edges. Moreover, on the vacuum bag side, unlike the flat mold side, the surface was uneven and not at all flat. This factor has been considered not satisfying for the overall quality of the parts, and especially for the strength of the shackles, which could bend, under axial loading, in an uneven way, considering the asymmetry. This was not the only issue, in fact some visible air voids have triggered a deeper analysis, which led to the section cut of the parts to examine the internal air voids.

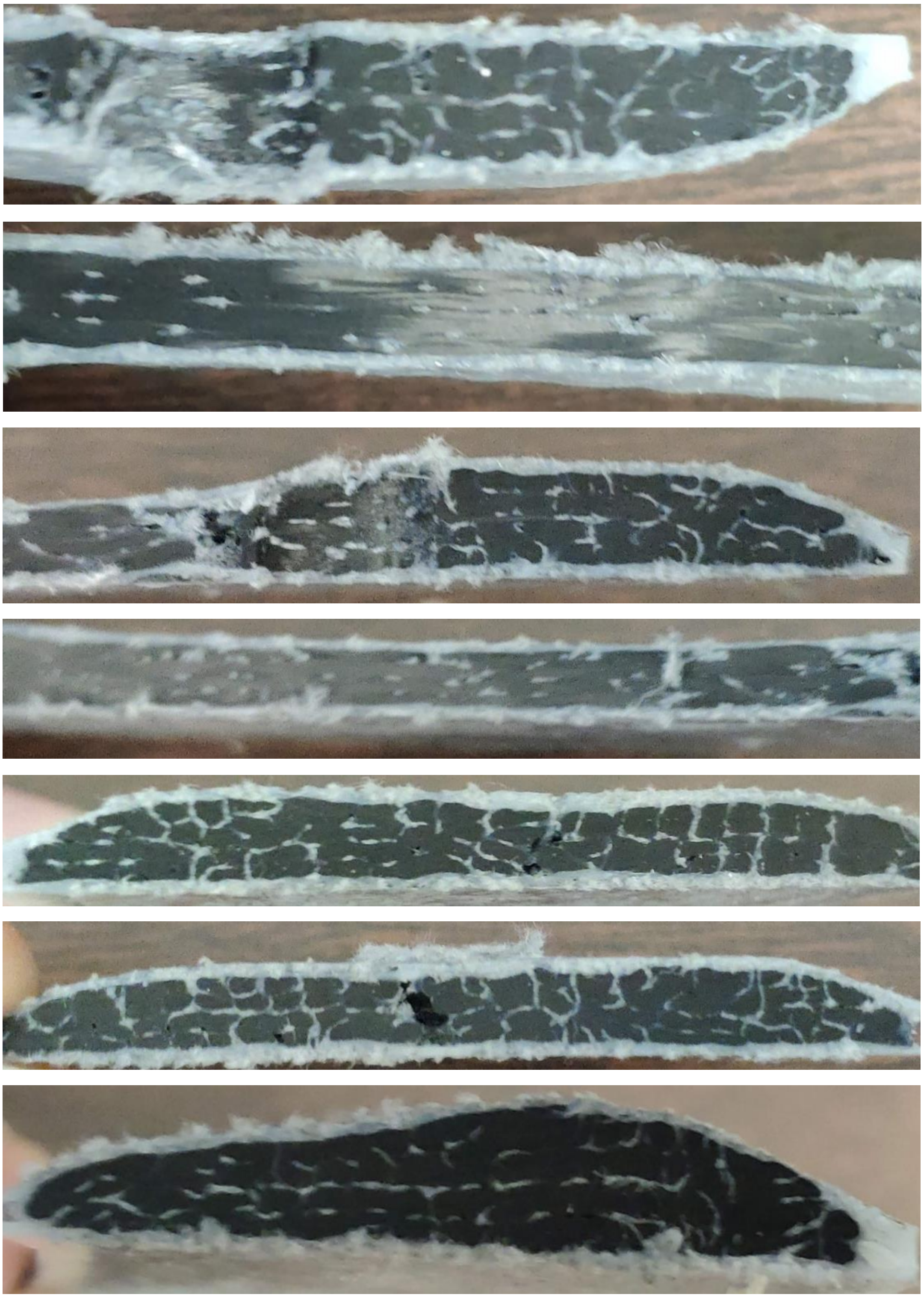

Figure 41 - Section cuts of the cured VARTM shackles

The presence of visible to the naked eye voids have later confirmed the initial doubts about the adequateness of the executed VARTM process, both for its intrinsic characteristics and for the practical execution of that specific batch. In fact, during the resin impregnation phase, some air bubbles were noted, likely due to some micro cracks in the vacuum bag.

Since the result was not satisfactory regardless of the internal air voids, it had been decided to switch to an in-mold hand lay-up, followed by a vacuum in-oven curing process.

7.2 In-mold hand layup

A proposed solution was the development of a mold, in which to cure the parts to obtain a better surface quality. The initial suggested idea was to infuse through vacuum the part enclosed in a mold (a similar concept to the RTM) and a concept mold was proposed in that sense.

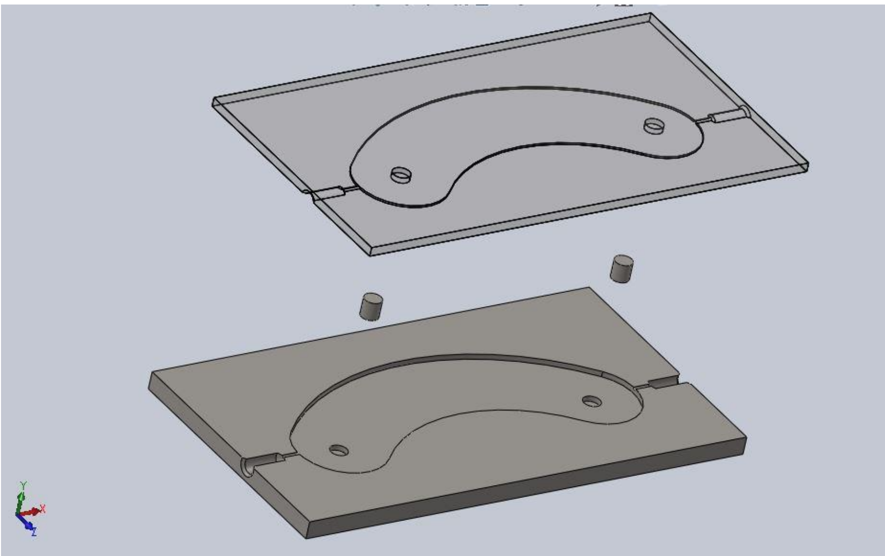

Figure 42 – Proposed mold concept

The concept consisted in a 2-parts mold, both females, and 2 inserts to keep the holes of the shackles open and at the right dimensions. The inlet and outlet ports could have also been placed in other positions. They were compatible with fittings for pressure sealing and should have been used to suck the resin throughout the cavity, while impregnating the preform. The concept has been judged too complicated and a simpler solution has been proposed, made of just one-sided female mold, enclosing the whole geometry of the part, which could be pressed/closed/sealed from a flat plate on the top. No holes should be designed in this new mold since the layup should have been a hand layup.

7.2.1 Mold design and manufacturing

Due to the decision of manufacturing also some tensile coupons for the material characterization and to the fact that there are two different shapes of shackles, a mold has been designed which enclosed all the different shapes and variants. This choice has been made both to save money and time, by milling the shapes on the same aluminum plate and at the same time.

Considering all the clearances and dimensions, a 12”x12” machinable aluminum plate was chosen, and a simple CAD design was elaborated to present the mold project.

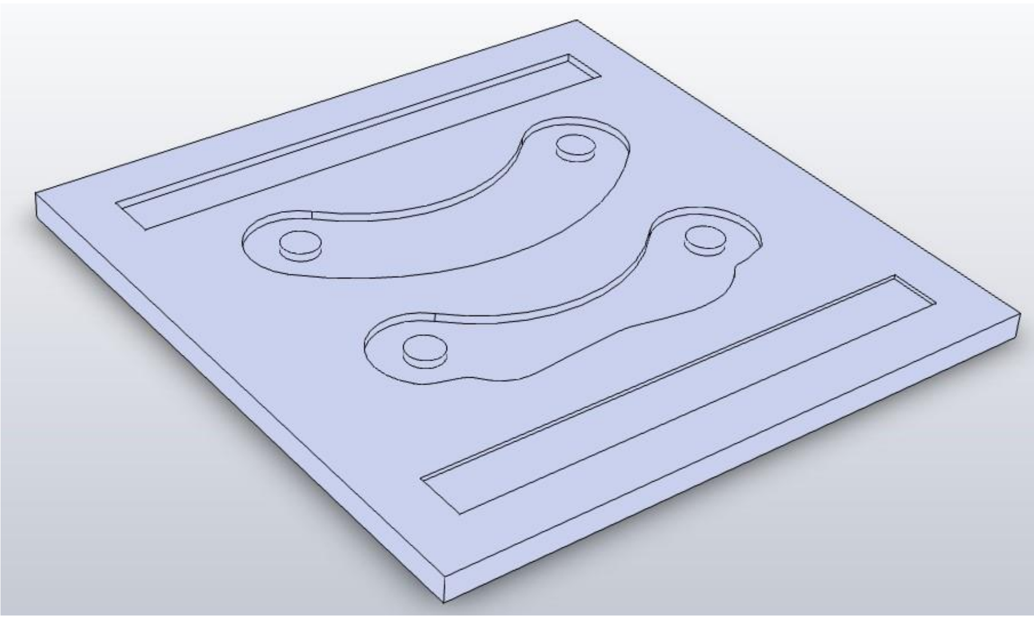

Figure 43 - Final mold design

From Figure 43 it is possible to see the 4 different shapes in the mold: the reference shackle, the net-shape shackle, and the two tensile coupons, one with a thickness of 4 mm and the other of 2 mm. The two shackles shapes both had a thickness of 4 mm. It is also possible to see that there are 2 pins for each shackle, meant to keep the holes open during the infusion and curing process.

The pins to keep the holes open were crucial, in fact, a drilling operation successive to the curing process, made to open or to bring back at the correct dimensions the holes, could damage the matrix, or, even worse, the fibers, bringing to a delamination caused by the peel stresses.

The manufacturing has been done at the CNC mill, and the mold was almost ready to be used, besides some finishing operations required to smoothen the edges.

Figure 44 - Finished mold

7.2.2 Process

The first concept of process proved itself wrong, in fact by just pressing a flat plate on top of the open side of the mold could just cause the exit of some resin (incompressible fluid) without any effect on either the geometry of the part nor the exit of air bubbles. Due to the lack of time, it was impossible to design and manufacture a completely new mold, so a solution was proposed to overcome this issue while using the very same mold. The solution consisted in closing the top side of the mold with a vacuum bag to suck the air out after a hand layup of the preforms, followed by an in-oven curing under vacuum.

This is a summary of the process:

- Cleaning of the mold surface with acetone and a specific product for mold preparation;
- Application of a release agent on the mold surface to facilitate the components removal after curing (lasts 15 releases);
- Application of seal tape on the edges of the mold;
- Mixing of two-components resin (resin : hardener = 100 : 30);
- Degassing process of mixed resin in vacuum for 10 mins.;
- Hand-layup of preforms by impregnation with a roller and manual positioning inside the mold;
- Positioning of transfer media ply;
- Positioning of breather cloth;
- Sealing of the mold with the vacuum bag;
- Insertion of the hose to suck vacuum;
- Final sealing of the mold;
- Creation of vacuum in the mold to compress the components and extract excess air and resin, the latter collected in a catch-can before the vacuum pump;
- Curing process in the oven: 2-hours ramp from RT to 60° C, 2 hours @ 60° C, 2 hours ramp to 122° C, 2 hours @ 122° C, 2 hours ramped cooling to RT.

Figure 45 - Impregnated preforms before sealing the mold

Figure 46 - Layup ready for in-oven curing

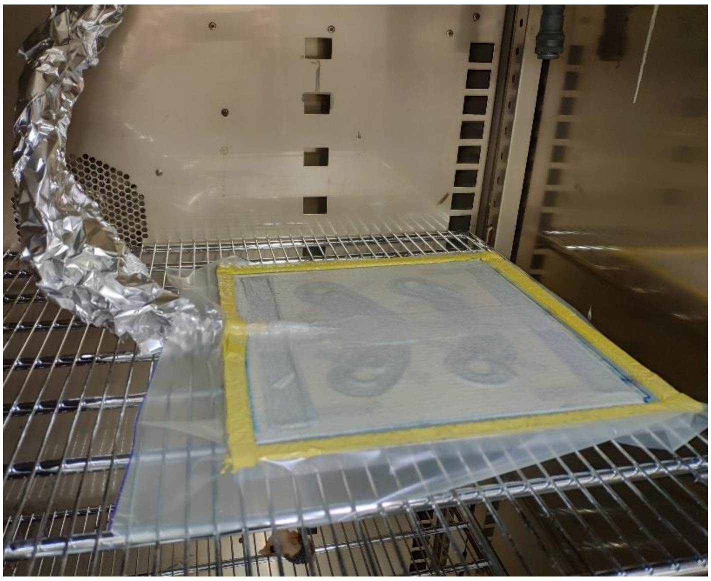

Figure 47 - In-oven curing of components

7.2.3 Results

The parts obtained with this method have revealed a better overall surface quality. Despite the side of the shackle in contact with the vacuum bag, the other sides have a very smooth surface. Due to this result, it was decided to continue to manufacture the parts following this technique.

The total production has been:

- 6 tensile coupons of a thickness of 2 mm;
- 6 tensile coupons of a thickness of 4 mm;
- 9 reference shape (‘boomerang’ shape) shackles;
- 9 net-shape shackles.

The final quality of each manufactured batch is depending on the impregnation and layup process. In the 4th batch, e.g., the vacuum bag had some flaws which caused some air bubbles to enter and remain inside the parts, while in the very first batch, too little resin was used, resulting in excessively dry components.

Figure 48 - 2 mm thick tensile coupon, upper face

Figure 49 - 2 mm thick tensile coupon, lower face

Figure 50 - 4 mm thick tensile coupon, upper face

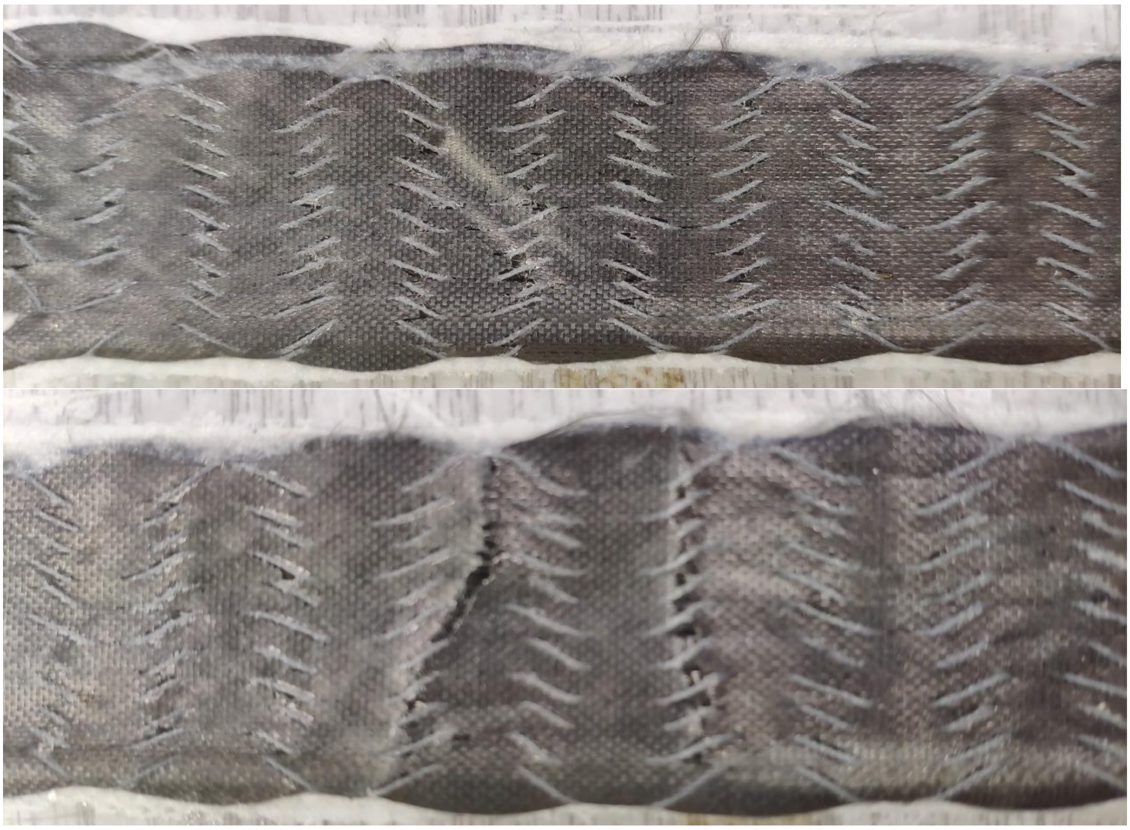

Figure 51 - Manufacturing defects in a tensile coupon due to the vacuum hose being pressed by the vacuum on the upper surface during curing process

Figure 52 - Cured shackle, before being pushed out of the mold

In Figure 52 it is visible a shackle just before being pushed out from the mold. The top surface is not perfectly flat due to the lack of geometry control on that side (vacuum bag side).

Figure 53 - Details of reference shape shackles defects

The defects in Figure 53 are areas where resin has not been kept during the curing. Despite the SC-15 being a low-viscosity resin, which should be a positive factor for the impregnation of the fibers, one of the emerging drawbacks of the TFA technique has been that because of the stitching, the fibers are tensioned longitudinally, and the fiber tow is compressed transversely. This lowers the permeability of the fibers making it harder for the resin to flow between them and fill the gaps, resulting in the presence in the finite product of residual voids.

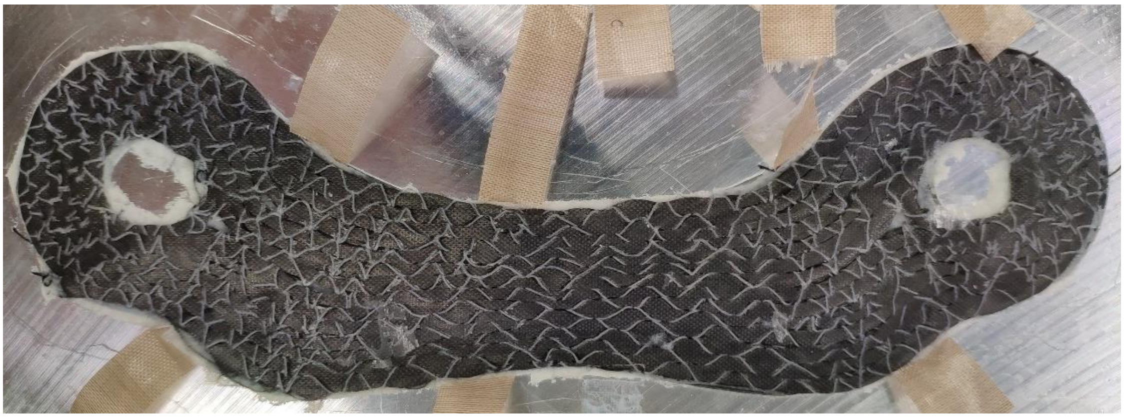

Figure 54 - Cured net-shape shackle

As showed in Figure 54, also the arrangement of the fibers plays an important role on how the resin can flow within the part. This is certainly a factor which must and can be improved in further development of this project.

Figure 55 - Residual voids between fiber tows in cured net-shape shackle

Though it is true that the defects showed in Figure 55 are relevant for the integrity of the component, it is also to be said that these defects were present only in the first manufactured batch, where too little resin was applied. In the next batches, even if present anyway, the entity of those flaws was smaller.

Figure 56 – Cured 4 mm tensile coupon, mold surface side

Figure 57 - Cured shackle, mold surface side

Figure 58 - Cured net-shape shackle, mold surface side

Figure 59 - Cured 2 mm tensile coupon, vacuum bag side

Figure 60 - Detail of cured 4 mm tensile coupon, mold surface side

From Figures 56-60 it is possible to evaluate the surface quality of the parts in the areas facing the mold surface. It is still evident a problem of resin infusion, since some areas present large voids, but the dimensional control is much more effective, and the flatness of the surface is ensured. Already at this point, one of the suggested solutions / improvements for the future development of this project is the manufacturing of a two-sided mold, through which realize a resin injection.

Unfortunately, as already mentioned, the lack of time prevented the resolution of several issues along the whole process, which have been put aside in order to get to a final, touchable, result. This should not mean, however, that these issues have been ignored or neglected, all of them have been noted down, and an analysis of the causes and possible solutions has been performed to address those who will eventually continue this project.

8. Testing

A wide set of experiments has been designed and implemented to collect as much information as possible on the material properties and on the shackles performances in terms of strength and failure mode. At first, the need to characterize the material, in order to get more reliable simulation results, has prevailed. To get those data, it has been necessary to realize some tensile coupons. In a second phase, also the shackles have been tested to assess their strength and their behavior under a uniaxial tensile load.

8.1 Tensile coupons test process

As already, mentioned, tensile coupons have been manufactured and tested to characterize the material properties.

8.1.1 Tensile coupons manufacturing

The coupons have been designed with a 10” x 1” rectangular shape, whose thickness is defined by two slayers of fibers stitched one on top of the other (half of the final composite shackles). The designed stitching path was relatively simple and representative of the stitching pattern of the components.

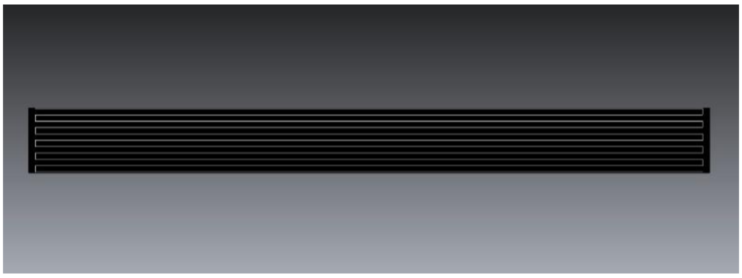

Figure 61 - Tensile coupon stitching pattern

As for what happened with the shackles, a first batch of six shackles was manufactured using the VARTM technique. These shackles had a very uneven surface, on the upper face and this result contributed to the decision to develop a mold to improve the final quality of the parts.

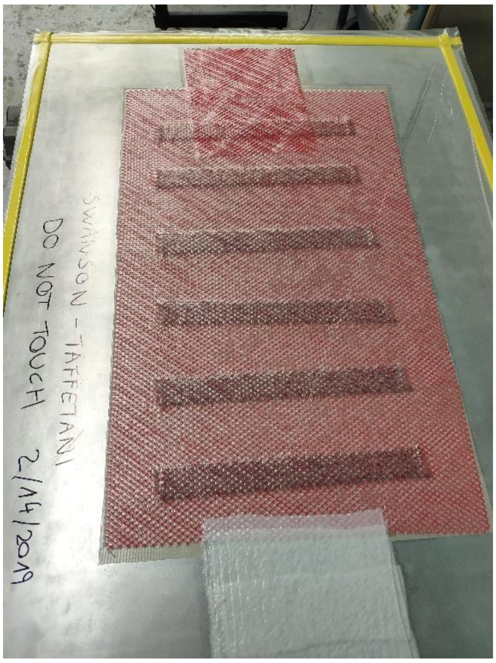

Figure 62 - Tensile coupons VARTM process

These coupons have then been finished by cutting off excess material and have been uniformed to a 1” x 9” shape.

After the first VARTM batch, it was decided to proceed with the design of the before mentioned mold, where 2 cavities have been realized to house the coupons’ shapes. One of them with a 2 mm thickness and the other with a 4 mm thickness.

The manufactured coupons had a quite good surface quality, especially on the mold surface face, and 6 batches have been realized.

The fact that both the 2 mm and 4 mm thickness were realized is because at the moment of the mold manufacturing, it was still unsure about which thickness size was to be used for the tests, and if an eventual comparison between the two was needed, so both were added to the mold for the sake of completeness and to guarantee a higher degree of freedom in the net steps of the project.

8.1.2 Gripping tabs

One of the problems generally encountered during composites testing is the choice of the tabbing configuration and the bonding of the of the end tabs onto test specimens. This is not a negligible part of the testing process, in fact the tabs protect the specimen and introduce the load into the specimen.

Following DOT/FAA/AR-02/106 "Tabbing Guide for Composite Test Specimens", 2002, "in contrast to metallic specimens, the testing of composite materials reinforced with high strength and/or high modulus fibers is not straightforward. […] Since a UD composite is the basic building block in structural composite laminates, its properties must well be characterized for use in lamination analyses". The main objective is to obtain a valid failure mode in the central gage of the specimen. To satisfy this condition, the stress state in the gage section of the specimen must have a considerably higher magnitude than anywhere else in the specimen, gripping tabs regions included. The axial strength of a general UD composite is high, compared to the transverse and shear strengths. This means that many specimens may fail in transverse normal and/or shear modes even under axial normal stress states.

For tension testing, the axial load is introduced through shear forces applied on the specimen surface. Shear forces are applied using some grips, which clamp the specimen surfaces at each end, through friction. A smooth, flat grip surface apply a uniform shear force to the specimen surfaces while producing minimal surface damage. However, smooth grip surfaces cause very low friction coefficients, and to overcome this, it is necessary to apply a relatively high clamping force to prevent grip slipping. Because of the typical low transverse compressive strength of a unidirectional composite, high clamping forces can result in significant through-thickness compressive stresses, and local crushing in the grip regions. Grip surface should therefore have an increased roughness to reduce clamping pressures at an acceptable level. Such a coarse face could damage the surface of the test specimen, so protective tabs are adopted and bonded onto the faces of the specimen grip regions. This enables the use of aggressive grip faces, decreasing the grip pressure and the likelihood of surface damage to the specimen. Moreover, tabs are used to reduce stress concentrations at the ends of the wedges.

From a functional point of view, gripping tabs are thickness-tapering elements, so that the central gage section of the specimen has a reduced cross-sectional area compared to the tabbed ends. The adopted way for metallic specimens is to have a width-tapered shape, but with composites this concept cannot be adopted because of the high probability of premature longitudinal splitting failure in the tapered region (the classic dog-bone shape).

Even though the tabs protect the surface of the specimen in the grip areas, they can behave as stress concentration factors, especially at their terminations, towards the central specimen gage. A solution to decrease this effect is to taper the tab at the gage section end, even though some stress concentration is still present. The only way to decrease this stress concentration effect is to properly choose the tabbing material, adhesive and tap taper geometry.

The selected tabbing material was NEMA Grade G-10 glass fabric/epoxy. It is very often adopted for gripping tabs, and its surface require a very minimal surface preparation. Moreover, it can be machined also after having been bonded to the composite test panel.

Also, the adhesive selection is no less of importance. The adhesive must be able to transmit the load into the specimen through shear and must withstand the compressive force exerted by the grips.

The adhesive is a Loctite bi-component epoxy which was available in the facility.

As written in the above-mentioned guide: "The purpose of tabbing a composite specimen is to introduce load into the test specimen without producing premature failure in an undesired failure mode. Thus, a successful tab configuration design is one that produces a valid failure mode within the central gage section of the specimen"[20]. To make this happen, the stress state in the gage section must be of greater entity than anywhere else in the specimen, including the grip region. That is why special attention must be payed to the tab configuration design, in order to minimize any stress concentration.

[20] DOT/FAA/AR-02/106 "Tabbing Guide for Composite Test Specimens", 2002

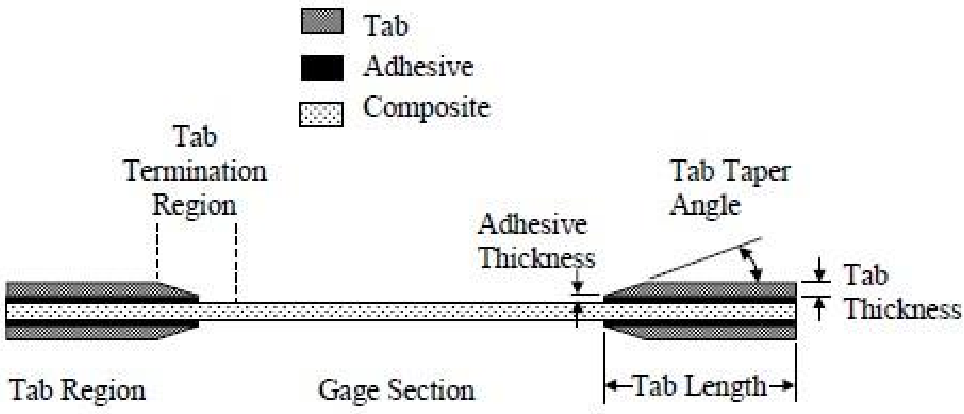

Figure 63 - Typical tabbed composite tension specimen (from DOT/FAA/AR-02/106 "Tabbing Guide for Composite Test Specimens", 2002)

The tabs where therefore realized as 1" x 1" square plates, and the tab termination region have been chamfered to a 45° angle to decrease the stress concentration factor.

The surface preparation for both the tabs and the specimens consisted in sanding the interested surfaces to increase the roughness of the surface. After that the tabs were bonded and left to cure with clamps, at room temperature, for 24 hours.

8.1.3 Testing with laser extensometer

The tensile testing of the specimens was performed to obtain the main material characteristics. Those characteristics were to be successively implemented in the FE model to improve its predictivity and trustworthiness.

The first tests have been conducted using the MTS-810 tensile test machine.

Figure 64 - MTS 810 Material Test System

In Figure 64 it is possible to see the machine, instrumented with a 100 kN load cell. The testing procedure has been determined to be displacement-controlled, following a ramp of 20 mm displacement in 120 seconds.

The system gives as an output:

- time
- load of the cell (N)
- displacement (mm)

With the addition of a laser extensometer, it is possible to obtain the strain of the specimen in the central section.

Figure 65 - Laser extensometer

Two very thin reflective tape strips are attached horizontally to the specimen surface, at a distance of 1" one from the other. The laser extensometer projects a vertical laser beam crossing both lines at their middle and from the reflected light can measure the distance between the two strips. The initial distance is recorded as a zero-time offset, and the next displacements from that initial distance are given, relatively from that initial offset, as a voltage signal to the control console of the test system, with an equivalence of 1 V = 1 mm. With this addition, it is possible to calculate the strains and the tensile stiffness in longitudinal direction of the composite specimen.

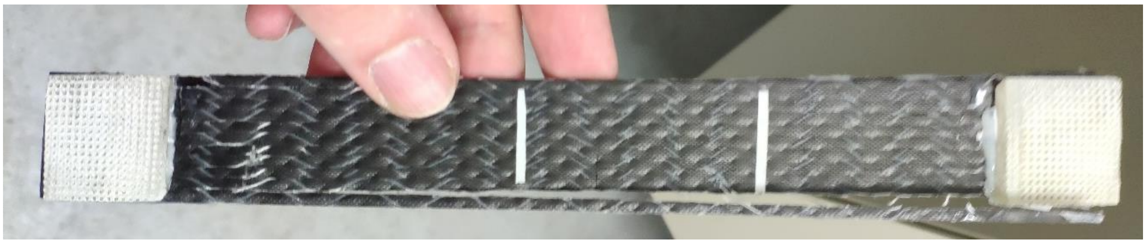

Figure 66 - Broken specimen with reflective tape stripes

The experimental plan can be resumed in this table:

VARTM	
Specimen	**Test method**
1	DIC
2	DIC
3	DIC
4	Laser extensometer
5	Laser extensometer
6	Laser extensometer
In-mold layup	
2 mm thick specimens	
Specimen	**Test method**
1A	Laser extensometer
2A	DIC
3A	Laser extensometer
4A	DIC
5A	Laser extensometer
6A	DIC
4 mm thick specimens	
Specimen	**Test method**
1B	Not tested
2B	Not tested
3B	Not tested
4B	Not tested
5B	Not tested
6B	Not tested

Table 6 - Experimental plan summary

The results of the tests are presented in the following plots:

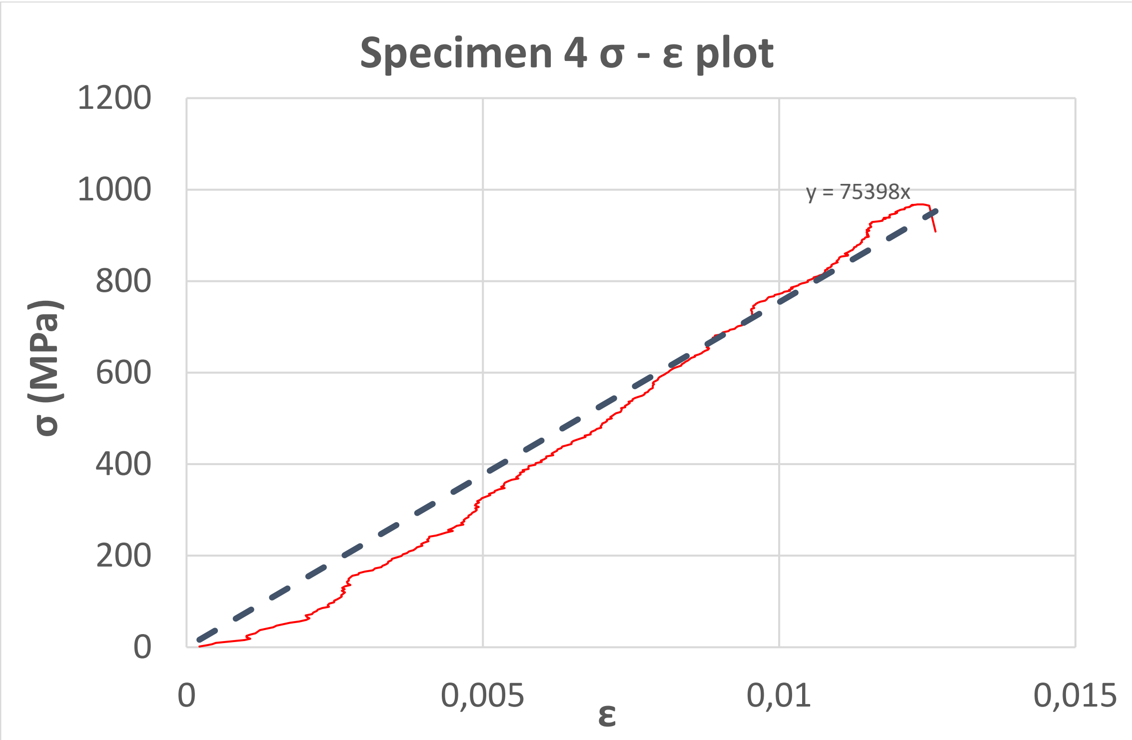

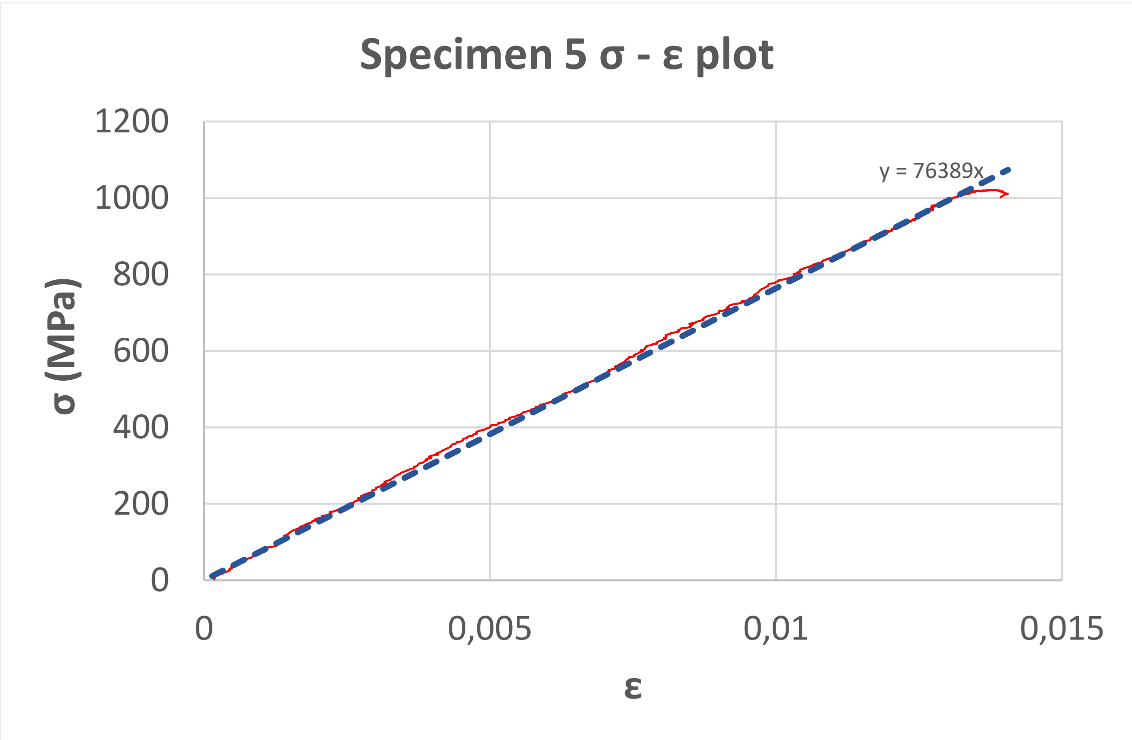

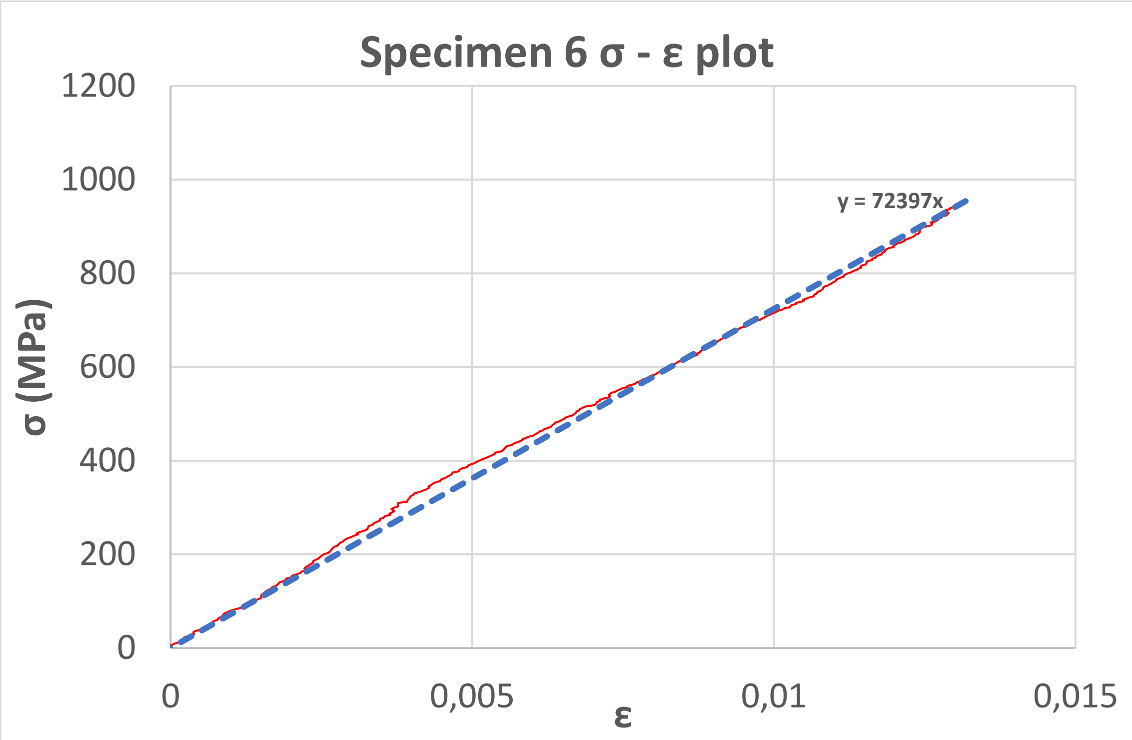
Specimen 6 σ - ε plot
σ (MPa)
1200
1000
800
600
400
200
0
0
0,005
0,01
0,015
ε
y = 72397x

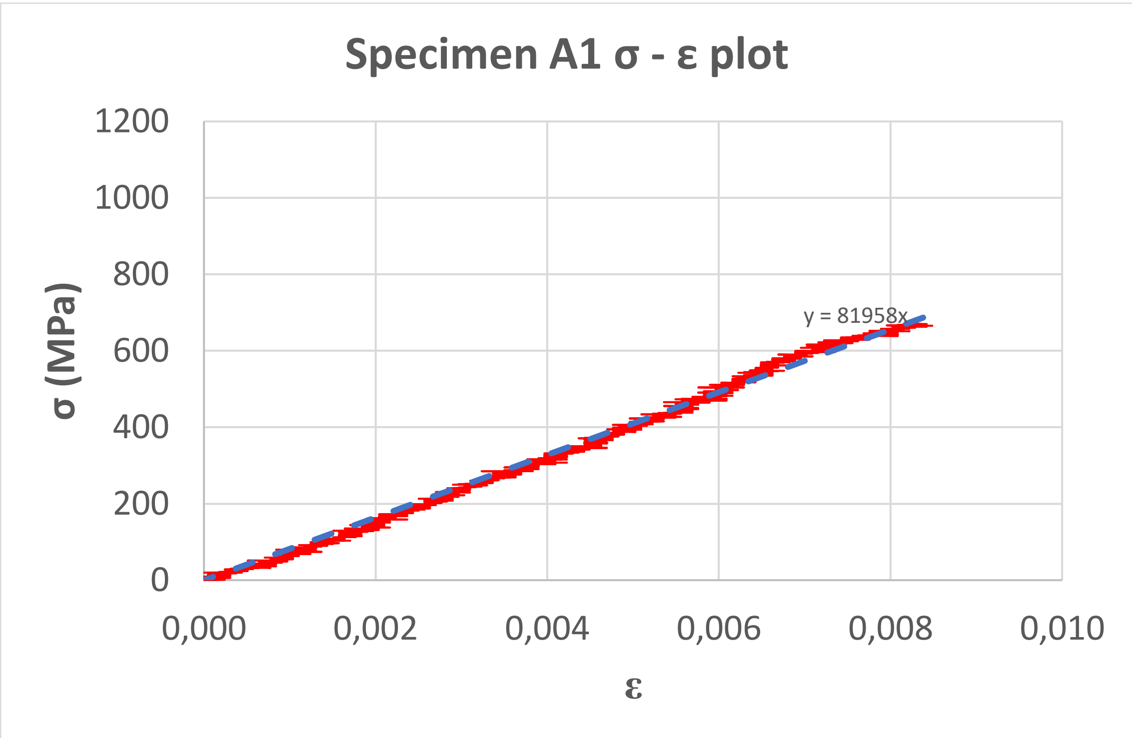
Specimen A1 σ - ε plot
σ (MPa)
1200
1000
800
600
400
200
0
0,000
0,002
0,004
0,006
0,008
0,010
ε
y = 81958x

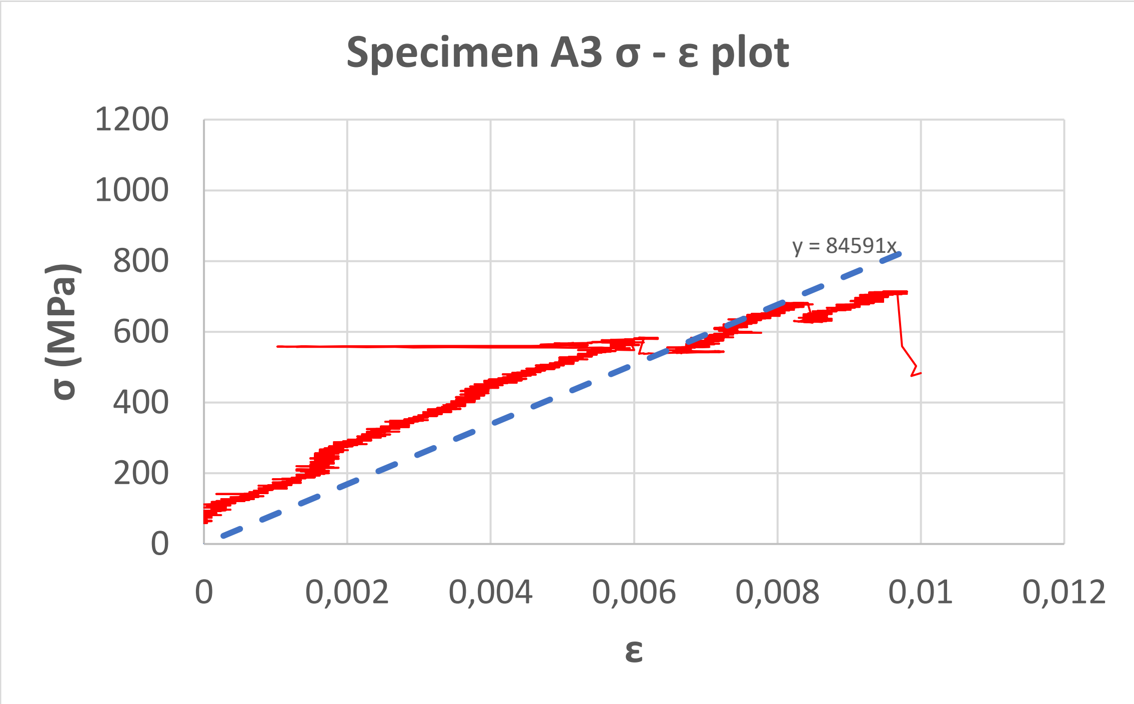

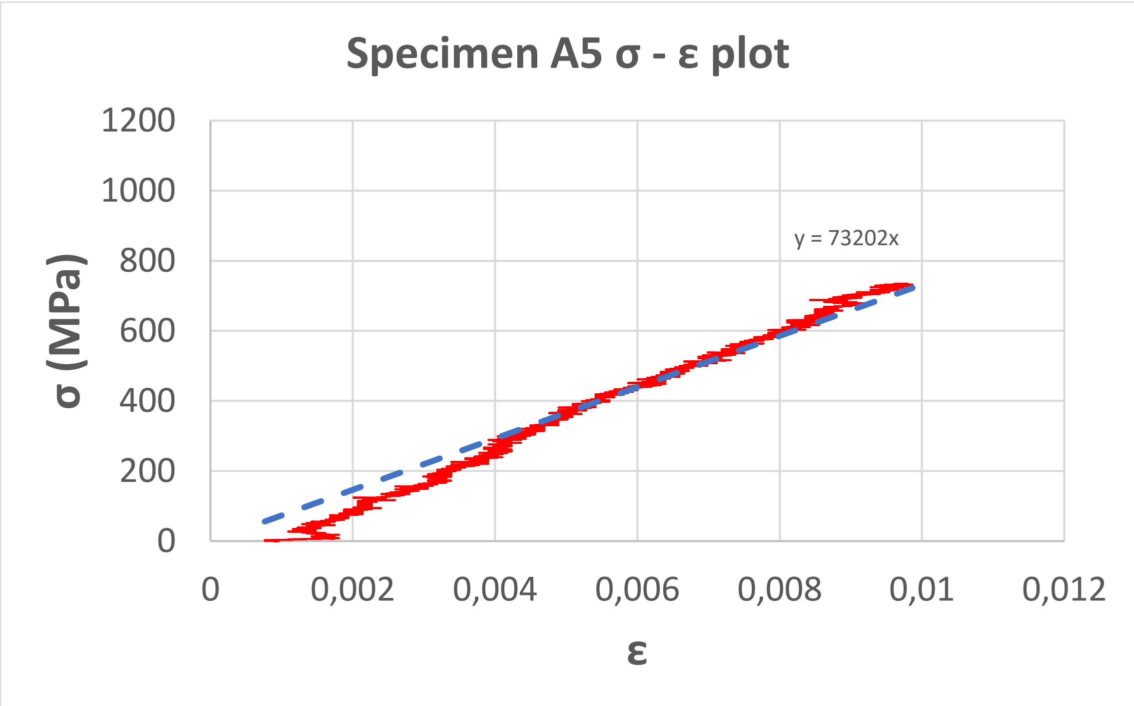

Figure 67 - Stress-strain plots from laser extensometer tensile tests

The results can be summarized in this table:

Specimen	Failure load (N)	Young's modulus (GPa)
4	44646	75,4
5	47075	76,4
6	48913	72,4
A1	28000	82,0
A3	29900	84,6
A5	30900	73,2
AVERAGE		**77,3**

Table 7 - Summary of tensile tests results from laser extensometer

From Table 7 it is possible to determine an average stiffness of the material, which results to be equal to 77.3 GPa. The stiffness has been calculated as the angular coefficient of the average line of the stress – strain diagram. The stress was obtained from the ratio between the output load of the load cell and the surface area of the cross section, measured for each specimen. This is the explanation of the fact that the obtained stiffnesses are in the same range of values, while there is a neat difference between the failure loads of the first three specimens (4, 5, 6), produced with the VARTM, and the last three (A1, A3, A5), produced in the mold. In fact, the cross-section area of the specimens was different between the two different manufacturing method, not only for intrinsic reasons such as the manufacturing method, but also the finishing operations performed after the manufacturing, to prepare the specimens for the testing.

8.1.4 Testing with Digital Image Correlation (DIC)

The measurements obtained through the laser extensometer are very useful to determine the longitudinal Young's modulus, that is the one in the 1-direction (E_1). But to get the other engineering constants that fully define the material, in order to feed them back into the FE model, it is necessary to adopt some other method which allow to measure the strains in other directions (e.g. 2-direction).

The adopted instrument to comply with this request was the Digital Image Correlation (DIC). This method consists in the preparation of the surfaces of the specimens in such a way to create a pattern of painted points and in the digital recording of the test with a high-speed camera or an equivalent tool. A software is successively capable of analyze the frames of the video recording and to identify, track and follow the displacements of the abovementioned dots which, being painted on the surface of the specimen, follow the specimen's displacements and strains.

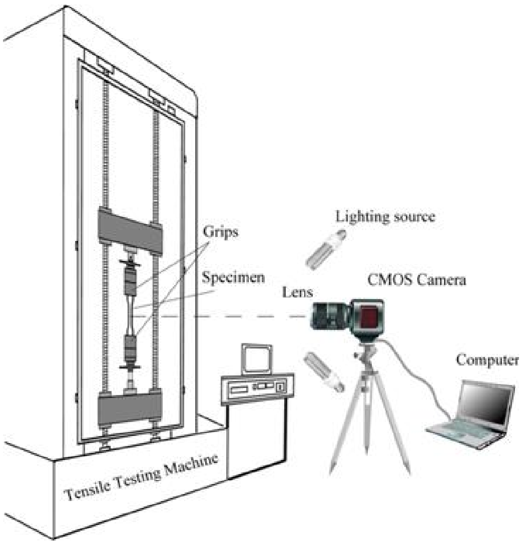

Figure 68 - Digital Image Correlation Setup (from Zhao, Zhao, "Investigation of Strain Measurements using Digital Image Correlation with a Finite Element Method", 2013)

The specimens have been prepared first being covered with a white spray paint, after that black spray paint drops have been scattered all over the white layer to create the dispersion of dots.

Figure 69 - Tensile coupon mounted in the MTS 810 test machine for DIC

Then the test is run, while recording a video with a camera perpendicular to the specimen. In this project, the strict timing has prevented the use of a digital camera or a high-speed camera, and the smartphone camera has been used, with a 30 FPS, 4K resolution. The video is then transferred to a laptop, where through a simple Matlab code several frames are extracted (a minimum of 100 or more, depending on the length of the video). Those frames are then imported in a commercially available software: GOM Correlate.

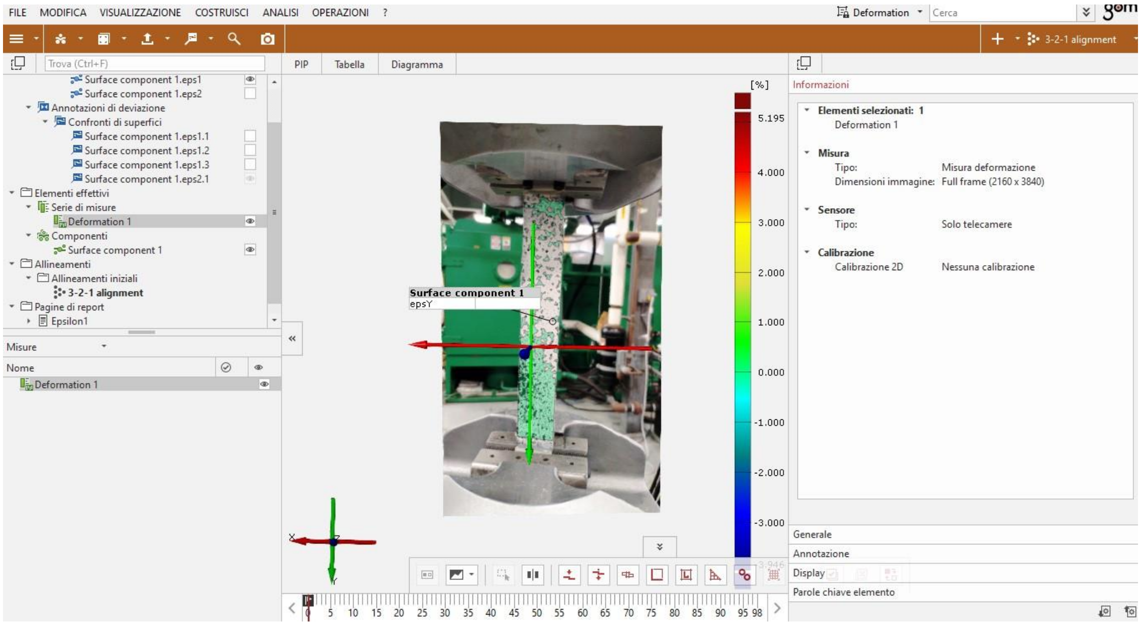

Figure 70 - GOM Correlate window

The steps followed within the software, for each tensile test, are:

- Importing of frames;
- Selection of the area for pattern recognition;
- Definition of the alignment of the part;
- Creation of the Surface component (recognition of dots pattern);
- Analysis of strains;
- Definition of query points where to visualize the exact strain values;
- Plotting of strain / timestep diagrams;
- Reporting.

A short overview of the tested specimens:

Specimen	Result
1	Bad camera focus, no useful data
2	Bad camera focus / dots pattern, only lower portion of specimen can be analyzed, and specimen slip in the grips area, no useful data
3	Bad camera focus / dots pattern, no useful data
A2	Good image recognition, useful data
A4	Good image recognition but specimen slipped in the grips area, no useful data
A6	Partial image recognition and slipped specimen, no useful data

Table 8 - Overview of DIC experiments

As Table 8 demonstrates, a combination of technical issues linked to the digital recording tool, and of failures of the adhesive between the gripping tabs and the specimen surfaces, has invalidated 5 out of 6 experiments. Only the specimen A2 has allowed to gather some useful data.

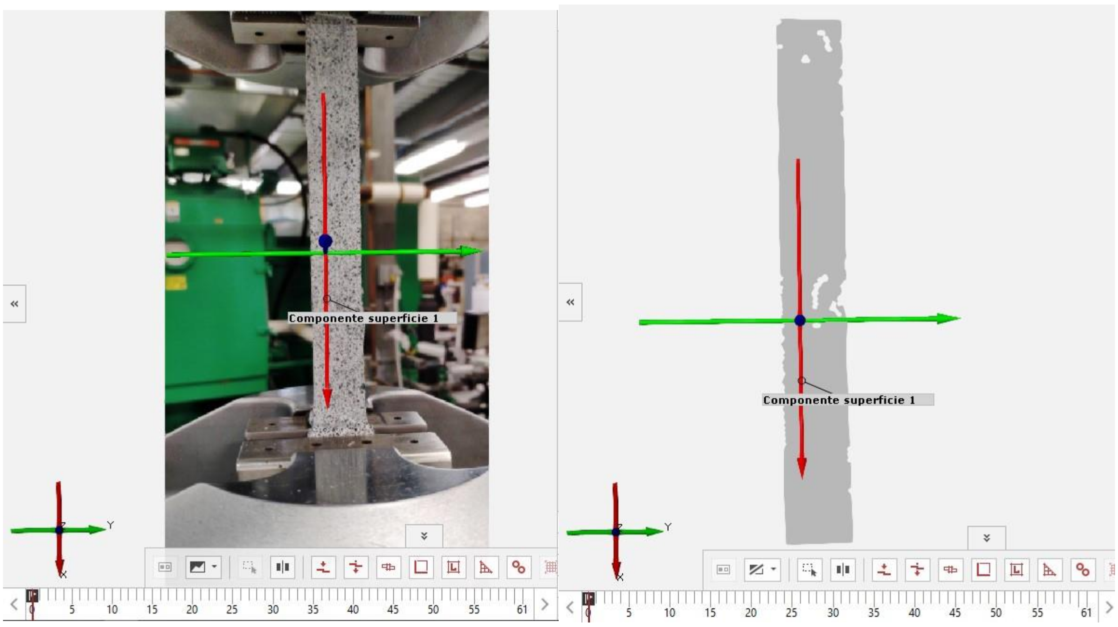

Figure 71 - First frame of Specimen A2 test (left) and recognized pattern for first frame of specimen A2 test (right)

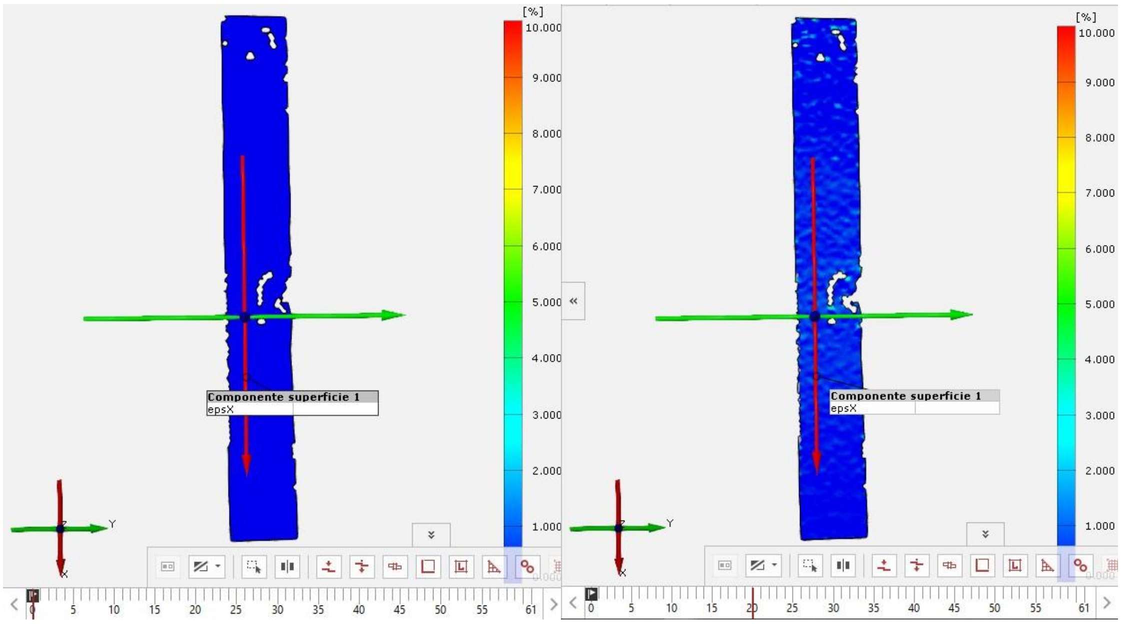

Figure 72 - Epsilon1 longitudinal strain frame 0 (left) and frame 20 (right)

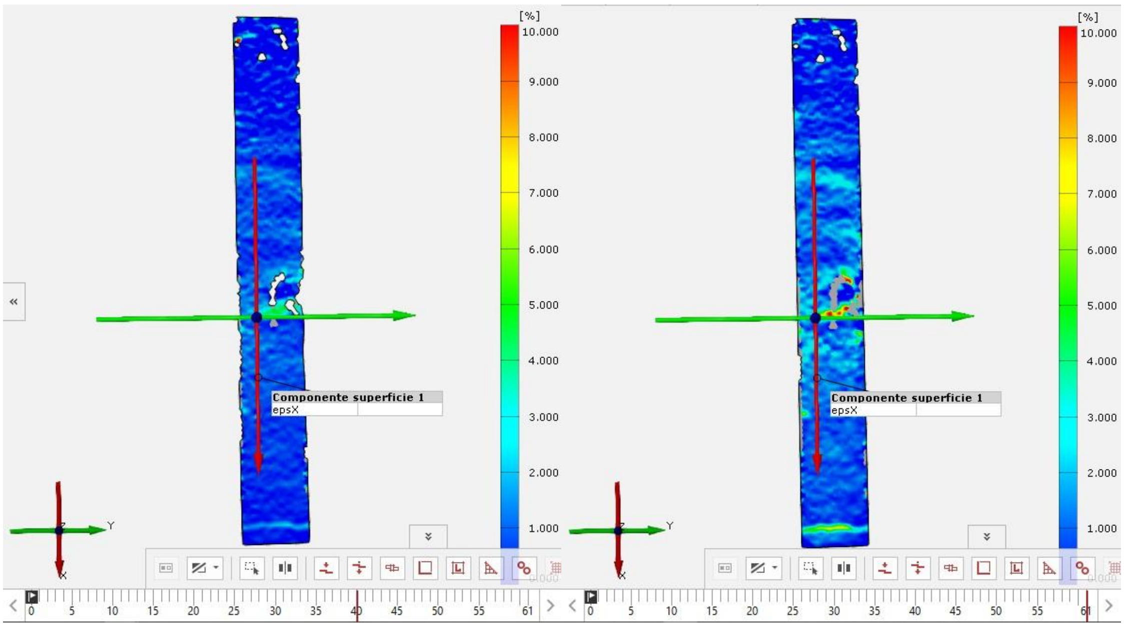

Figure 73 - Epsilon1 longitudinal strain frame 40 (left) and final (right)

In Figure 71 it is possible to see how the software maps the scattered dots to create a surface. In Figures 72 and 73 it is possible to see the evolution of the longitudinal strain ε_1 during the experiment in the frames from the start of the experiment to the first crack (not the ultimate failure).

It is possible to plot the same results for the transversal strain ε_2:

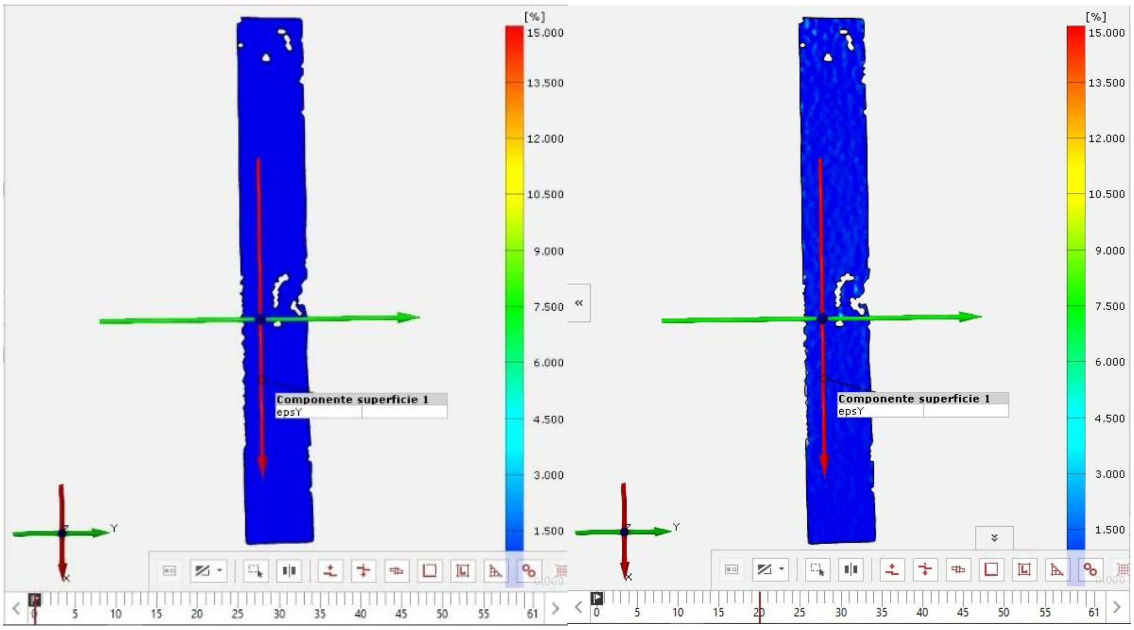

Figure 74 - Epsilon2 at frame 0 (left) and 20 (right)

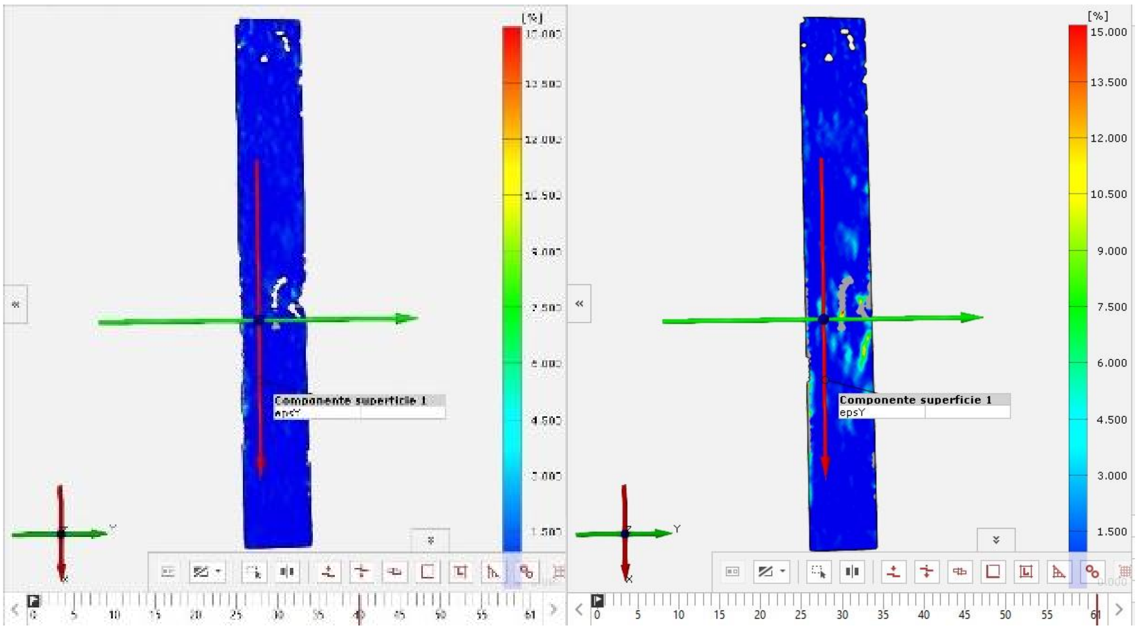

Figure 75 - Epsilon2 at frame 40 (left) and final (right)

It is interesting to observe that for the analysis of the longitudinal strain (Figures 72 and 73) it is possible to see some horizontal fringes, and more interesting (Figures 74 and 75), for what concerns the lateral strain (in 2-direction) is that is possible to see in the last frame before the first crack appearance, some vertical lines which are useful to describe the main failure mode that has been seen for these specimens: the detachment of the various fiber tows, one from the other, in the resin-rich areas between them.

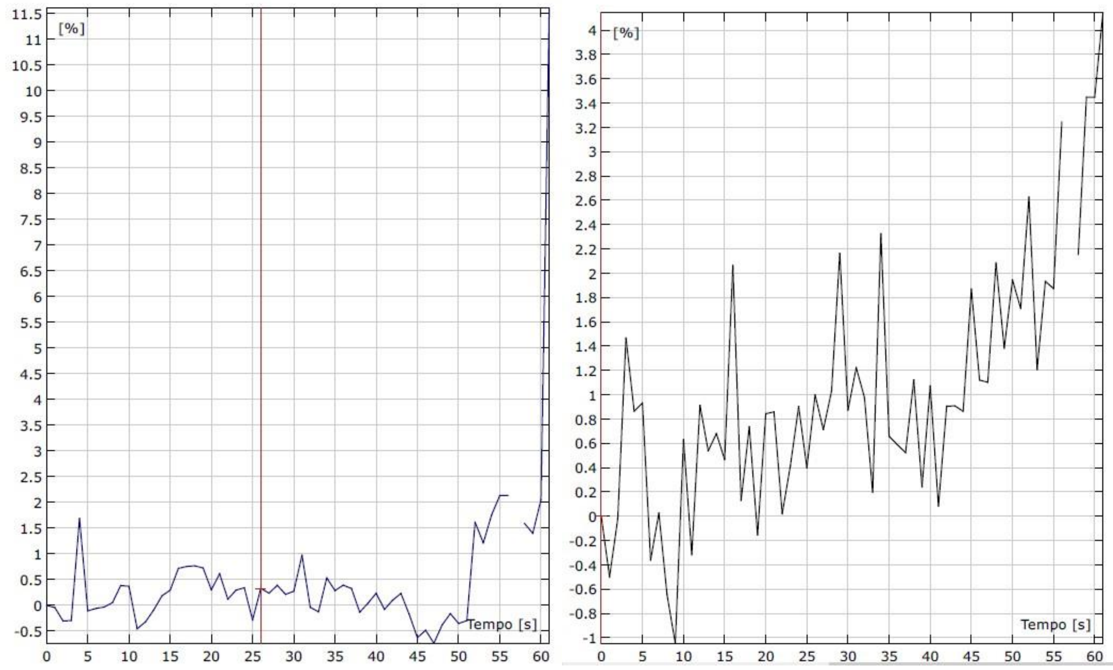

Figure 76 - Epsilon1 (left) and Epsilon2 (right) historical value in one query point

In Figure 76 there are the historical values of the ε_1 and ε_2 along the test from the beginning of the test to the appearance of the first crack. They have been both measured in the same location, close to where the first crack appeared. The signal appears to be quite noisy and only in the ε_2 plot there is a sort of growing trend which corresponds to what is possible to see in the contour plot and to what happened before the first failure. It is also true that the noisy but constant in average strain value in the longitudinal direction can be justified by the very high stiffness of the material. In fact, the deformation is very little also in presence of high loads, and only when the first crack appears the signal has a spike towards more than 10% strain. Probably, with a better setup of the acquisition system and a better digital tool, the accuracy of this software can be improved, and the results can be more useful than what obtained during these experiments.

8.1.5 Failure modes

The observed failure modes during the tensile coupons tensile tests have been mainly two:

1. Inter-fiber tows failure
2. Gripping tab failure and specimen slip
3. Horizontal fracture near the tab edge (stress concentration)

Consequently, only the first of the three can be considered the "correct" failure mode, while the second is just a consequence of the malfunction of the adhesive bond between the gripping tab and the specimen surfaces and the third is caused by a bad design of the tabbing system.

Figure 77 - Failed specimen 1

Figure 1 shows the failed Specimen 1, that is the first from the VARTM manufactured batch. In the picture it is possible to see the perfect example of the first two failure modes at the same time. In fact, it is evident the detachment due to the inter-fiber tows failure between the different fiber tows, with all the vertical cracks running along the matrix-rich areas. It is also clearly visible, in the top portion near the grip area, a black area of exposed fibers, which has slipped out from the bonded area.

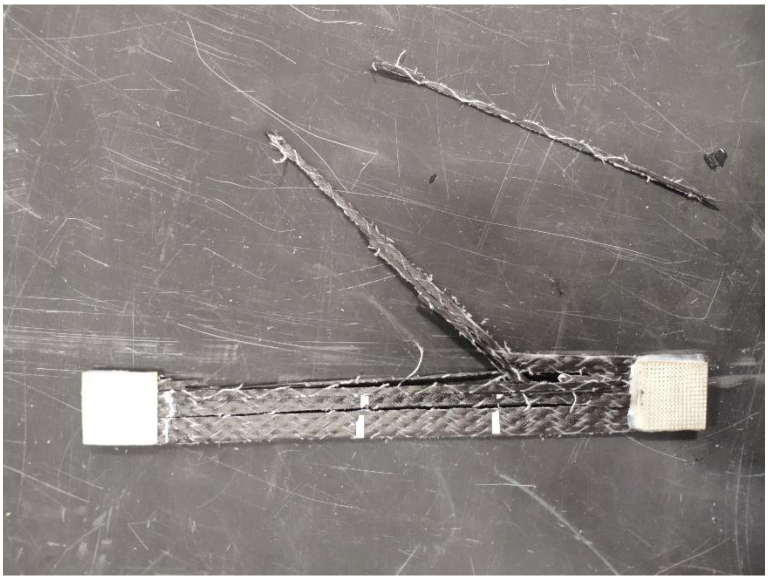

Figure 78 - Failed specimen after tensile test with laser extensometer

Another example of the first failure mode can be seen in Figure 78, where it is displayed a failed specimen after a tensile test with the use of the laser extensometer. On the left of the specimen, near the gripping tab, it is possible to see a horizontal crack caused by the stress concentration induced by the cross-section reduction in correspondence of the tabs end. Even if the tabs were tapered on the gage side at 45°, in some cases it has not been enough to avoid that kind of failure.

Figure 79 - Stress concentration induced cracks

8.2 Shackles test process

The testing campaign has not been limited to material characterization only (specimens testing), but also the shackles, both the reference-shape and the net-shape, have been tested, to understand how they fail and if some design modifications can be done to improve their performance. Furthermore, the experimental results can be compared with the numerical simulations' ones and the predictive capability of the finite element model can be assessed.

8.2.1 Test fixture design and manufacturing

The first necessary step to proceed with shackle testing, was to build a test fixture. In fact, while the tensile specimens could be tested simply clamping them on the tensile test machine grips, the load on the shackles is inserted via two bolts inserted in the holes of the shackle plate. Therefore, a system capable of providing an interface to transmit the load, from the test machine grips to the bolts had to be designed and made.

A couple of C-shaped brackets were already available in the lab, they provided the interface between the grips and had some holes, which have been used as a reference to build two couples of plates to allow the connection between the brackets and the shackles.

Figure 80 - First fixture design

In Figure 80, it is possible to see the first developed design for the test fixture. At both ends of the assembly there are the two steel C-shaped brackets, provided with surfaces that can be clamped in the wedges of the test machine. Then on the left it is possible to see a couple of steel plates (in green) ¼” thick, with a ¼” bolt connecting them to the shackle. On the right side, the ¼” bolt is connecting directly the shackle to the bracket.

However, this design has been judged too weak to stand the test loads, and the proposed solution was to adopt larger diameter bolts. The plates have then been modified and another couple of plates has been made to allow the connection between the shackles and the brackets. 5/8” bolts have been used.

Figure 81 - Final fixture design (detail of bolted plates)

8.2.2 Digital Image Correlation (DIC)

Here is an overview of the tests:

Shackle	Method	Photo
A1	DIC	No image available
B1	DIC	No image available
A2	DIC	No image available
B2	DIC	
A3	DIC	

B3	DIC		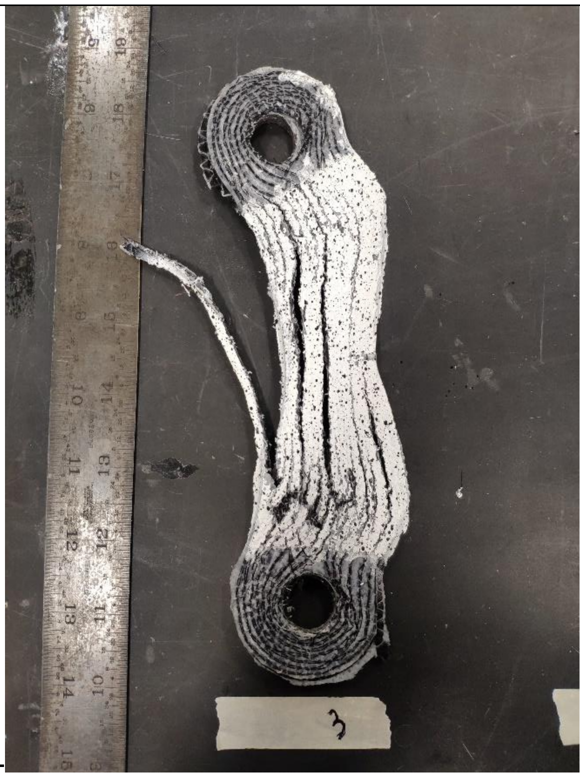
A4	DIC		

B4	DIC		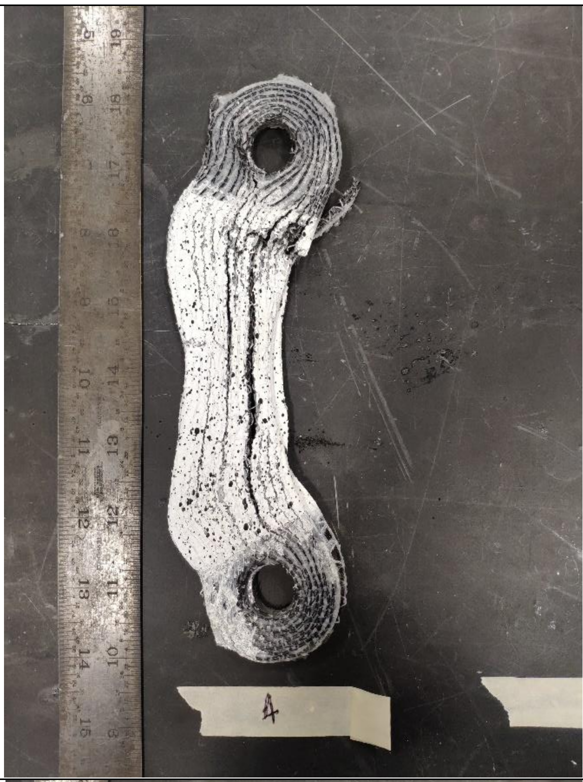	
A5	DIC		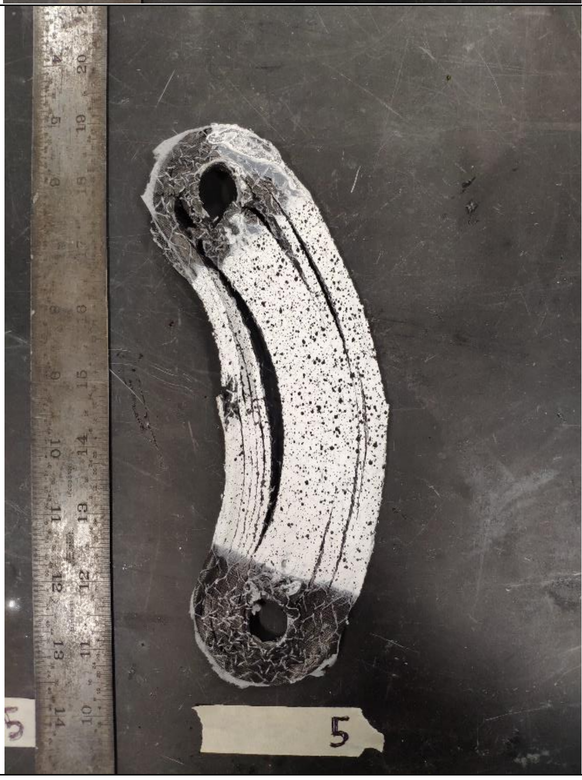	

B5	DIC		
A6	DIC		

B6	DIC		

Table 9 - Shackle tests results

Where the letter A or B identify the shape of the shackle (A for the reference shape and B for the net-shape), and the number the production batch number (from 1 to 6).

These tests have provided very useful knowledge on how the components fail and, as a consequence, on how the design can be improved to increase the strength of the component and to obtain a better performance.

8.2.3 Results and failure modes

In this paragraph the main results from the shackles testing will be presented. An experimental campaign has been carried on with the aims of understanding the strength, performance and failure modes of the shackles.

First of all, an overview of the failure loads of the tested shackles is given:

Shackle	**First crack load (N)**	**Ultimate failure load (N)**
Reference shape		
A1	2850	7800
A2	6300	6600
A3	5700	7800
A4	5700	6900
A5	5700	5900
A6	6900	6900
Avg.	**5525**	**6980**
Std. dvtn.	**1395**	**730**
Netshape		
B1	3700	4000
B2	4500	5000
B3	4300	6800
B4	4250	7900
B5	3200	7750
B6	4000	6900
Avg.	**3990**	**6390**
Std. dvtn.	**475**	**1560**

Table 10 - Results overview of shackles tests

From Table 10 it is already possible to deduce some information. First of all, the strongest shape is the reference one, with an average ultimate failure load 9.2% higher.

The analyzed failures have given an indication on how the shackles break and from that information, an improvement in the design concept can be achieved.

The basic failure pattern of all the shackles is this one:

1. Bending of the plate

Figure 82 - Shackle specimen

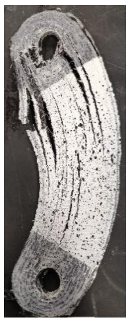

Figure 83 - Broken specimen

2. Detachment of adjacent fiber tows, due to shear stress between one tow and the next one. (Crack initiation)
3. Crack propagation
4. Compression on the external curved side, tension on the internal curvature. The fibers on the internal side can break under tension.

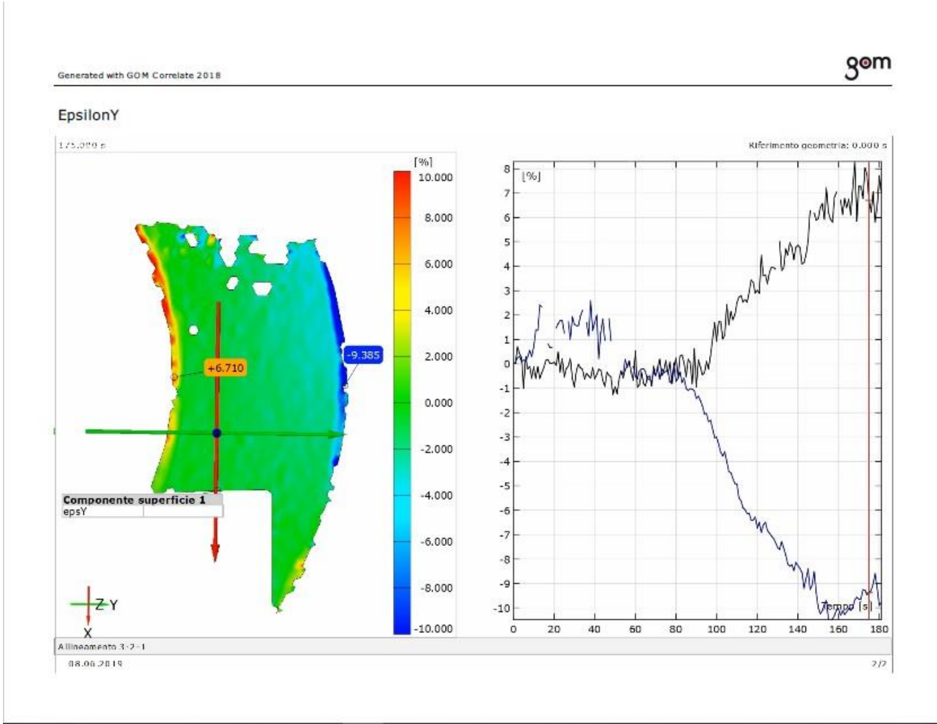

Figure 84 - DIC analysis of reference shape shackle #A3

This is a general failure mode of both the reference and net-shape shackles. The main difference between the two is due to the main difference in their design. In fact, while the net-shape shackles have all the fibers passing around the two holes, the reference shackles have only some of them circling around the holes: some fibers are just in the middle section (Figures 85 and 86).

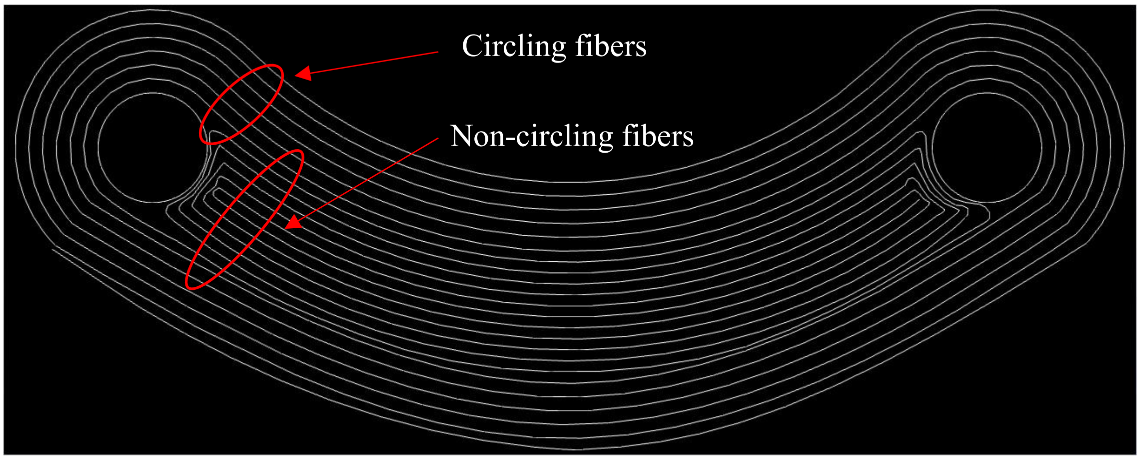

Figure 85 - Stitching pattern of reference shape shackle

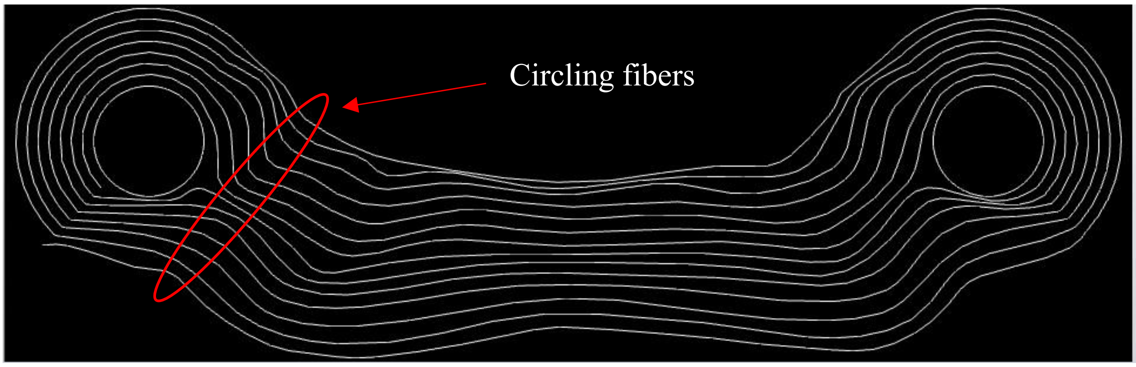

Figure 86 - Stitching pattern of net-shape shackle

This difference explains the fact that the reference shape shackles break in the area between the fiber reinforcement around the hole and the central portion of non-circling fibers, in fact in that area the main load is not aligned with the local 1-direction of the composite part, but with its 2-direction (transversal). While in the net-shape shackles, there is a resin rich area right under the holes, which gives start to the crack propagation.

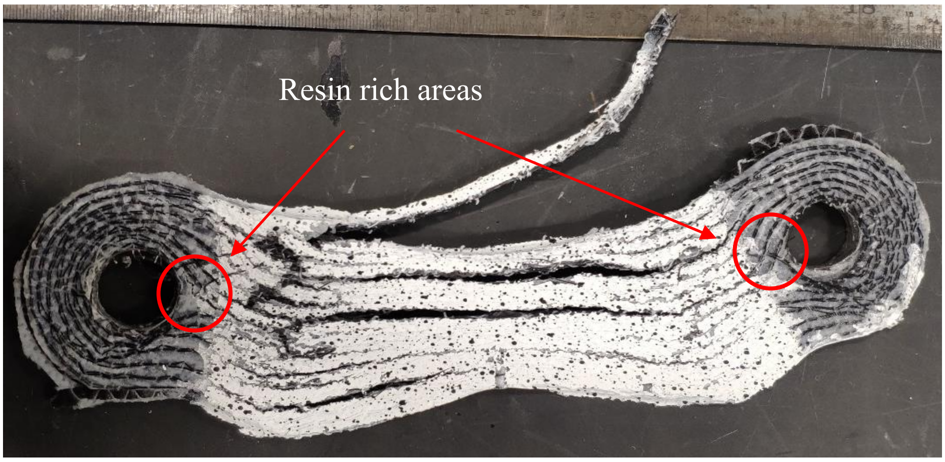

Figure 87 - Broken specimen #B3

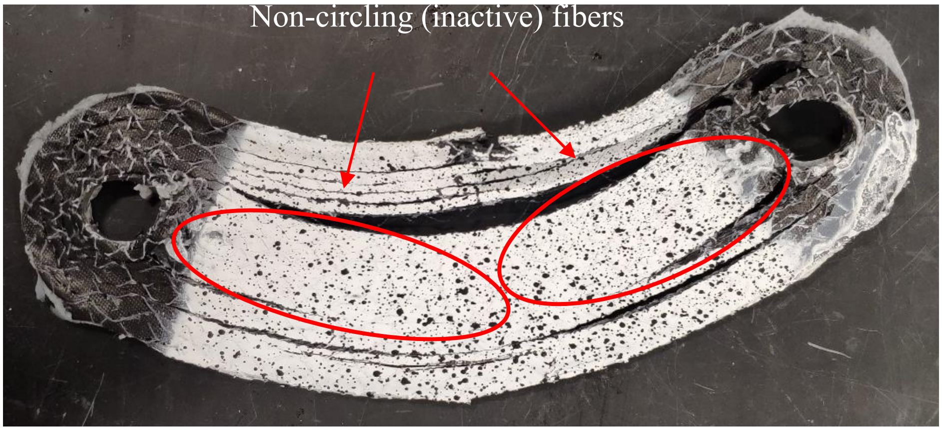

Figure 88 - Broken specimen #A5

A proposed solution for this issue was to use different complementary layers of stitched fibers, instead of superposing two or more identical layers. This could not be done during the development of this work due to timing constraints, but it is clearly a weak spot of the design of the components.

9. Feedback of material properties into the FE model

The next step, after the testing campaign, was to implement the material data into the FE model, with the aim to obtain results as coherent as possible. From the data collected through the testing of the tensile coupons, the engineering constants, necessary to define the material have been identified.

9.1 Material data

As reported in Table 7, the average tensile stiffness, that means the one in the longitudinal direction (1-direction) was 77.3 GPa. Considering a 10% safety factor the chosen E_1 stiffness for the FE model was 70 GPa. As far as the transversal stiffness, some criticalities appeared, in fact the coupons tested with the DIC, did not give good results. This is due to a combination of two factors, lack of image quality of the recording camera system, and bad dispersion of the spray paint dots on the specimen. As already mentioned several times before, the timing of the project did not allow to perform additional tests and, moreover, the results were analyzed only after the end of the project, making it impossible to execute them again. Due to these issues, the safest and also more reasonable choice (considered the failure mode of the specimens and of the shackles, being intrinsic with the TFA technique) was to consider the pure SC-15 epoxy stiffness, equal to 2.4 GPa. In fact the fiber tows are aligned along the longitudinal direction, so it makes sense to assume that the transversal modulus, E_2, is the one of the epoxy matrix. And analogously for the E_3 stiffness. The Poisson's ratios have been set to $\nu_{12} = 0.3$, $\nu_{13} = 0.3$ and $\nu_{23} = 0.1$, respectively. The shear stiffnesses have been calculated using the formula:

$$G_{ij} = \frac{E_i}{2(1 + \nu_{ij})}$$

Equation 42 - Shear modulus

Following Equation 42, the results are: G_{12} = 27 GPa, G_{12} = 27 GPa and G_{23} = 1.1 GPa. Having all the nine engineering constants, the material was defined and ready to be used in the FE analysis.

Engineering constants	
E1	70 GPa
E2	70 GPa
E3	2.4 GPa
ν_{12}	0.3
ν_{13}	0.3
ν_{23}	0.1
G_{12}	27 GPa
G_{13}	27 GPa
G_{23}	1.1 GPa

Table 11 - Stitched and cured carbon fiber tows/epoxy engineering constants

Once that all the data have been stored and applied to the model, the simulation has been re-run for both the reference and the net-shape shackle.

The applied conditions were a load transmitted to the external semi-circle of one of the bolt holes, and a fixed constraint to the opposite semi-circle of the other hole.

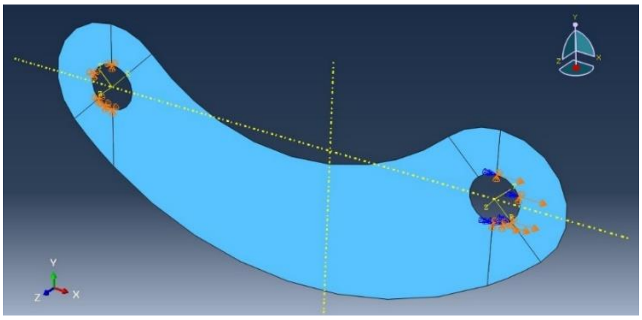

Figure 89 - Loadstep of FE model for the reference shape shackle

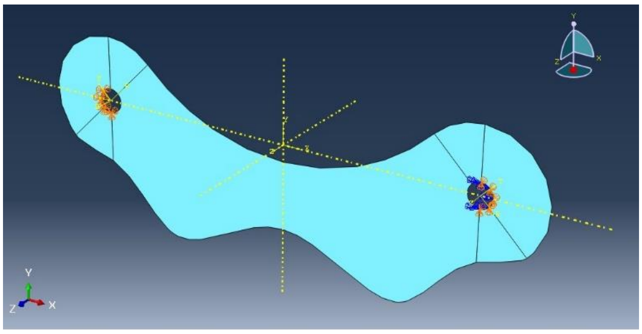

Figure 90 - Loadstep of FE model for the netshape shackle

The load was not directly defined, instead was applied a ramped displacement of 200 mm in 120 s to recreate the same conditions of the tensile test. The choice of limiting the displacement to 200 mm, even if during the tests it was bigger, is due to the fact that in average at that displacement the specimens were still showing an elastic behavior, where the model conditions still applied. After that the specimens started to show crack formation and propagation and the model would not be able anymore to follow those phenomena, being optimized for an elastic behavior. This is also the reason why the model is intrinsically unable to predict the failure of the component. It has been modeled as a homogeneous orthotropic material, and it was given material orientation in order to follow the direction of the actual fiber tows, yet it is not capable of represent the tows and the matrix separately. That is why an accurate failure mode prediction cannot be expected from this model.

9.2 FEA results

The results of the FE analysis have been compared to the ones gathered during the experimental campaign. The chosen comparison term has been the E22 strain in the transversal direction. In fact, this strain is the main indicator of an upcoming failure (since failure mode consists in the transversal detachment of two adjacent fiber tows). The closer the prediction to the measured values the better prediction capability of the model. The E22 strain has been measured in the same position in both the FE model and the experimental specimens: at the middle of the inner curved section of the shackle plate.

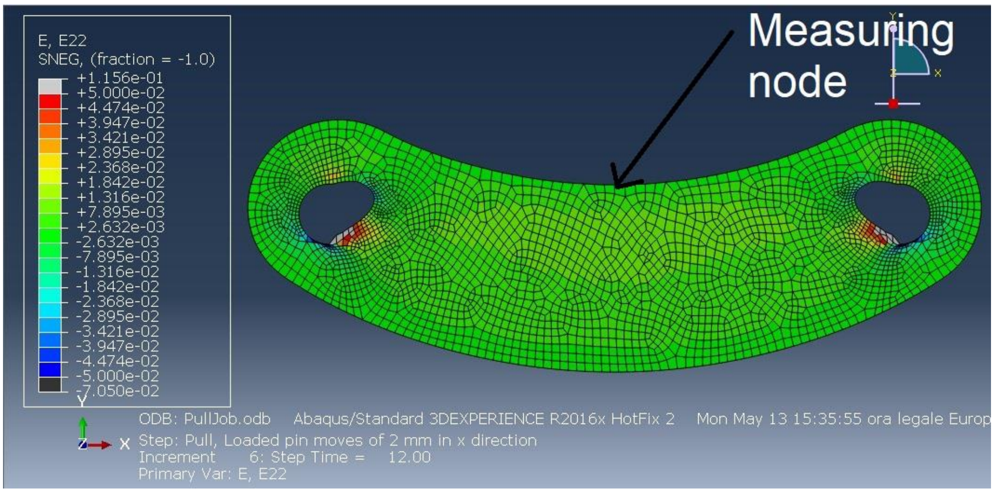

Figure 91 – Reference shape E22 strain contour plot

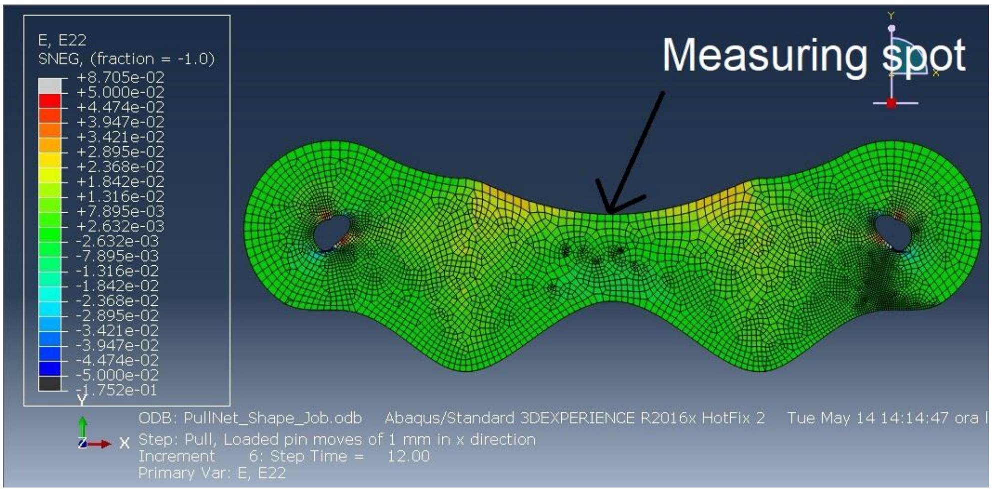

Figure 92 - Net-shape E22 strain contour plot

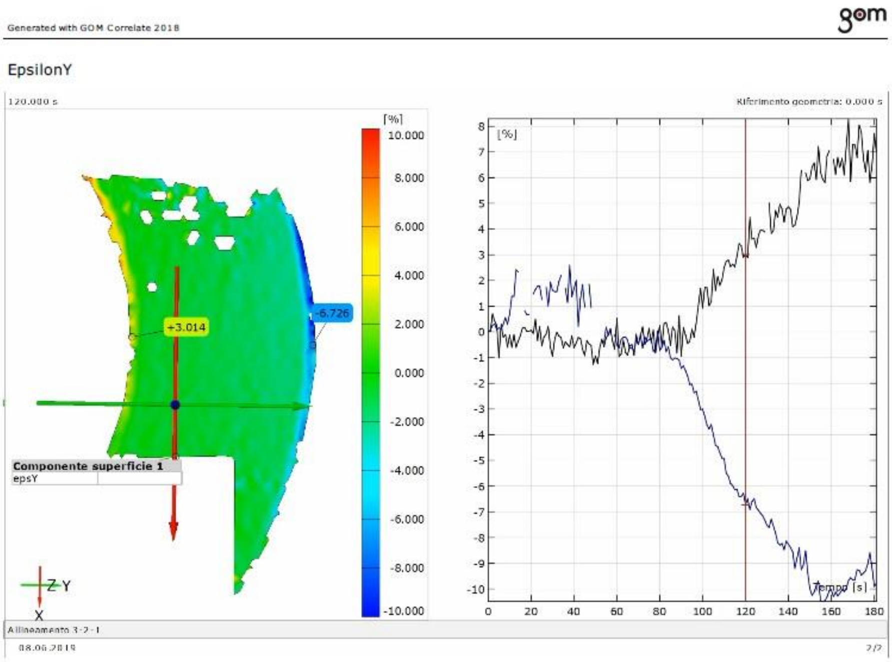

Figure 93 - DIC experimental E22 strain contour plot

In the following table the numerical values are listed:

Specimen	E22 strain
Reference shape FEA	0,002854
A1	0,04765
A2	0,02538
A3	0,03014
A4	0,0019
A5	DIC data not usable
A6	0,00939
Net-shape FEA	0,001935
B1	0,0004
B2	0,00372
B3	0,02942
B4	DIC data not usable
B5	DIC data not usable
B6	0,00067

Table 12 - FEA results comparison vs experimental results

The average value for the reference shape shackles is 0,022892, which is 8 times the value obtained from the FEA. As far as the net-shape shackles, the average measured transversal strain is

0,008553, which is 4,4 times the resulting value from the FEA. Therefore, the conclusion is that the model is overestimating the stiffness of the component. It is also true that the accuracy of the implemented DIC method can be greatly improved, so that a deeper analysis has to be carried out to draw the right conclusions.

In the next chapter, the whole process is analyzed, and the results will be commented with the aim to validate the process and to build a starting point for the next development of the project.

10. Results and conclusion

In this chapter, the main results of the thesis project will be presented. After that, there will be a brief summary of the next steps needed to improve the quality of the project and to go deeper into each step of the whole process.

10.1 Target strength

The first parameter to be evaluated is the compliance of the component with the strength requirements. Considering the average first crack load of the reference shape shackle of 5525 N, and decreasing it of a 1.2 safety factor, the resulting average strength of the reference shape shackle is

$$\frac{Avg. first\ crack\ load}{safety\ factor} = \frac{5525\ N}{1.2} = 4604\ N > 2670\ N$$
$$= target\ minimum\ failure\ load$$

The average reference shape shackle is exceeding 1.72 times the target strength. Analogously, the net-shape shackle has an average first crack load of 3990 N, which, decreased of a 1.2 safety factor is equal to 3325 N, still higher than 2670 N target failure load. The net-shape shackle is 1.25 times stronger than the minimum target, yet is 38% weaker than the reference shape shackles.

10.2 Weight

A big advantage of the composite materials is the light weight. In fact, compared to the base steel shackle considered at the beginning, the composite shackles are much lighter, keeping the same or even better performances. Compared to the steel shackle, which has a calculated weight of around 400 g, the composite one weighs just 48 g (reference shape shackle) and 36 g (net-shape shackle), thus having a weight reduction of 88% and 91% respectively. This is not just a huge material saving, but also a big decrease of the vehicle weight. Furthermore, it is not just the overall vehicle weight to decrease, which just by itself produces a better fuel economy, but also a reduction of the non-suspended masses. In fact, the suspension elements are partly considered within the non-suspended masses and decreasing them improves the vehicle drivability and ride comfort.

10.3 Next steps

As previously mentioned, the approach of this project has been a holistic approach. This means that every step of the process from the design to the manufacturing has been covered. Due to the very narrow time window, the priority has been given to the completion of the whole process, rather than to focus more deeply on just one of the several steps needed. The reason to do that was to give to the trainee a global understanding on the composite design, testing and manufacturing sectors. The downside of this choice has been, of course, a lower quality level in each step. Every decision made was the result of a tradeoff between the need for project advance and scientific and technical quality of the process. Even if the quality of the finite components and of the FE model is not the best, all the necessary actions to improve it are already clear and defined, since all of them have been evaluated and studied.

The steps which should be developed more deeply and further analyzed to improve the quality of the project are:

- Finite element model;
- Stitching pattern;
- Manufacturing process;
- Testing setup.

10.3.1 FE model improvement

The FE model needs to be refined, to obtain a higher failure prediction capability. In this case, e.g., the model, if calibrated, would be able to represent some strain and stiffnesses of the actual component, but will never have the failure prediction capability.

The two main improvements should come from:

- better data from experimental testing;
- development of a model able to reproduce the different behavior of fiber tows and resin-rich areas (homogeneous → heterogeneous material).

Having good data from the experimental testing allows to define the material in a more realistic way, which adheres to the real-life behavior. While the setup of a model which is able to recreate the interactions between fiber tows and resin-rich areas, allows to replicate and then predict the failure mode of the component in a very precise way.

10.3.2 Stitching pattern improvement

From the testing campaign, one of the weak spots that has emerged is the stitching pattern. Not having a representative FE model, the only way to understand how to increase the effectiveness of the stitching pattern was to test the specimens, but due to time constraints, no change in the design was possible after the first one. The use of complementary layers can help to decrease the matrix-rich areas, and to improve the component strength. In fact, one of the biggest constraints during the definition of the stitching pattern was to have all the fibers laid down along a single continuous path. With the application of complementary layers, it will be possible to gain a degree of freedom which will allow to optimize the fibers direction.

By complementary layers, it is intended the super-position of differentiated layers, unlike what was done in this project, with the super-position of 2 identical double layers. This means that 2 or more different layers are stitched, and then joined together during the component curing phase, to reduce resin-rich areas, by reciprocally filling each other gaps between stitched fiber tows.

10.3.3 Manufacturing process

The manufacturing process has got a lot of room for improvement. From the materials side, the choice of the fibers and matrix system can be analyzed. The materials used in this project were adopted because of their properties but also because already present in the manufacturing facility. The possibility of widening the choice could improve the effectiveness of the manufacturing process and hence the final properties of the component to be manufactured. Furthermore, the support cloth onto which the fibers are stitched, at the moment in fiber-glass in this project, could be chosen to "disappear" in the finite product. In fact, the current cloth is remaining still during the infusion and curing phases and it is visible in the finished part, disrupting the surface finish, and the aesthetics of the component. A possible choice could be to adopt a water-soluble support cloth, which can be washed away after the end of its support function for the fiber tows once they are placed in the mold.

Another critical issue in the manufacturing process to be corrected is the mold. In this project a one-sided CNC-milled aluminum mold has been used, but the surface quality was on target only on the side facing the mold surface, while the other side, facing the vacuum bag, is not satisfactory. To solve this issue, a 2-parts, male-female mold should be designed, with inserts for the shackle holes, and one inlet and one outlet holes for vacuum lines through which realize a vacuum-assisted resin transfer molding. In that way the geometry and surface quality control should be optimal. A first concept of it has been already designed, but it needs to be further engineered and manufactured.

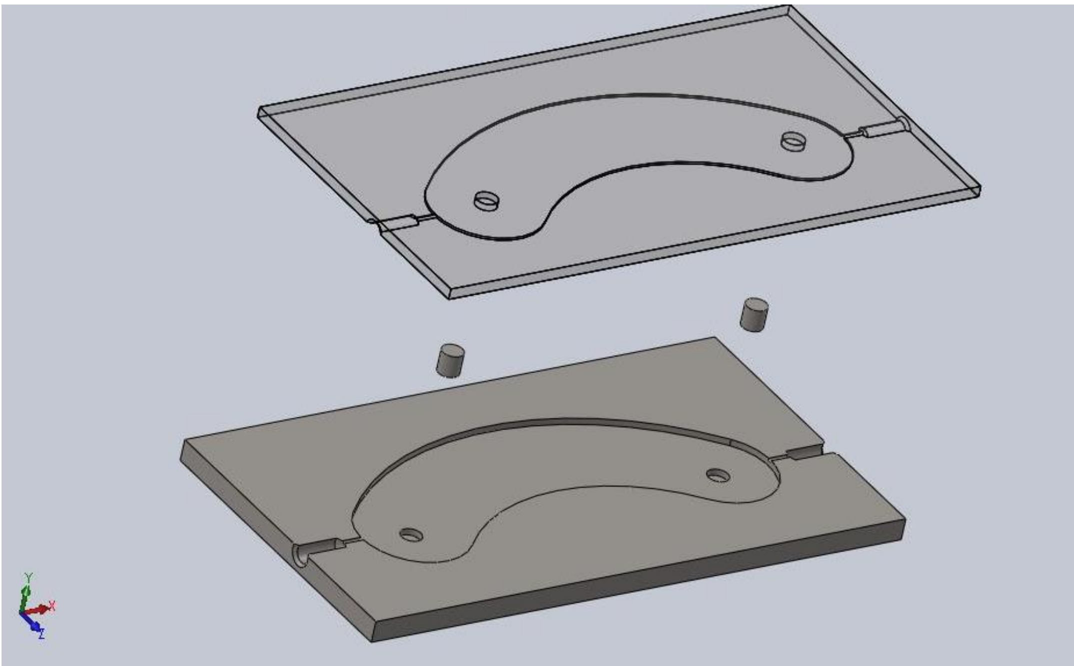

Figure 94 – Concept design of 2-sided mold for VARTM

10.3.4 Testing setup

The experimental test setup is fundamental for the success of the project. This relevance is clearly due to the importance of having meaningful and usable data from the experiments to characterize the material and understand the failure modes of the components. Unfortunately. for this project no professional DIC equipment was available and the smartphone camera used to capture the videos of the tensile tests has not been good enough to provide reliable data. In fact, the optimal setup should have at least 2 high frequency cameras to obtain correct strain and displacement data. Furthermore, the gripping tabs bonding needs to be analyzed in a deeper way, even with a specifically dedicated FE model, to understand it better and avoid gripping tabs failure which invalid any measurement taken. In addition to that, the realized test fixture for the shackle specimens was adapted from some scratch equipment found in the laboratory and was not designed for the purpose. This means that some tradeoffs had to be made in order to use it, e.g. the orientation of the specimen during the test was not parallel to the machine, but perpendicular, so that the camera had to put sideways of the machine, even worsening the conditions for video recording.

11. Conclusions and acknowledgements

The overall outcome of the project must be evaluated very critically. The solid result is that a finished prototypal part was made. The basic minimum requirements of strength are matched with a surplus. The weight reduction is significant, leading, per each vehicle to a saving of around 750 g.

It is also true that this cannot be considered as a finished project. The stage of development can be identified as a "proof of concept", and this is the idea with which it was started. A holistic approach to the use of TFA technique for a practical automotive application to lay down the path, from design to manufacturing and testing. Each one of these steps has to be developed in depth, bringing a higher scientific and technical content.

Nevertheless, the followed trail has given a basement onto which further results can be built and obtained.

Moreover, I have to say thank you to Politecnico di Torino and Michigan State University, and more directly to Prof. Giovanni Belingardi and Prof. Mahmoodul Haq, for having followed my path and guided me towards the right direction.

Thank you also to Fiat Chrysler Automobiles, which has funded the scholarship of the project.

And a big thank you goes also to all the smart and outstanding colleagues working in the Composite Vehicle Research Center, who have always helped me whenever I needed a tip or an opinion, to proceed along the development of the thesis project.

Last but not least, a huge thank you is for my girlfriend Cecilia who has borne the weight of my distance still keeping all her support for me and this project, and to my family, which has always provided everything to me without asking anything in return.

Bibliography

Carbon composites one of top 10 emerging technologies. (2014). *World Economic Forum.*

Company, S. G. (1963). *Chambrey, France Patent No. 1435739.*

Crothers, & al. (1996). Tailored fibre placement to minimize stress concentrations.

Fitzer, & Kunkele. (1990). *High Temp. - High Pressures journal 22(3)*, pp. 239-266.

Gibson. (2011). *Principles of Composite Material Mechanics.*

Gliesche, & al. (2002). Application of the tailored fibre placement (TFP) process for a local reinforcement of an “open-hole” tension plate from carbon/epoxy laminates.

Gotro. (2016). *Polymer Composites Part 3: Common Reinforcements Used in Composites*. Retrieved from Polymer Innovation Blog: https://polymerinnovationblog.com

Inagaki. (2000). *New Carbons - Control of Structure and Functions.*

Jaeger, H. (2014). *cheaper carbon fiber will slash auto making costs manufacturer*. Retrieved from reuters: https://www.reuters.com/article/sgl-fibers/cheaper-carbon-fibre-will-slash-auto-making-costs-manufacturer-idUSL5N0MP2RP20140328

Khaliulin, & al. (2014). Prospects of Applying the Tailored Fiber Placement (TFP) Technology for Manufacture of Composite Aircraft Parts”.

Koricho, & al. (2014). Innovative tailored fiber placement technique for enhanced damage resistance in notched compo-site laminate.

Mazumdar, S. (2019). *The Glass Fiber Market.* Retrieved from Composite Manufacturing Magazine: http://compositesmanufacturingmagazine.com

Pichler, D. (2019). *The Carbon Fiber Market.* Retrieved from Composite Manufacturing Magazine: http://compositesmanufacturingmagazine.com

Ramesh, & Singh, V. (2012). *Damage and Failure of Composite Materials.*

Richter, Uhlig, Spickenheuer, Bittrich, Mäder, & Heinrich. (2014). THERMOPLASTIC COMPOSITE PARTS BASED ON ONLINE SPUN COMMINGLED HYBRID YARNS WITH CONTINUOUS CURVILINEAR FIBRE PATTERNS.

Salil, K. R., & Manas, C. (2006). *Plastics Technology Handbook.*

Tosh, & Kelly. (2000). On the design, manufacture and testing of trajectorial fibre steering for carbon fibre composite laminates.

Zhu, & al. (2018). Variable Angle Tow reinforcement design for locally reinforcing an openhole composite plate.